Advanced Monitoring and Control Strategies for Li-Ion Batteries and Smart Energy Systems

Thesis Submitted by

Abhijit Dey

Doctor of Philosophy
(Engineering)

Electrical Engineering Department
Faculty Council of Engineering & Technology
Jadavpur University
Kolkata, India

2025

Jadavpur University
Kolkata – 700032, India

INDEX NO. 205/19/E

1. **Title of the Thesis:**

   Advanced Monitoring and Control Strategies for Li-Ion Batteries and Smart Energy Systems.

2. **Name, Designation & Institution of the Supervisors:**

Dr. Kesab Bhattacharya
Professor,
Electrical Engineering Department,
Jadavpur University

Dr. Sovan Dalai
Professor,
Electrical Engineering Department,
Jadavpur University

3. List of Journals Published:

- **A. Dey**, S. Mondal, B. Chakraborty, S. Dalai and K. Bhattacharya, "Online Internal Resistance Computation-Based Early Sensing of Thermal Runaway for Smart Fault Handling System (FHS) of Li-Ion Batteries," in *IEEE Embedded Systems Letters*, vol. 17, no. 4, pp. 284-287, Aug. 2025, doi: 10.1109/LES.2025.3535836.
- **A. Dey,** S. Mondal, B. Chakraborty, S. Dalai and K. Bhattacharya, "Microcontroller Based Real-Time Power Monitoring Module by Hybrid Power Factor Selection Algorithm," in *IEEE Embedded Systems Letters*, doi: 10.1109/LES.2025.3602829**.**

4. List of Patents:

Nil

5. List of Presentations in National/International Conferences:

- **A. Dey**, B. Chakraborty, S. Dalai, and K. Bhattacharya, "Insights and New Practices for Advanced Metering Infrastructure and Smart Energy Metering Framework in Smart Grid—A Case Study," in Proc. IEEE Calcutta Conference (CALCON), Kolkata, India, pp. 323–326, 2022.

- **A. Dey**, K. R. Hasabnis, B. Chakraborty, S. Mondal, S. Dalai, and K. Bhattacharya, "Enhancing Power System Resilience with DG Using GA Based Relay Coordination and FCL Integration," in Proc. IEEE 4th Int. Conf. on Applied Electromagnetics, Signal Processing, & Communication (AESPC), pp. 1–6, 2024.

- **A. Dey**, S. Dalai, S. Mondal, and K. Bhattacharya, "Advancements in Li-ion Battery Materials for Battery Energy Storage Systems," in Proc. 2025 Devices for Integrated Circuit (DevIC), Kalyani, India, Apr. 5–6, 2025.

Statement of Originality

I, **Abhijit Dey** registered on **4th July 2019,** do hereby declare that this thesis entitled "***Advanced Monitoring and Control Strategies for Li-Ion Batteries and Smart Energy Systems***" contains a literature survey and original research work done by the undersigned candidate as part of Doctoral studies.

All information in this thesis has been obtained and presented in accordance with existing academic rules and ethical conduct. I declare that, as required by these rules and conduct, I have fully cited and referred to all materials and results that are not original to this work.

I also declare that I have checked this thesis as per the "Policy on Anti-Plagiarism, Jadavpur University, 2019", and the level of similarity as checked by iThenticate software is 3 %.

Abhijit Dey 09.10.2025
(Signature of Candidate)

Date:

Certified by Supervisors:
(Signature with date, seal)

1. K Bhattacharya 09/10/2025
Dr. Kesab Bhattacharya
Professor
Electrical Engineering Department
JADAVPUR UNIVERSITY
Kolkata-700 032

2. 09/10/2025
Dr. Sovan Dalai
Professor
Electrical Engineering Department
Jadavpur University
Kolkata-700032

Certificate from the Supervisors

This is to certify that the thesis entitled "*Advanced Monitoring and Control Strategies for Li-Ion Batteries and Smart Energy Systems*" submitted by **Shri Abhijit Dey**, who got his name registered on **4th July, 2019** for the award of Ph. D.(Engg.) degree of Jadavpur University is absolutely based upon his own work under the supervision of **Prof. Kesab Bhattacharya and Prof. Sovan Dalai,** and that neither his thesis nor any part of the thesis has been submitted for any degree/diploma or any other academic award anywhere before.

K Bhattacharya 09/10/2025

Signature of the Supervisor and date with Office Seal

Dr. Kesab Bhattacharya
Professor
Electrical Engineering Department
JADAVPUR UNIVERSITY
Kolkata-700 032

09/10/2025

Signature of the Supervisor and date with Office Seal

Dr. Sovan Dalai
Professor
Electrical Engineering Department
Jadavpur University
Kolkata-700032

Acknowledgment

The author expresses his sincere appreciation and deep gratitude to his esteemed guides, Prof. Kesab Bhattacharya and Prof. Sovan Dalai of the Electrical Engineering Department, Jadavpur University, for their invaluable guidance in carrying out the thesis work. This work has reached this stage with their expertise, encouragement, and valuable criticisms. The author also expresses his sincere gratitude towards his supervisors for granting the essential freedom for his work, while the close oversight from the mentor directed the work towards excellence.

The author expresses his deep sense of appreciation to the Head of the Department of Electrical Engineering, Jadavpur University, for her kind accordance in providing the necessary departmental facilities for the implementation of this work.

It is the author's pleasure to acknowledge his respected teachers, Prof. Biswendu Chatterjee, Prof. Biswanath Roy, and Prof. Madhubanti Maitra, for their advice and encouragement in completing the research work.

The author also wants to acknowledge the contributions of Mr. Supratik Mondal and K. R. Hasabnis in the course of the research work.

The author is thankful to his colleagues, Mr. Biswajit Chakraborty, Mr. Sandipan Kumar Paul, and Mr. Soumyadeep Maity, for providing support in various ways for carrying out the work.

The author would like to express his heartfelt gratitude to all his family members and relatives for their never-ending support and encouragement during the course of the thesis work.

The author also extends thanks to all the members of the High-Tension Laboratory of the Electrical Engineering Department, Jadavpur University, for making it possible to work in a homely atmosphere. Last but not least, the author remains indebted to all the resources that he was fortunate to have during the work.

Abhijit Dey.

Dedicated to
My Parents, Wife, Child, and Teachers

Table of Contents

List of Figures

List of Tables

List of Abbreviations

Abbreviation	Full-Form
Li-ion	Lithium-Ion
IR	Internal Resistance
TR	Thermal Runaway
BESS	Battery Energy Storage System
SES	Smart Energy Systems
AMI	Advanced Metering Infrastructure
DG	Distributed Generation
EMS	Energy Management System
PV	Photovoltaic
RES	Renewable Energy Source
SOC	State of Charge
ECM	Equivalent Circuit Model
SEI	Solid Electrolyte Interphase
NMC	Nickel Manganese Cobalt Oxide
LFP	Lithium Iron Phosphate
LMO	Lithium Manganese Oxide
LCO	Lithium Cobalt Oxide
NCA	Nickel Cobalt Aluminum Oxide
LTO	Lithium Titanium Oxide
UPS	Uninterruptible Power Supply
DOE	Department of Energy
BNEF	Bloomberg New Energy Finance
TOU	Time-of-Use
V2H	Vehicle-to-Home
V2G	Vehicle-to-Grid
MCU	Microcontroller Unit
IoT	Internet of Things
ETRS	Early Thermal Runaway Sensing
BTE	Battery Testing Experiment
FHS	Fault Handling System
ATS	Arrival Time Stamp
IRT	Internal Resistance Threshold
ATG	Alarming Time Gap
VOC	Volatile Organic Compounds
CA	Cell Array
TDM	Time Division Multiplexing
CCR	Charging Control Relay

API	Application Programming Interface
AWS	Amazon Web Services
OCR	Over Current Relay
DOCR	Directional Over Current Relay
CTI	Coordination Time Interval
PSM	Plug Setting Multiplier
TMS	Time Multiplier Setting
GA	Genetic Algorithm
FCL	Fault Current Limiter
HIL	Hardware-in-the-Loop
HPFSA	Hybrid Power Factor Selection Algorithm
ZCD	Zero-Crossing Detector
LAP	Load Analysis Process
SCADA	Supervisory Control and Data Acquisition
SOH	State of Health
AMCD	Advanced Metering Communication Device
AMCC	Advanced Metering Control Computer
AMRC	Advanced Metering Regional Collector
USDP	Universal Service Delivery Point
FTS	File Transfer Service
MDN	Message Disposition Notice
AS2	Applicability Statement 2
LDC	Local Distribution Company
NAN	Neighborhood Area Network
WPG	WebSphere Partner Gateway
RTF	Real Time Framer
PPF	Post Processing Framer
MDM/R	Meter Data Management/Repository

List of Mathematical Symbols

Symbol	**Meaning**
I	Current
V	Voltage
R_{int}	Internal Resistance
T	Temperature (K)
t	Time (s)
P	Power
E	Energy
η	Efficiency
$SOC(t)$	State of Charge at time t
SOH	State of Health
U_{OCV}	Open Circuit Voltage
R_0, R_1, R_2	Battery Resistances (Ohmic, Polarization, Concentration)
C_1, C_2	Battery Capacitances (Electrochemical, Concentration)
P_{true}	True Power
P_{app}	Apparent Power
V_{rms}	RMS Voltage
I_{rms}	RMS Current
ΔT	Temperature Rise
Δt	Time Difference / Coordination Time Interval
V_H	Hall Voltage
V_{offset}	Offset Voltage
I_{sensor}	Sensor Current
P_{out}	Output Power
V_k	k-th voltage sample (V)
I_k	k-th current sample (A)
$f_{threshold}$	Threshold frequency
IR_{max}	Maximum measured IR (mΩ)
T_{onset}	Thermal runaway onset temperature (°C)

Chapter 1

1.1.Introduction

The global shift towards clean and sustainable energy has underscored the vital role of energy storage systems, particularly lithium-ion (Li-ion) batteries, in supporting the evolving needs of modern power networks. The growth of renewable energy integration, electric mobility, and distributed generation has driven the demand for Battery Energy Storage Systems (BESS) that are not only efficient but also intelligent and fault resilient. These developments align with the vision of Smart Energy Systems (SES), which aim to optimize energy flow through the integration of digital intelligence, automation, and real-time communication across energy generation, storage, and distribution assets [1].

In this context, Li-ion batteries offer superior gravimetric and volumetric energy densities, faster response times, and a favorable lifecycle cost, positioning them as the preferred choice for energy storage in microgrids, smart homes, electric vehicles, and hybrid renewable power plants. Their widespread adoption has also amplified safety concerns due to the occurrence of catastrophic failures such as thermal runaway (TR), cell swelling, and electrolyte leakage. The onset of such shortcomings is often preceded by internal electrochemical imbalances that manifest through subtle changes in system-level electrical characteristics such as internal resistance (IR) [2]. The reliable deployment of Li-ion batteries in large-scale and embedded systems requires a comprehensive monitoring and control framework capable of early fault detection and health-aware operation. While conventional Battery Management Systems (BMS) rely on voltage, current, and temperature sensing, recent studies [3] have discussed the significance of online IR estimation in detecting precursors of TR. The diagnostic sensitivity of internal resistance measurements provides a practical and computationally feasible alternative to invasive sensing techniques, making them suitable for real-time health estimation.

Furthermore, smart energy networks incorporate intelligent communication and control infrastructures such as Advanced Metering Infrastructure (AMI), fault-tolerant distributed generation (DG) controllers, and embedded microcontrollers to support dynamic reconfiguration and energy flow optimization. As explored in [4, 5], AMI and embedded sensing frameworks not only enhance data visibility but also create the foundation for predictive diagnostics, grid-interactive energy storage, and adaptive fault management. However, challenges persist in the practical implementation of such intelligent battery systems. These include material-level degradation phenomena, such as lithium plating and SEI growth, which influence IR evolution, as well as systemic issues like communication latency in AMI and coordination in DG (BESS) systems.

1.2.Fundamentals of Energy Systems

The 21st-century energy landscape is undergoing a profound transformation, driven by global imperatives to reduce carbon emissions, enhance energy efficiency, and decentralize power generation. Traditional fossil-fueled, centralized energy systems are being replaced by more dynamic and responsive architectures that incorporate distributed energy resources (DERs), renewable energy sources (RES), and intelligent control systems. This paradigm shift has given rise to what is broadly known as smart energy systems (SES), a multifaceted integration of power electronics, communication technologies, digital intelligence, and real-time energy management [1].

At the heart of SES lies the requirement for flexible, reliable, and responsive energy storage systems. Battery Energy Storage Systems (BESS), particularly those based on lithium-ion (Li-ion) technology, have emerged as the most promising solution to meet these requirements. They serve as both energy buffers and enablers of critical grid services such as frequency regulation, voltage support, demand-side response, renewable smoothing, and black start capabilities [6, 7]. Their rapid response time, modular deployment, and favorable energy density have made them indispensable in smart grid environments, off-grid renewable installations, and electric mobility infrastructures.

However, the integration of energy storage into SES extends beyond the electrochemical performance of the battery cells themselves. It encompasses embedded diagnostic systems, communication protocols, and intelligent control architectures capable of interacting with grid elements in real time [5]. These smart setups allow for continuous assessment of battery health, detection of degradation trends, and execution of control decisions based on predictive analytics. For instance, monitoring parameters like internal resistance (IR), terminal voltage, charge-discharge profiles, and temperature not only reflect the battery's current performance but also its impending failure modes [8]. The ability to interpret such data in real time, through embedded microcontrollers or edge computing platforms, enables proactive fault mitigation strategies, as demonstrated in [3].

Another layer of complexity is introduced by the heterogeneity of DERs, which includes solar photovoltaics (PV), BESS, wind turbines, diesel generators, and fuel cells, all of which may operate under different control logics and temporal dynamics. In such cases, the coordination of power flows, fault management, and optimal energy dispatch requires intelligent energy management systems (EMS) that interact seamlessly with the BESS [5]. These systems must account for battery aging, load profiles, environmental conditions, and network topology in their decision-making.

Concurrently, the communication backbone of SES plays a critical role in ensuring interoperability, data integrity, and timely control actuation. Protocols such as Modbus, IEC 61850, and DNP3 facilitate data exchange between local energy management units, smart meters, and central utility control rooms [9]. Furthermore, the deployment of Advanced Metering Infrastructure (AMI) provides a two-way communication channel between the consumer and the utility, enabling demand-side participation, time-of-use billing, and remote fault diagnostics. BESS units, when interfaced with AMI systems, can respond to grid events, participate in ancillary markets, and enhance grid observability [4].

Despite these advancements, several challenges persist, particularly in the areas of system reliability, safety, and scalability. Li-ion batteries, while offering many operational benefits, are inherently prone to degradation mechanisms such as lithium plating, electrolyte breakdown, and thermal runaway, especially under high load or fault conditions [10], [11]. These failure mechanisms necessitate the development of robust fault diagnostic methods, many of which are based on internal resistance tracking, thermal modeling, and gas detection techniques [3], [12]. Moreover, the effectiveness of these diagnostics hinges on the fidelity of equivalent circuit models (ECMs), the resolution of embedded sensor data, and the timeliness of the communication infrastructure.

1.2.1 Li-ion Batteries

Lithium-ion (Li-ion) batteries represent a cornerstone technology in the transition to decarbonized and decentralized energy systems. Introduced commercially in the early 1990s by Sony, the technology has evolved significantly over the past three decades to dominate applications ranging from portable electronics and electric vehicles (EVs) to stationary energy storage for grid and microgrid systems [11]. Their widespread adoption is primarily attributed to their superior electrochemical properties: high energy density (150–250 Wh/kg), long cycle life (typically 2000–5000 cycles), low self-discharge rates, and high coulombic efficiency (>99%) [1], [13].

At the core of a Li-ion cell is the intercalation mechanism, where lithium ions shuttle between a cathode (typically a transition metal oxide) and an anode (usually graphite), embedded in an organic electrolyte with a separator to prevent direct electronic contact. This chemistry supports a nominal cell voltage of approximately 3.6–3.7 V, enabling compact high-voltage battery modules. Various chemistries have been developed to optimize performance trade-offs between energy, power, safety, and cost. Some of the most common cathode materials include:

i. Lithium Cobalt Oxide (LCO) – high energy but low thermal stability.
ii. Lithium Nickel Manganese Cobalt Oxide (NMC) – balanced energy and safety.
iii. Lithium Nickel Cobalt Aluminum Oxide (NCA) – high energy density, used in Tesla batteries.
iv. Lithium Iron Phosphate (LFP) – long life and excellent thermal safety [14].

Anode materials also influence overall performance. Conventional graphite offers good structural stability, but newer designs incorporate silicon-based materials and lithium titanium oxide (LTO) to improve capacity and rate performance, though challenges related to volume expansion and lower energy density, respectively [15].

The relevance of Li-ion batteries to smart energy systems lies not only in their energy storage capability but also in their ability to respond quickly and effectively to transient conditions. Their low internal impedance makes them well-suited for applications such as:

i. Fast frequency response and frequency containment reserves.
ii. Ramp-rate control for photovoltaic or wind systems.
iii. Short-duration backup in uninterruptible power supply (UPS) applications [6].

However, despite these advantages, Li-ion batteries are prone to degradation and safety hazards when operated outside optimal conditions. Factors such as high C-rate charging/discharging, extreme temperatures, overvoltage, and deep cycling accelerate aging and reduce capacity retention [16]. Degradation mechanisms include:

i. Solid Electrolyte Interphase (SEI) layer growth on the anode,
ii. Lithium plating during fast charging or low-temperature operation,
iii. Electrolyte decomposition, and

iv. Gas generation and swelling [12].

In large-scale or embedded applications, cell-to-cell inconsistency further complicates reliable operation. As observed in [8], slight variations in internal resistance and capacity among cells in a module can lead to current imbalance, localized heating, and early onset of thermal runaway in stressed cells. Therefore, accurate, real-time monitoring of parameters such as internal resistance, cell temperature, and voltage spread is critical. These indicators provide early warning of abnormal behavior, enabling timely intervention through control algorithms or active thermal management systems. The use of internal resistance (IR) as a real-time health marker, as demonstrated in [3], has proven particularly effective in embedded platforms where simplicity, speed, and reliability are essential.

Li-ion batteries also exhibit chemistry-dependent aging profiles, necessitating tailored Battery Management System (BMS) configurations and diagnostic models for each use case. For instance, LFP systems exhibit stable voltage curves, which challenge SoC estimation but benefit cycle life, whereas NMC chemistries offer higher energy density but greater sensitivity to thermal and cycling stress [17]. The evolution of battery technologies continues to progress with the emergence of solid-state batteries, lithium-sulfur, and sodium-ion alternatives. However, the extensive deployment history, mature supply chain, and improving safety of Li-ion systems ensure their dominance in the near-to mid-term across all sectors of smart energy systems.

1.2.1.1 Basic Structure and Operation

The Li-ion batteries have shown an increment in GED from ∼80 Wh/kg to ∼260 Wh/kg in recent years [18], with a benchmarking of a typical energy density value of Li-ion batteries to be 265 to 280 Wh/kg [5]. But still, its acceptance is widely uncomfortable in the BESS power system network due to its inability to meet a threshold GED of ∼350 Wh/kg, which is provided by gasoline and other adjacent compounds [19]. Fig. 1.1 describes the year-wise trend of GED growth of Li-ion batteries. Besides single transition metal oxides, mixed transition metal oxides are now being globally recognized due to their many positive sides. Emerging compounds such as NMC (Nickel Manganese Cobalt Oxide) are likely to be used as a cathode in Li-ion batteries along with new anode materials (such as Silicon) for meeting the target of achieving high GED along with specific capacity in 2030 [21, 22], because of its high rate and charge capacity along with good structural stability.

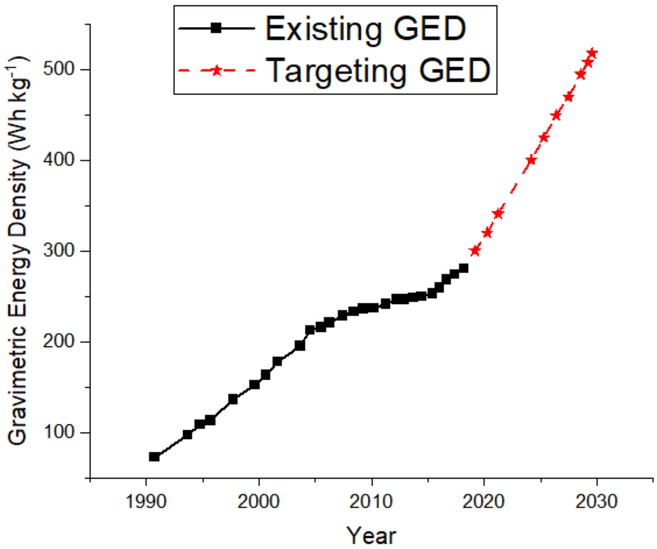

Fig. 1.1. GED growth over years. Data taken from [20].

Fig. 1.2 shows the comparison diagram for 5 types of Li-ion cells, which are NMC, LFP (Lithium Iron Phosphate), LMO (Lithium Manganese Oxide), LCO (Lithium Cobalt Oxide), and NCA (Lithium Nickel Cobalt Aluminum Oxide), providing a better understanding of the difference between different material Li-ion cells. So, it is also quite evident from the figure that NMC has maximum specific energy, and it is very much optimized compared to other cells, in terms of all the presented parameters in the diagram. A detailed comparison between different Li-ion cells can also be investigated from [23, 24]. Recently, Quan Li et al manufactured pouch Li-ion cells having a GED of ~700 Wh/kg under specialized conditions and a Volumetric Energy Density (VED) of ~1650 Wh/L by incorporating a high-capacity rich manganese-based cathode along with a lithium anode having high specific energy [25]. These developments can contribute hugely to BESS for the power system network.

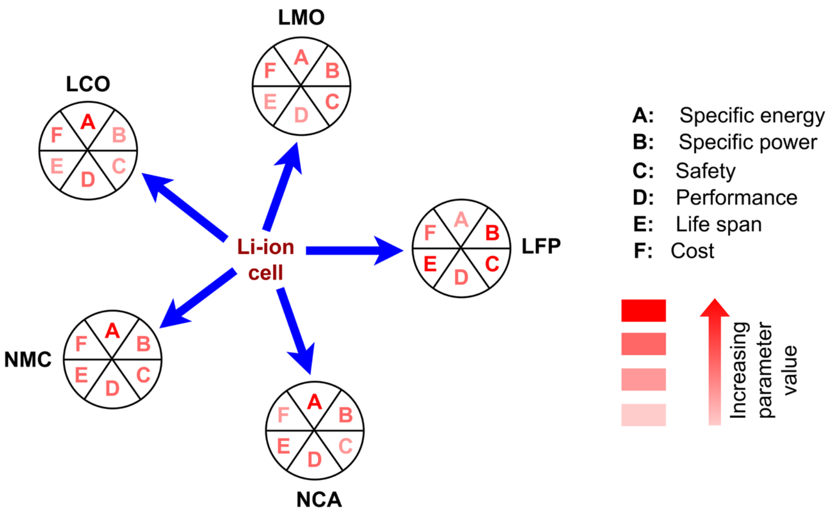

Fig. 1.2 Li-ion cell comparison diagram. Redrawn from [26]. Copyright © 2019, MDPI.

1.2.1.2 Common Chemistries

A Li-ion battery is made up of "n" number of Li-ion cells. Each Li-ion cell has three most important components, namely anode, cathode, and electrolyte. Li-ion chemistry consists of intercalating any foreign molecules/ions into host molecules. The intercalation chemistry changes the conductivity as well as the structural design of the host molecule. Whittingham et al were the first to develop a rechargeable Li-ion cell based on intercalation chemistry in which a Titanium Sulphide (TiS_2) was used as cathode material, a lithium metal anode, and a liquid electrolyte consisting of lithium salts dissolved in organic solvents were incorporated [27]. But as time passes, new anode, cathode, and electrolyte materials with better features have played vital roles in cell chemistry. The main components of Li-ion cells are discussed here as follows.

1.2.1.2.1 Anode

The anode plays a very crucial role in the electrochemical operation of Li-ion cells. Both the anode and cathode enable the current flow in the outer circuit. The anode acts as an electron donor and Li-ion acceptor during charging, and an ejector during discharging. Selecting proper anode material having high specific capacity and other required characteristics is of utmost importance for operation of Li-ion batteries in different applications. Table 1 briefs about different trending anode materials along with their properties, merits/demerits, and applications. Mostly graphite (C_6) is used as the anode material in Li-ion cells because of its flat structure (suitable for Li ions intercalation), low cost, and operating potential along with excellent life cycle [29, 38]. The capacity of graphite is moderate 372 (mAh/gm) [39]. The diffusion rate of graphite is also better than the lithium-carbon combination, which makes it suitable for production of efficient Li-ion batteries for various applications. Lithium metal is also researched for incorporation as anode material in Li-ion batteries because it has a high specific capacity (3860 mAh/gm) and lowest density, but low coulombic efficiency and enhancement in uncontrollable Li-dendrite growths restrict its worldwide acceptance [40]. As listed, graphene is gaining worldwide popularity as an anode material because of some of its excellent features such as high electrical conductivity, good mechanical strength (providing suitable mechanical stability of the structure), high mobility of Li-ions, and large surface area [29]. However, the Li-ion absorption ratio is quite similar to graphite. Studies [41, 42] have found that cascading graphene sheets can resolve this aforementioned problem up to a certain extent (increasing the weight of the structure up to a certain level). So, there is a trade-off between the number of cascading graphene sheets and the required Li-ions absorption ratio. Besides these carbon-based compounds, other anode materials like alloy-based materials, conversion-type transition metals, and silicon-based compounds are also gaining researchers' interest gradually because of their special intrinsic characteristics and morphology. Further research is still going on for selecting appropriate anode materials having high power densities, and high capacity along with suitably high diffusion rates for fast diffusion of Li-ions into the anode material and other required characteristics for reliable use of Li-ion batteries in the modern era.

1.2.1.2.2 Cathode

Besides the anode, the cathode also plays a key role in cell chemistry. To meet the high-power density, energy density, and specific capacity targets in 2030, the selection of electrode materials is of utmost importance. The cathode is the positive terminal, which is used for injecting electrons (during charging) and accepting electrons (discharging). Cathode materials have several nano and micro-structures, among which are particularly spherical secondary aggregates (SSAs) and single-crystal cathodes (SCCs). SSCs are quite similar to SSAs but are quite different in terms of physical as well as chemical properties. SSCs/SSAs are crystal-like sub-micrometer or micrometer structures for cathode materials with exposure to facets and other dispersion characteristics [43, 44]. Merits and demerits of SSCs/SSAs structures along with their chemical and physical structural details have been detailed in [43]. The selection of appropriate single as well as mixed transition metal oxide materials as cathode plays a crucial role in Li-ion battery chemistry. Table 1.2 summarizes some of the cathode materials along with their chemical, and physical details and applications. From Table 1.2, LMO is bearing a quite high GED, so it should be researched critically for its faithful applications. But [58] have reported a significant negative side of LMO called the Jahn–Teller (J–T) effect, which restricts some of its use. J-T effect states that any nonlinear molecular system having a spatially degenerate electronic zero state undergoes a geometrical distortion to lower the overall energy and remove this degeneracy, thus forming a low-energy compound [59]. Substitution/doping method has been adopted in LMO materials to inhibit the J-T effect by increasing structural stability (by altering the atomic structure). NCA also has quite similar features to NMC but lacks in cost. In NMC, nickel (Ni) provides good specific energy but lacks structural as well as thermal stability; however, the incorporation of Manganese (Mn) and Cobalt (Co) improves the stability problem (structural, thermal, and magnetic) [60].

As the GED and cell-specific capacity of cathodes are the main parameters behind the popularity of a Li-ion battery, various researchers have modified the existing cathode materials with doping, coating, surface quality modification, etc. Other than these enlisted cathode materials other cathode materials with quite high GED and high intercalation voltage, such as phosphate poly-anions $LiCoPO_4$ (800 Wh/kg) [58], $LiMnPO_4$ (700 Wh/kg) [61], Li_2CoSiO_4 (1200Wh/kg) [5, 62], FeS_2/C (1273 Wh/kg) [5, 63] are also in the focus of current research work.

Table 1.1 Comparison of different Li-ion battery anode materials

Sl. No.	Anode Materials	Capacity (mAh/gm)	Merits	Demerits
1	Graphene	744[28], 770-1115 [29]	Good flexibility, electrical and thermal conductivity, high Li-intercalation rate, and high capacity.	Low coulombic efficiency and high cost.
2	Carbon Nanotubes (CNTs)	1116, 1100 [29], ~550 (MWCNTs) [30]	Cost-effective, better tensile strength, good thermal conductivity, and high reversible capacity.	Low electronic conductivity and low capacity at high discharge rates.
3	Silicon	2800-5149 [29, 31-33]	High specific capacities, energy densities, and better safety features.	Limited life cycle and irreversible capacities.
4	Germanium	1623 [29]	High specific capacity, good performance, and high cycling reliability.	Frequent volume fluctuation during lithium intercalation.
5	Transition Metal Oxides (e.g., TiO_2, SiO_2)	320-1200 [34-35]	Good specific capacity, cost-effective, and eco-friendly.	Poor coulombic efficiency, high voltage hysteresis, and

				low life cycle.
6	Alloys with Lithium	993, 2234, 536, 994 [19]	High specific capacities and high Li-ion intercalation sites.	Structural instability due to high volume changes.
7	Lithium-Germanium Alloys	1624, 1384 [36]	High specific capacities and particle pulverization rate.	Volume expansion leads to anode instability.
8	Lithium-Silicon Alloys	4212, 3579 [19]	Good performance and cycling reliability.	370% volume expansion.
9	Lithiated Siligraphenes	1286, 2090 [37,38]	High storage capacity, stability, low volume expansion, and electrical conductivity.	Limited Li/graphene interaction.

Table 1.2 Comparison of different Li-ion battery cathode materials

Sl. No.	Cathode Materials	GED (Wh/kg)	Capacity (mAh/gm)	Applications
1	LCO	250, 274 [45]	180, 140 [19, 29]	Cell phones, tablets, etc.
2	LMO	184.64 [19, 46]	108 [44], 148 [48]	Heavy Vehicles and medical devices.
3	LFP	90-140 [41, 49]	212 [49], 170 [50]	EVs, Grid Energy Storage System (GESS), etc.

4	NMC-111	190 [51]	170 [52], 160 [51, 53]	Low-power devices (tablet, laptop), EVs, etc.
5	NCA	250-300 [54], 869 [55]	279 [56], 277 [57]	Medical applications, Power grids, etc

1.2.1.2.3 Electrolyte

Electrolytes are substances that bridge the gap between the anode and cathode. Appropriate selection of electrolytes is the key factor for the safe operation of Li-ion batteries. The ionic conductivity, volatility, solubility, Li-ions mobility, Solid Electrolyte Interphase (SEI) formation capability with anode current collector, thermal safety, and non-inflammable characteristics are critical parameters that determine a suitable electrolyte for any appropriate application [64, 65]. As EV industries are now dominating the world and Li-ion batteries are fuelling these development processes, the thermal characteristics of any Li-ion batteries are of critical interest. Studies [64, 66] detail the thermal characteristics of various electrolytes with their existing problems, along with their respective remedies. Electrolytes such as ionic liquids, polymeric ionic liquids, and polymer electrolytes are now replacing conventional electrolytes ($LiPF_6$) as they are more optimized than $LiPF_6$ in terms of the aforementioned parameters.

1.2.1.3 Equivalent Circuit Models and Monitoring Techniques

Appropriate modelling of the Li-ion battery is essential for studying battery dynamics during the charging and overcharging process.

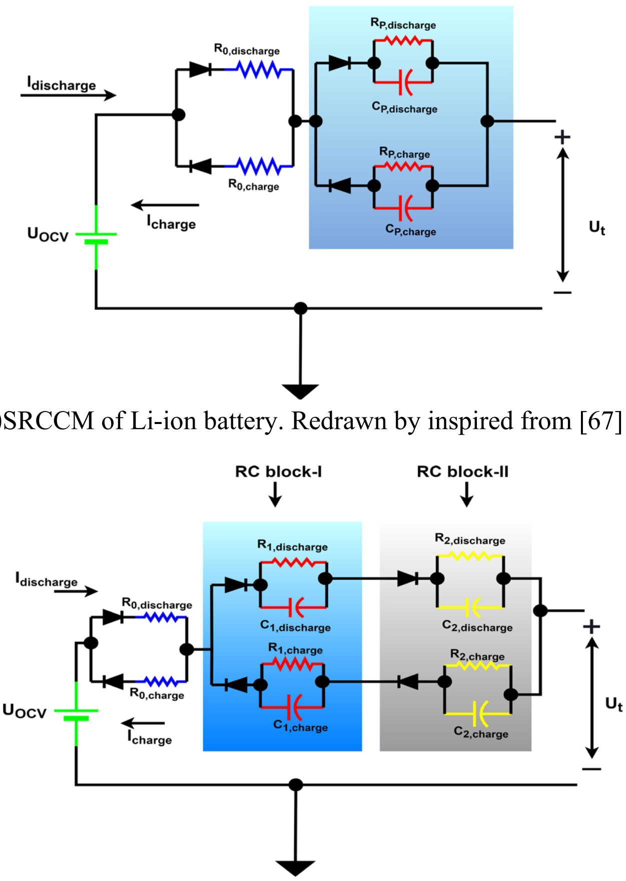

(b)TRCCM of Li-ion battery. Redrawn by inspired from [68]

Fig. 1.3. Typical Equivalent Circuit Models of a Li-ion Battery

Three types of models that are applicable for determining battery dynamics are the electrochemical model, the empirical model, and the Equivalent circuit model. Different battery models bearing different properties are adopted for various purposes. Table 1.3 shows the merits and demerits of different battery models along with their applications [75]. This study concentrates on discussions related to ECM. The Single RC Circuit Model (SRCCM) was the first model to be used in analyzing battery dynamics. Now it is also utilized for its much-optimized accuracy and simplicity. Fig. 1.3a shows a typical SRCCM of a Li-ion battery. In the diagram, "U_{OCV}" is the open circuit voltage of the cell, "I" is the branch current, "U_t" is the battery terminal voltage, "R_0" is the internal resistance of the cell which signifies the opposition nature of the electrolyte present (Ohmic polarization), "R_P" and "C_P" are the resultant polarization resistance and capacitance which denotes the transient behavior of the model due to various reactions that happens at the electrode-electrolyte interface and bulk electrolyte solution. Here, the diode connections are given for automatic selection of battery parameters according to the charging or discharging process. In this context, the term polarization refers to the potential drop due to various internal activities of the cell [76]. Though it is used for its aforementioned advantages, but two main disadvantages which restricts its utilization in some applications are 1) Not able to reflect detail insights about some specific reaction, polarization process and non-linear dynamics in Li-ion battery 2) As R_0, R_P, C_p and U_{OCV} depends on some intrinsic or/and extrinsic battery parameters (such as SoC, temperature, branch current, etc.), so, ignoring that may lead to inaccurate battery analysis [77]. Several literatures [78] have proposed Two RC Circuit Model (TRCCM) or so-called Dual polarization (DP) model. This battery model solves the first disadvantage of the basic SRCCM up to a great extent, by reproducing different polarization (electro-chemical and concentration polarization) process (and non-linearities) with the in- corporation of double RC blocks, thus reflecting the transient behavior accurately. Other proposed models with incorporation of different modifications are also floating in the research domain. Table. 1.4 gives information about the different proposed models along with their area of modifications and cause. Fig. 1.3b shows a TRCCM of a Li-ion battery (having two RC blocks). In the diagram, "U_{OCV}" is the open circuit voltage of the cell, "I" is the current branch, "U_t is the battery terminal voltage", "R_0" is the internal resistance of the cell which basically signifies Ohmic polarization, "R_1" and "C_1" are the electro-chemical polarization resistance and capacitance, "R_2" and "C_2" are the concentration polarization resistance and capacitance. Here also diodes arrangement shows automatic selection of battery parameters according to charging or discharging of the battery. But for simplicity the bi-direction battery parameters are kept as quite similar for the ease of online implementation. As the number of RC blocks increases in the ECM of the Li-ion cell, the accuracy also increases along the same manner, because it incorporates other side minor polarization effects, but the complexity of the circuit increases making its computational burden higher, forcing the analysis to be done through iterative numerical methods or any robust ML algorithms. So, in regards of this n-RCCM of Li-ion battery, there always has been a question of optimization between the accuracy and the complexity in selecting the number of RC blocks. It is quite evident from the Pulse Discharge (PD) characteristics of both SRCCM and TRCCMs in [90], that the TRCCM resembles much better with the experimental plot having a maximum relative error of ~0.71% than the SRCCM, which has a maximum error of ~1.04%.

Table 1.3: Comparison of Different Battery Equivalent Models

Sl. No.	Models	Merits	Demerits	Applications
1	(E-ChM)	Good, High degree of non-linearity	High execution time and a huge number of execution parameters	Cell dynamics study and cell design [69, 70]
2	EM	High degree of linearity, easy online implementation	Low accuracy and fewer details about battery dynamics	BESS, Grid-connected network [71, 72]
3	ECM	Optimized accuracy and complexity, easy online implementation	Not too high accuracy, not accurate SOC estimation, and not too much adjacent to physical interpretation	Estimation of OCV, SOC, and other battery parameters in frequency and time domain [73, 74]

Table 1.4: Comparison of Different ECMs for Li-ion Battery

Sl. No.	Existing Models	Modified element(s)/ Circuit(s)	Cause for modification	Reference
1	Diffusion Resistance Model	Adding extra resistance in series with	Replicating the diffusion process in low frequency	[79]

		the internal resistance.		
2	Gaussian Noise Model	In series with an ohmic resistance	For reproducing miscellaneous battery dynamics in the whole frequency range	[80]
3	Fractional Order Model	Adding a temperature and SOC-dependent phase element (CPE) in parallel with the polarization resistance	For reflecting the phenomena of change in polarization reactions and frequency dispersion due to the SEI layer	[81, 82]
4	Self-discharge run-time-based model	Adding an extra parallel R-C section with a variable current source	For indicating the self-leakage activity when the battery is idle	[83]
5	Hysteresis Equivalent Model	Extra series R-C section with variable voltage source	To mitigate the hysteresis gap in OCV during charge-discharge	[84, 85]
6	—	Extra series capacitor with ohmic resistance	For LFP battery modeling to increase accuracy and physical representation of internal resistance	[86]
7	—	Extra series and shunt resistors and	For representing chemical/physical aspects: double	[87]

		capacitors	layer formation, cell interconnections, self-discharge, etc.	
8	n-RC integral circuit model	'n' number of R-C blocks in series	To showcase multiple side reactions and polarization phenomena accurately	[88, 89]

1.2.1.4 Applications Across Grid and Embedded Domains

As the global energy landscape shifts towards decarbonization, decentralization, and digitalization, the efficient utilization of renewable energy sources is becoming imperative. This transition demands enhanced stability, flexibility, and controllability in power systems, which has driven widespread adoption of Battery Energy Storage Systems (BESS). Li-ion batteries, with their superior electrochemical properties, fast dynamic response, and modular scalability, have emerged as a central technology for both grid-scale and embedded system applications.

Due to their capability for rapid charge-discharge, high energy density, and deep cycling performance, Li-ion batteries are extensively deployed in BESS for critical grid applications such as short-term peak shaving, voltage and frequency regulation, load leveling, energy arbitrage, and ancillary services [91]. According to the U.S. Department of Energy (DOE), frequency regulation remains one of the most dominant applications of Li-ion-based BESS, particularly in deregulated energy markets [92].

In the context of market dynamics, the study in [93] shows how a reduction in Li-ion battery pack costs has catalyzed broader deployment of BESS across utilities and industrial sectors. In particular, New York has reported a significant cost reduction to approximately $32/kWh for battery cells (and around $133/kWh for battery packs) in 2023 [94]. Bloomberg New Energy Finance (BNEF) forecasts this cost to decrease further, reaching nearly $80/kWh by 2030. These declining costs are accelerating the penetration of Li-ion BESS into both centralized and decentralized grid architectures. Li-ion batteries also play a vital role in smart distribution networks, acting as compensators and buffers in embedded applications such as smart homes, commercial buildings, and microgrids. Their integration into behind-the-meter (BTM) setups enables functionalities such as self-consumption optimization, peak demand mitigation, and time-of-use (TOU) arbitrage for consumers. The flexible operation of Li-ion batteries under embedded control systems also supports load forecasting, voltage stabilization, and enhances resilience during outages [95]. Recent works [96] highlight the escalating demand for BESS in national grids, reflected in year-wise capacity installations. As reported, the United States alone recorded 8,900 MW of installed power capacity and 11,100 MWh of energy capacity in Li-ion-based BESS by the end of 2022. These figures indicate a rapid transition toward battery-integrated grids capable of managing renewable intermittency and load volatility.

1.2.1.4.1 BESS Applications for Grid

BESS is in the umbrella of high demand due to its services, which include voltage and power support, frequency regulation, black-start, energy arbitrage, behind-the-meter, etc. [97].
Insights about some important BESS services are given below.

- Voltage imbalance in the power grid can occur due to unbalanced loads and improper reactive power management. Incorporation of BESS helps to address this issue by consuming (charging) or providing (discharging) active power, which balances load and indirectly aids in maintaining voltage stability. This active power compensation becomes more crucial when the line impedance ratio value is 1 or close to 1. Again, as in recent times roof-top photovoltaic cells associated in a microgrid structure are being utilized in several smart homes, so power distribution and generation process of the same should be studied properly. Literature such as [98, 99] provide enough information about the generation-distribution power of photovoltaic cells. Among which, the voltage irregularity problem is quite significant due to fluctuations/ intermittency in solar intensity. So, to mitigate this problem BESS has been introduced with each local roof-top photovoltaic cell. Various publications [101, 102] have focused on designing various efficient BESS algorithms for local voltage regulations in roof-top photo-voltaic cells by performing programmed charging or discharging during voltage rise or voltage down issues, respectively.

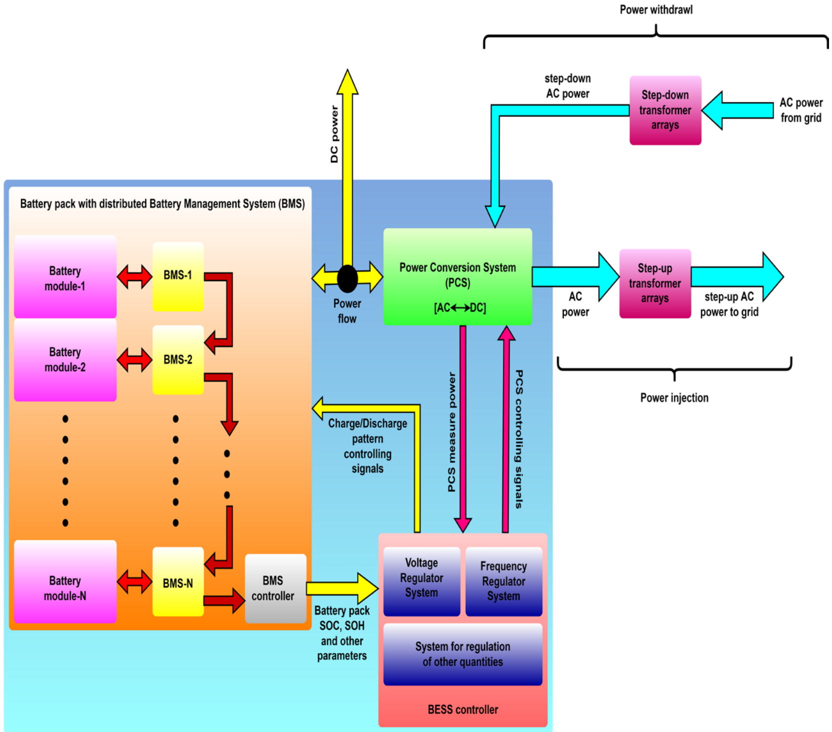

Fig. 1.4 Simplified BESS structure. Redrawn by inspired from [100].

• Frequency imbalance is a significant issue in power grid systems, often stemming from the disparity between power generation and load demands. In such cases, the distribution of active power, crucial for frequency control, may vary at the load end. So, the frequency controlling is a major activity that should be done in the power grid system. BESS are utilized in the grid to mitigate this frequency imbalance issue. Fig. 1.4 shows a basic block diagram representation (BDR) of the BESS in the power grid. According to the diagram, Power Conversion System (PCS) plays the major role in frequency regulation. During the time of low frequency power distribution in the load end, the BESS discharges more power into the PCS thus injecting more frequency dependent power to the load, called as up-regulation and similarly during high frequency power distribution in the load end, the BESS charges by taking active power from the PCS thus withdrawing frequency dependent power from the load (down-regulation) [103,104]. The key parameters for frequency control are response time, provision time, and power output [103]. Among these parameters, response time plays a vital role in determining the frequency response capability of BESS. Typically, BESS responses in withdrawing/delivering the frequency-dependent power at the output as soon as there is a frequency imbalance power supply at the output. So, normally, it has very little response time and good response speed. As the permission of frequency control service of BESS is given by higher authorities of different operators, so, different operators like European Network of Transmission System Operators for Electricity (ENTSO-E) in Europe, Federal Energy Regulatory Commission (FERC) in the US, etc. have adopted various nomenclatures for efficient frequency regulation service in the power grid. [105] summarizes nomenclature and other details of the frequency control service adopted by different operators in Europe.

• Energy arbitrage is one of the applications of BESS, which includes the storage of energy (charging of battery pack) by BESS when the price is low (low demand) and then dispatching the stored energy in the grid (discharging of battery pack) when the price is high (high demand) [106, 107]. Energy arbitrage is very much required in this era of renewable energy, due to the irregularities of power sources (solar, wind, hydro, etc.) in different parts of the day. Thus, an efficient algorithm should be programmed inside the BESS controller so that it can send charge/discharge signals to the battery packs by inspecting the energy prices in the market. But the problem may arise in predicting the future energy prices as it is highly stochastic in nature [108].

•Blackout situations are seen frequently in power grid systems, which occur due to any natural hazards, malfunctioning in the transmission cables, load-shedding in power lines, or any faults, etc. [109]. So, after these blackout conditions, the power system should be started by consuming some energy. BESS also provides black start by injecting electric power to the distributed system (or other electrical system) without letting the system rely on an external power supply [110]. For implementing this black-start service of the BESS, efficient restoration principal algorithms should be dumped inside the BESS controller such that the sub-system/system responds quickly by maintaining system reliability and not allowing any adverse environment impact. Publications such as [111] give various BESS black start based blackout restoration principles for faithful utilization of the service.

1.2.1.4.2 Application Across the Embedded Domain

In addition to grid-level deployment, Li-ion battery systems are increasingly integrated into embedded energy systems, especially in smart homes, microgrids, commercial buildings, and electric vehicles (EVs). These embedded domains are characterized by decentralized, often self-sufficient, energy generation and storage units that rely heavily on battery-based systems for enhanced autonomy, reliability, and optimization of energy flows. A common scenario in embedded systems is the use of rooftop photovoltaic (PV) systems in smart residential buildings. These systems, when coupled with Li-ion BESS, enable consumers to generate, store, and manage their own energy, effectively reducing dependency on the utility grid and lowering energy bills. However, intermittency in solar irradiance leads to voltage fluctuations and localized instability. To counteract this, researchers have proposed localized BESS controllers that dynamically manage the charge/discharge behavior of the battery to mitigate voltage rise during excess generation and voltage drop during sudden load conditions [112], [113], [114], [115].

Further, BESS in embedded systems enables load shifting and peak demand management by storing energy during low-demand periods and releasing it when demand surges. This practice not only improves operational efficiency but also offers economic benefits by avoiding high energy tariffs during peak hours. Moreover, these systems support time-of-use optimization and net metering, which are integral components of smart home energy strategies [116]. In mission-critical infrastructures such as hospitals or data centers, BESS provides seamless uninterruptible power supply (UPS) services. These embedded BESS setups are often configured with real-time diagnostic and control systems, allowing predictive fault management and battery health estimation through internal resistance monitoring and state-of-charge (SOC) tracking [117], [118].

Another domain of embedded applications is electric mobility. EVs utilize Li-ion BESS not only for propulsion but also for regenerative braking and bidirectional vehicle-to-home (V2H) or vehicle-to-grid (V2G) energy exchange. These embedded BESS configurations contribute to grid stability and demand-side energy balancing in distributed energy networks [119], [120]. Thus, the application of Li-ion BESS in embedded domains is not limited to energy storage but extends to system-level integration, intelligent control, and cyber-physical interfacing, forming a backbone for modern distributed smart energy systems.

1.2.2 Smart Energy Management Systems

The integration of Battery Energy Storage Systems (BESS), renewable generation, and intelligent load control mechanisms has led to the emergence of Smart Energy Management Systems (SEMS). These systems use real-time data acquisition, analytics, and control algorithms to dynamically balance energy supply and demand, enhance energy efficiency, and maintain system reliability at both grid and localized levels. SEMS can operate across diverse domains, including grid-tied environments, microgrids, and embedded systems, where they coordinate distributed energy resources (DERs) such as photovoltaics, wind turbines, and Li-ion batteries. With the rise in electrification, particularly in transportation and buildings, SEMS serve as the technological interface between consumer energy requirements and grid-side flexibility provisions. A typical SEMS architecture consists of smart meters, renewable generators, energy storage units, power electronic converters, and embedded controllers running supervisory control algorithms. The implementation of SEMS has enabled real-time demand response, peak shaving, load forecasting, dynamic pricing, and fault-tolerant energy scheduling, all of which are vital in achieving the goals of decentralized, decarbonized, and digitalized energy infrastructures.

In the following subsections, the role of Li-ion batteries as enabling storage units within SEMS is explained, followed by an examination of their influence in the transition to distributed smart architectures.

1.2.2.1 Role of Li-Ion Batteries in Modern Smart Energy Systems

The role of lithium-ion (Li-ion) batteries in modern smart energy systems has become increasingly critical due to their superior energy density, high efficiency, rapid response capability, and long cycle life. These attributes position Li-ion batteries as the backbone of decentralized and intelligent power infrastructures, where reliability, flexibility, and responsiveness are fundamental operational requirements.

In smart energy systems, Li-ion batteries are integrated as dynamic storage components capable of balancing intermittent generation from renewables, regulating voltage and frequency, and ensuring continuity of power during supply-demand mismatches. Their fast-discharge characteristics enable real-time load balancing, particularly in systems with fluctuating renewable energy inputs such as rooftop PV or wind installations [121]. In residential and commercial smart buildings, Li-ion batteries function as behind-the-meter storage to support demand-side management, peak shaving, self-consumption enhancement, and backup power provisioning during outages [122]. Furthermore, Li-ion batteries support grid-scale smart applications by participating in ancillary services, such as frequency response, spinning reserve, and voltage regulation. Their participation in energy arbitrage and real-time market operations improves economic efficiency, especially in deregulated and time-of-use tariff structures.

Smart energy systems are also characterized by interconnectivity and data-driven decision-making, and Li-ion batteries play a central role in such cyber-physical ecosystems. Embedded battery management systems (BMS) utilize data from sensors and communication protocols to optimize battery usage, estimate state-of-charge (SOC), state-of-health (SOH), and implement predictive fault diagnostics. Integration of Li-ion batteries with smart inverters and digital controllers enhances their compatibility with IoT-enabled energy networks, allowing coordinated energy dispatch across distributed resources [123], [124]. The advancement of energy storage algorithms further improves the operational reliability of smart energy systems. Model Predictive Control (MPC), fuzzy logic, and AI-based optimization techniques have been developed to schedule charge-discharge cycles of Li-ion batteries in response to forecasted energy profiles and real-time pricing signals [125]. These control strategies not only extend battery life but also contribute to sustainability goals by enhancing renewable utilization and reducing fossil fuel dependence. The convergence of Li-ion battery technology with communication systems, embedded control, and artificial intelligence continues to transform smart energy infrastructures into resilient, responsive, and self-optimizing entities.

1.2.2.2 Energy Transition to Distributed Smart Architectures

The contemporary energy sector is undergoing a paradigm shift from centralized, fossil-fuel-based generation to distributed, renewable-driven smart architectures. This transition is primarily fueled by global decarbonization objectives, increased penetration of distributed energy resources (DERs), and the proliferation of digital communication and control technologies within the power grid. The conventional top-down approach of energy distribution is increasingly being replaced by bottom-up architectures, where local generation, storage, and consumption are managed intelligently to meet both user-level and system-wide objectives. Distributed smart architectures integrate key technological components such as rooftop solar photovoltaics, wind turbines, Li-ion battery energy storage systems, smart inverters, advanced metering infrastructure (AMI), and embedded control platforms. These systems form energy clusters or microgrids, which can operate in grid-connected or island modes, offering resilience during disturbances and operational flexibility under normal conditions [126], [127].

A critical feature of these architectures is the implementation of bidirectional power flow and peer-to-peer energy exchange, which fundamentally redefines the role of end-users as active participants, "prosumers", instead of passive consumers. Li-ion batteries in such systems serve not only for energy storage but also as real-time balancing agents, enabling the compensation of generation-demand mismatches, facilitating demand response, and enhancing system stability [128]. The energy management system (EMS) in distributed smart setups serves as the supervisory layer, gathering data from distributed assets, performing analytics, and dispatching control signals to optimize energy utilization. EMS modules are increasingly embedded with AI-based algorithms, capable of forecasting load and generation, detecting faults, and managing cyber-physical threats. The tight integration of energy assets with the Internet-of-Things (IoT) devices and machine-to-machine (M2M) protocols ensures real-time monitoring and adaptive control across multiple layers of the system hierarchy [129], [130].

Furthermore, regulatory frameworks and policy reforms in several countries are actively encouraging distributed smart grid implementations. Initiatives such as the IEEE 2030 standards, the EU's Clean Energy Package, and India's National Smart Grid Mission (NSGM) are promoting investments in decentralized infrastructures. These policies are complemented by dynamic tariff structures, net metering provisions, and open-access mechanisms, which economically incentivize consumers to deploy BESS and participate in ancillary services markets. The transition to distributed smart architecture represents a foundational step toward a resilient, low-carbon, and consumer-centric energy ecosystem. Li-ion battery-based energy storage systems, when embedded within such architectures, are instrumental in ensuring operational continuity, economic viability, and environmental sustainability.

1.3.Challenges in Existing Systems

Despite significant advancements in battery-integrated energy systems, numerous technical, environmental, and systemic limitations continue to hinder widespread, reliable adoption across grid and embedded domains. These challenges are particularly critical in the context of Li-ion batteries, which, while enabling enhanced flexibility, bring forth issues concerning thermal stability, communication interoperability, and sustainability.

This section discusses the fundamental challenges that persist in existing systems, grouped under three primary domains: thermal risks and safety concerns, integration and communication hurdles associated with distributed generation (DG), and environmental and economic considerations. These limitations must be addressed to realize the full potential of smart, scalable, and safe energy systems.

1.3.1 Thermal Safety and Operational Risks in Li-Ion Batteries

Li-ion batteries, despite their widespread use across energy storage and mobility applications, present significant thermal safety concerns due to their complex electrochemical behavior and sensitivity to environmental and operational conditions. As these batteries operate within a narrow thermal stability window, thermal runaway, capacity degradation, and mechanical or electrical abuse can lead to irreversible damage, fire hazards, or even catastrophic system failures [131], [132].

Thermal runaway in Li-ion batteries refers to a self-accelerating exothermic reaction that occurs when the internal temperature exceeds a critical threshold (typically around 150°C–200°C). This condition is often triggered by internal short circuits, overcharging, external heating, or mechanical puncture. The exothermic reactions involve the decomposition of the solid electrolyte interphase (SEI), electrolyte oxidation, and cathode material breakdown, releasing flammable gases such as CO, CO_2, and hydrocarbons [133].

Moreover, non-uniform temperature distribution within battery packs exacerbates the imbalance of cell performance. Variations in temperature lead to uneven current distribution, unequal state-of-charge (SOC) among cells, and accelerated degradation of certain cells over others, leading to cycle life reduction and efficiency loss [134].

Table 1.5. Major Thermal and Operational Risk Factors in Li-Ion Batteries

Risk Factor	**Cause**	**Effect**	**Mitigation Techniques**
Overcharging	Poor BMS, charger failure	Thermal runaway, cell swelling	Overvoltage protection, redundant BMS checks
High ambient temperature	Inefficient cooling, external heat	Accelerated aging, electrolyte breakdown	Active/passive thermal management systems
Internal short circuit	Manufacturing defect, dendrite formation	Sudden heat surge, fire risk	Advanced separator designs, internal resistance-based monitoring
Mechanical deformation	Impact, vibration, or puncture	Short circuit, electrolyte leakage	Shock-absorbing casing, structural reinforcement
Over-discharge	Excessive depth-of-discharge	Copper dissolution, SEI damage	Voltage threshold regulation
Thermal propagation in pack	Heat transfer from one cell to another	Cascading failure of adjacent cells	Fireproof separators, cell spacing, thermal barriers
Repeated fast charging	Excessive C-rates	Lithium plating, gas formation	Controlled charge profiles, adaptive charging algorithms

In energy storage systems, particularly in stationary applications like grid-connected BESS or embedded microgrids, safety-critical environments demand real-time monitoring of thermal parameters. Several studies have emphasized the importance of internal resistance estimation and temperature-sensitive modeling of cells for accurate fault diagnostics and predictive safety control [135], [136]. Integration of infrared thermal imaging, distributed temperature sensors, and advanced battery thermal models in embedded controllers further enhances early fault detection capabilities. Moreover, the selection of cell chemistry also plays a vital role in thermal behavior. For instance, $LiFePO_4$ (LFP) batteries exhibit higher thermal stability compared to $LiCoO_2$ (LCO) or NMC chemistries, making them more suitable for safety-critical applications, though often at the cost of energy density [137].

In high-power embedded applications such as electric vehicles (EVs), aerospace, or robotics, the thermal dynamics of Li-ion batteries are even more critical due to the compact design and high current throughput. Real-time embedded systems must implement battery thermal models, model predictive control (MPC), and state estimation algorithms to dynamically regulate cell temperatures and prevent thermal runaway. The multi-dimensional nature of thermal risks in Li-ion systems necessitates a holistic approach encompassing material design, packaging architecture, thermal management, and system-level monitoring algorithms, to ensure safe, long-life operation under varying load and ambient conditions.

1.3.2 Integration of DG and Communication Challenges

The increasing integration of Distributed Generation (DG) into energy networks, particularly from renewable sources such as solar PV, wind, and bioenergy, presents several challenges related to synchronization, stability, control, and real-time communication within smart energy architectures. While DG offers significant benefits in terms of decarbonization and localization of energy resources, its operational unpredictability and intermittency necessitate the deployment of advanced control frameworks and robust communication infrastructures [138], [139]. DG systems operate at various voltage levels, often with asynchronous output characteristics, and must be interfaced with the central grid through power electronic converters, inverters, and phase-locked loops (PLLs). The harmonization of frequency and voltage, particularly in weak grids, becomes a technical bottleneck. These systems are vulnerable to phase instability, unintentional islanding, and voltage fluctuations, especially during sudden changes in load or irradiance or wind conditions [140].

Furthermore, the coordination of DG units in a decentralized energy environment requires real-time monitoring, dispatch control, and data exchange, all of which depend heavily on communication protocols such as IEC 61850, DNP3, and Modbus. The heterogeneity of communication standards and the absence of unified interoperability guidelines can cause latency, data loss, and control mismatch, ultimately reducing system efficiency and safety [141].

The communication infrastructure faces several technical constraints, including:

i. Bandwidth limitations in rural or remote installations.
ii. Latency and jitter affect the timing of control signals.
iii. Cybersecurity threats, which can compromise system integrity via unauthorized access or malicious data injections [142].

These issues are further compounded when DG systems are interfaced with Battery Energy Storage Systems (BESS) and Advanced Metering Infrastructure (AMI) in a multi-layered energy ecosystem. Synchronizing the operation of such systems requires not only robust communication pathways but also time-synchronized data logging, fault detection and isolation, and network redundancy strategies. Addressing the integration and communication challenges of DG requires a multidisciplinary approach, combining advances in control theory, embedded system design, communication engineering, and cybersecurity practices. The deployment of edge computing, machine learning for adaptive control, and blockchain for secure energy transactions are promising future trends aimed at resolving these limitations.

1.3.3 Environmental and Economic Considerations

The integration of Li-ion battery-based energy systems in modern power architecture must contend not only with technical constraints but also with profound environmental and economic implications. As energy storage systems scale globally, particularly in smart grids, electric mobility, and decentralized generation concerns related to resource availability, lifecycle emissions, waste management, and economic feasibility are becoming increasingly central to system planning and policy discourse.

From an environmental standpoint, the extraction and processing of critical raw materials such as lithium, cobalt, nickel, and graphite have a large negative impact on the environment. Mining operations, particularly in regions with weak environmental regulations, are associated with soil degradation, water contamination, and the release of toxic byproducts. For instance, cobalt mining in the Democratic Republic of Congo has raised concerns over environmental harm and human rights violations, prompting a push for alternative materials or improved recycling methods [143], [144].

In terms of emissions, while Li-ion batteries are often considered zero-emission during operation, their production and end-of-life stages contribute to greenhouse gas emissions, resource depletion, and chemical leakage risks. Lifecycle assessment (LCA) studies indicate that battery manufacturing accounts for approximately 50–70 kg of CO_2 equivalent per kWh of capacity, depending on the supply chain and energy source used for processing [145]. Moreover, the disposal and recycling of Li-ion batteries present significant challenges due to the presence of flammable electrolytes, toxic metals, and complex component structures. Although battery recycling technologies (e.g., pyrometallurgical and hydrometallurgical processes) are under development, their energy intensity, cost, and limited recovery rates hinder widespread adoption. The lack of standardized recycling frameworks globally further exacerbates the environmental risk of improperly discarded battery modules [146].

On the economic front, while the cost of Li-ion battery packs has declined substantially reaching approximately $130 per kWh in 2023, the overall Levelized Cost of Storage (LCOS) remains high for certain applications, particularly in developing markets or off-grid systems [147]. Factors contributing to high LCOS include capital expenditure (CAPEX), operational and maintenance costs, battery degradation, and uncertainty in second-life applications. Additionally, the financial viability of deploying Li-ion storage is heavily influenced by regulatory frameworks, market design, and incentive structures. Time-of-use pricing, demand response programs, and renewable integration mandates can enhance economic returns, but such mechanisms are not uniformly implemented across regions. Uncertainties in battery lifespan, especially under diverse thermal and cycling conditions, further complicate long-term return on investment (ROI) projections [148].

Therefore, addressing the environmental and economic challenges associated with Li-ion battery systems necessitates a combination of material innovation, recycling infrastructure development, policy support, and system-level optimization. Future pathways include the exploration of solid-state batteries, lithium-sulfur alternatives, and battery-as-a-service (BaaS) models to align storage deployment with sustainability and affordability goals.

1.4. Advanced Monitoring Methods for Thermal Runaway Mitigation

Thermal runaway is a critical safety concern in Li-ion batteries, particularly in high-capacity and high-density configurations employed in grid-integrated and embedded energy systems. The complex interaction of thermal, electrical, and electrochemical phenomena under fault conditions leads to abrupt temperature escalation, which can result in fire hazards or system failures. As Li-ion systems are increasingly deployed in sensitive environments, the development of advanced thermal monitoring and mitigation frameworks has become indispensable.

Advanced monitoring strategies aim to detect the onset of thermal anomalies, enable real-time health diagnostics, and initiate preventive or corrective control actions before a critical failure occurs. Among these, temperature-based sensing, internal resistance-based estimation, gas vent detection, and model-based predictive techniques form the core of modern thermal runaway prevention methodologies. This section presents the most widely adopted methods, starting with temperature-based monitoring.

1.4.1Temperature-Based Monitoring Techniques

Temperature-based monitoring is the most basic and widely adopted method for detecting early signs of thermal instability in Li-ion batteries. As thermal runaway is preceded by a gradual or sudden rise in temperature, observing temperature variations allows system operators to predict and mitigate safety risks. This technique is embedded in virtually all commercial battery management systems (BMS), making it an indispensable line of defense in thermal safety assurance [149].

In practical implementations, various sensors such as thermistors, resistance temperature detectors (RTDs), and thermocouples are strategically placed on cell surfaces, between modules, or embedded within the pack enclosure. These sensors are used to continuously monitor cell, module, and ambient temperatures across different spatial locations in the system. The gathered data allows for real-time detection of abnormal thermal patterns, enabling protective measures like load disconnection, forced cooling, or system shutdown before the onset of thermal runaway [150]. Threshold-based monitoring is commonly employed, where the absolute temperature, rate of temperature rise (dT/dt), and temperature differential across cells are compared to predefined safety limits. For instance, temperature increases beyond a certain value, typically between 60–80°C for most chemistries, trigger fault flags or emergency shutdown procedures. Moreover, standards such as IEC 62660 specify operating limits and test protocols for thermal safety evaluation [151].

The major benefit of this technique lies in its simplicity, affordability, and ease of integration. Since it requires no intrusive internal measurements, it is highly scalable for multi-cell and grid-level installations. However, one limitation is that temperature sensors often lag the actual internal fault progression. As they are mounted externally or on the surface of battery cells, they tend to detect heat only after it has propagated outward. This leads to delayed detection, especially in cases involving internal short circuits or dendrite formation, where the thermal hotspot originates deep within the cell [152]. In high-performance embedded systems and fast-charging applications, temperature-based data are frequently integrated with intelligent diagnostics, such as Kalman filtering, trend analysis, or thermal modeling. These hybrid approaches help interpret temperature fluctuations within the broader electrochemical and thermal dynamics of the battery. For example, combining dT/dt with current and voltage data allows for the identification of unexpected thermal spikes during normal operation, which can be early indicators of abnormal internal behavior [153].

Temperature monitoring is also the basis of active thermal management systems (ATMS), where real-time feedback is used to initiate dynamic control actions such as activation of cooling loops, heat sinks, or phase change materials (PCM). The integration of such systems has proven crucial in maintaining uniform cell temperatures across battery packs, especially in electric vehicles, aerospace, and high-density BESS installations [154]. Nevertheless, temperature monitoring should not be relied upon in isolation for comprehensive thermal fault detection. Its effectiveness improves significantly when used in conjunction with internal resistance analysis, voltage response modeling, and gas vent detection. When properly integrated, temperature-based techniques contribute effectively to safe, robust, and intelligent thermal management systems in modern battery-powered infrastructures.

1.4.2 Internal Resistance-Based Thermal Runaway Detection

Monitoring internal resistance has emerged as a reliable and proactive approach to predicting thermal runaway events in Li-ion batteries. Unlike temperature-based methods, which often detect issues only after significant heat has been generated and dissipated to the sensor, internal resistance monitoring allows for early identification of internal degradative mechanisms such as electrode delamination, solid-electrolyte interphase (SEI) breakdown, electrolyte decomposition, and internal short-circuit formational of which are potential precursors to thermal runaway [155].
Internal resistance, often referred to as equivalent series resistance (ESR) or impedance, represents the cumulative opposition to charge movement within the battery. It encompasses resistive losses due to current collectors, electrodes, electrolyte, and interfacial phenomena. Under normal operation, internal resistance remains within a predictable range; however, abrupt or accelerated increases in resistance are strong indicators of internal cell abnormalities [156]. This resistance increase leads to enhanced Joule heating (I^2R) during charging or discharging operations, which further elevates the temperature and promotes a positive thermal feedback loop, potentially initiating a runaway process [157]. Internal resistance can be estimated through various methods. The most direct approach involves current-pulse or voltage-step techniques, where a transient current is applied and the immediate voltage response is analyzed to extract resistive characteristics. While accurate, these techniques are often limited to laboratory settings or offline diagnostics. In practical systems, model-based estimation methods, such as Extended Kalman Filtering (EKF) and Equivalent Circuit Modeling (ECM), are preferred due to their ability to perform real-time, online resistance estimation without interrupting battery operation [158]. Among the ECM topologies, the R_{int} model, the Thevenin model, and dual-polarization RC networks are commonly used to characterize the dynamic behavior of batteries. These models are calibrated using voltage, current, and temperature measurements and then fitted to estimate real-time resistance values. By analyzing the rate of change, absolute magnitude, and deviation from expected resistance profiles, faults can be detected even before surface temperature begins to rise [159].
Another significant advantage of resistance-based detection is its insensitivity to ambient conditions. Unlike temperature or pressure measurements, which are susceptible to external environmental fluctuations, resistance is an

intrinsic electrochemical parameter and hence offers greater reliability in both grid-connected and embedded environments. For instance, in systems with high current ramp rates (e.g., UAVs, automotive propulsion), resistance-based monitoring provides rapid fault identification even under transient loads [160].

Despite its advantages, resistance monitoring is not without limitations. The internal resistance of a battery is highly dependent on state of charge (SOC), temperature, current amplitude, and cell aging. Therefore, context-aware interpretation algorithms must be employed to distinguish between normal resistance variations and those indicative of failure. Moreover, consistent calibration and compensation for hysteresis effects are necessary for accurate tracking across different operational regimes [161]. In recent years, hybrid diagnostic frameworks have been proposed, integrating internal resistance estimation with temperature, voltage, and gas detection metrics for multi-parameter fault modeling. Such frameworks significantly improve the reliability of thermal runaway prevention mechanisms and have become an essential part of advanced battery management systems (BMS) in aerospace, defense, and grid-scale energy storage domains.

1.5.Control Strategies for Grid-Integrated Battery Energy Systems

The integration of Battery Energy Storage Systems (BESS) with modern power grids plays a critical role in ensuring flexibility, reliability, and resilience. With increasing deployment of Distributed Generation (DG) sources, such as rooftop solar PV, wind turbines, and microturbines, alongside BESS, the system dynamics become more complex, necessitating advanced and coordinated control strategies. These strategies must address not only the energy balancing and fault management requirements but also the protection system coordination, particularly relay coordination, which becomes increasingly challenging in DG-rich networks [162].

In conventional grid systems, overcurrent protection devices and directional relays are coordinated based on predictable fault current paths and system topologies. However, with multiple DG sources interfaced through inverters or directly to the grid, fault current magnitudes and directions become uncertain and bidirectional. This significantly complicates relay grading, time–current curve coordination, and selectivity of protection schemes [163]. Furthermore, the presence of BESS introduces dynamic power injections during transient or fault conditions, influencing fault currents depending on its control logic and state of operation.

As such, the control strategies for grid-integrated BESS must be designed to ensure both power flow optimization and protection selectivity, enabling the system to distinguish between normal DG-induced current injections and actual fault events. Modern control schemes embed adaptive relay coordination algorithms within the BESS controller or centralized protection coordination units. These algorithms dynamically adjust relay settings, such as pickup current, time delay, and directionality, based on the real-time grid topology, DG status, and BESS operating mode [164].

In terms of control hierarchy, the grid-integrated BESS operates under a multi-layered framework:

i. Primary control ensures voltage and frequency regulation at the point of common coupling (PCC), handling instantaneous disturbances.
ii. Secondary control performs load sharing and reference restoration.
iii. Tertiary control addresses economic dispatch, energy arbitrage, and coordination with market signals [165].

In the context of protection, primary and secondary controllers are also responsible for interpreting protective signals from relays and integrating them into the BESS operation logic. For example, in case of upstream faults, the controller can command the BESS to disconnect or shift to islanding mode, based on relay coordination signals. In this way, the BESS supports protection zone selectivity and minimizes nuisance tripping of upstream devices. To mitigate relay coordination conflicts, especially under bidirectional flow and fault current variability, several solutions have been proposed:

i. Directional overcurrent relays (DOCRs) that discriminate against fault directions based on DG and BESS locations.
ii. Differential protection schemes that can locally sense faults without relying on current magnitude alone.
iii. Communication-assisted relays using IEC 61850 GOOSE messaging to coordinate trip commands between relays and BESS controller in real-time.
iv. Adaptive setting groups stored within intelligent electronic devices (IEDs), triggered by system topology or DG operation mode changes [166].

Moreover, the BESS controller often incorporates grid-support functionalities such as:

i. Grid-forming and grid-following control to either establish grid references in island mode or synchronize with utility parameters.
ii. Black-start capabilities in coordination with protective relays to safely energize de-energized zones.
iii. Fast frequency response (FFR) and voltage ride-through compliance, ensuring contribution to grid stability during transient faults or DG intermittency [167].

In DG-dense microgrids, the coordination of BESS and DG must also address fault location accuracy, islanding detection, and selective load restoration. Relay coordination, in this case, is tightly coupled with real-time monitoring of BESS state-of-charge (SOC), thermal limits, and discharge availability, which influences whether BESS can support loads post-fault or needs to isolate itself. To ensure seamless operation, a protection-aware control strategy is required, where BESS dynamically aligns its power injection, fault ride-through, and disconnection protocols in accordance with the relay settings and grid protection philosophy. These strategies are critical in achieving selective fault isolation, system reliability, and safe operation under varying fault scenarios.

In conclusion, the interplay between relay coordination and BESS control strategies is a crucial design consideration in modern power systems with integrated DG. Advanced algorithms leveraging real-time grid intelligence, communication, and adaptive protection are essential for fault-resilient operation and grid-supportive behavior of BESS in such contexts.

1.6. Scope of the Thesis

This thesis focuses on developing advanced monitoring and control methodologies for Li-ion batteries integrated into smart energy systems. The scope is motivated by the increasing need for intelligent, real-time diagnostics and operational strategies to enhance the reliability, safety, and efficiency of battery-based distributed energy frameworks. The thesis also aims to address limitations in existing protection and control infrastructures by proposing integrated solutions spanning from embedded system design to grid-scale energy management. The framework of this thesis has been presented in Fig. 1.5.

A key contribution of this research lies in the formulation of a real-time internal resistance-based monitoring framework for early detection of thermal runaway events in Li-ion batteries. This includes the development of a dedicated hardware-software prototype and its validation under controlled testing environments. The framework is designed to detect precursors to thermal faults, thereby initiating smart fault-handling mechanisms to avoid catastrophic failures.

In addition to battery diagnostics, the thesis addresses the challenges associated with the protection and coordination of Distributed Generation (DG) systems in smart grids. A relay coordination methodology is proposed that incorporates fault current limiter (FCL) devices and simulation studies to optimize relay operating times, especially in the presence of DG units. This enables improved system resilience and selectivity under fault conditions.

The research also proposes a microcontroller-based hybrid power factor control algorithm, tailored for real-time energy management in embedded environments. This algorithm is designed to optimize the power factor dynamically based on load characteristics and frequency sensitivity, thereby improving energy efficiency and reducing stress on the grid.

Another area of focus in the thesis is on the integration of smart metering infrastructure (AMI) with grid and energy systems. The information flow, data processing, and analytics required for intelligent energy control are explored in depth, with particular attention to microcontroller interfacing, load forecasting, and demand-side analytics.

The scope spans across six interlinked research domains:

Chapter 2 outlines the design of a real-time Fault Handling System (FHS) for Li-ion batteries, with emphasis on early detection using internal resistance estimation techniques.

Chapter 3 presents a resilient protection framework for distributed energy systems, integrating relay coordination schemes and fault current limiters to enhance fault response.

Chapter 4 describes the implementation of a real-time hybrid power factor control algorithm, including logic-level design and its performance evaluation on embedded platforms.

Chapter 5 addresses the smart metering infrastructure necessary to support intelligent grid-interactive battery systems, detailing AMI components, protocols, and energy analytics.

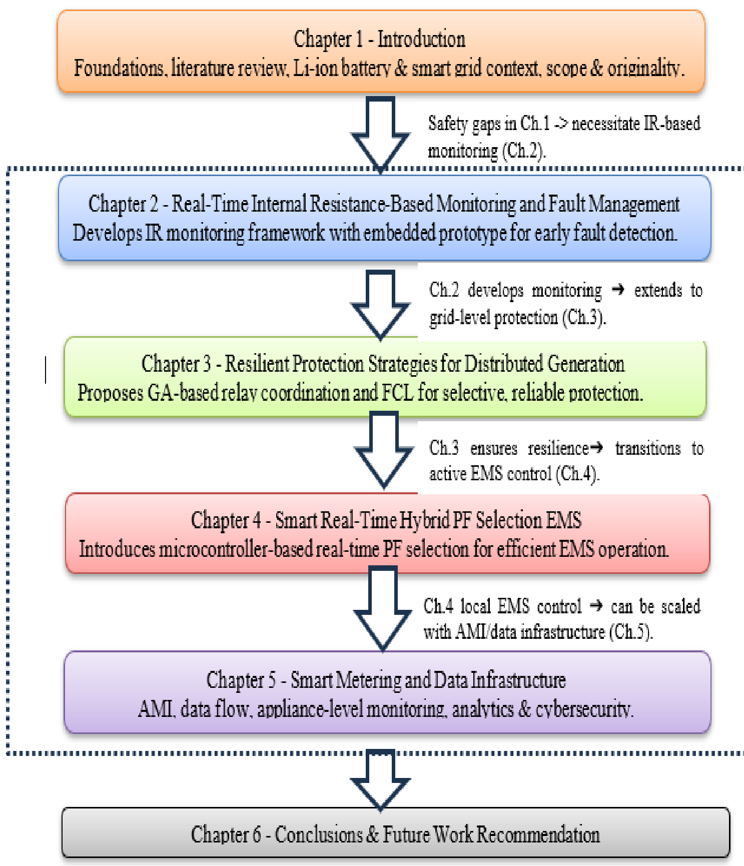

Fig. 1.5 Comprehensive framework of this thesis.

Chapter 6 synthesizes all the research outcomes and proposes recommendations for future developments in battery-integrated smart energy networks.

The overarching scope is to unify diagnostic precision, protection adaptability, and energy intelligence within a single coordinated framework. The methodologies developed herein are applicable to a broad range of smart grid, microgrid, and embedded energy storage applications, aligning with global trends in decarbonization, digitalization, and decentralization.

1.7. Originality of the Thesis

To the best of the author's knowledge, the current work has made the following original contributions:

- *Development of an internal resistance-based real-time fault handling system (FHS) for Li-ion batteries and its validation through embedded implementation.*

- *Analysis of relay operating characteristics and coordination time intervals under various DG penetration levels and with and without fault current limiters (FCLs).*

- *Prototyping and testing of a frequency-aware energy monitoring platform using a microcontroller-based architecture.*

Chapter 2

Real-Time Internal Resistance-Based Monitoring and Fault Management in Li-Ion Batteries

2.1. Introduction

Nowadays, due to environmental concerns and the fuel crisis with traditional vehicles, Electric Vehicle (EV) industries are expanding rapidly worldwide. Similarly, Battery Energy Storage System (BESS) industries are also expanding significantly due to their ability to stabilize the grid through various services. Their safety mainly depends on the type of battery used and the design of the Fault Handling System (FHS) in the Battery Management System (BMS). Li-ion batteries are widely used in these industries because they offer high energy density, long cycle life, and a low self-discharge rate. One of the major safety concerns in these battery-operated systems is Thermal Runaway (TR) [168]. During overcharging, the battery eventually develops internal chemical abnormalities, leading to the release of gases and exothermic reactions that trigger TR [169]. Another important event during overcharging is the change in the battery's Internal Resistance (IR), which occurs due to internal chemical reactions and subsequent polarizations. Various studies [169, 170] have investigated the chemical and electrical behaviour of Li-ion batteries during overcharging and proposed several Early Thermal Runaway Sensing (ETRS) methods from a theoretical perspective. Previous ETRS methods include mechanical strain detection, gas venting, and electrochemical impedance spectroscopy (EIS) [171, 172]. However, these approaches have limitations such as low detection sensitivity, safety risks from vent gases, and complex setup requirements. Some other studies have explored internal resistance monitoring methods, but these typically works offline or rely on data-driven analysis, requiring system shutdown or post-event analysis [173]. To overcome these limitations, this work proposes an online internal resistance monitoring system that operates continuously during system activity, offering real-time diagnostics without interrupting battery operations. In this study, an efficient and low-cost microcontroller-based prototype of an ETRS module for a smart FHS has been developed. This module enables ETRS using an online IR sensing mechanism and simultaneous monitoring of both temperature and internal resistance through two microcontroller units, thereby reducing the risk of data corruption. Additionally, the proposed method sends SMS alerts via IoT to notify users, helping to prevent critical fire accidents in the battery pack.

2.2. Proposed Methodology

In this work, a commercial Nickel Manganese Cobalt Oxide (NMC) cylindrical cell (NMC 18650) having diameter and height of 1.85 cm and 6.56 cm respectively, electrical capacity of 2000 mAh and maximum charging voltage of 4.2V has been utilized. Initially, the cell was discharged to a voltage of ~4V for further processes.

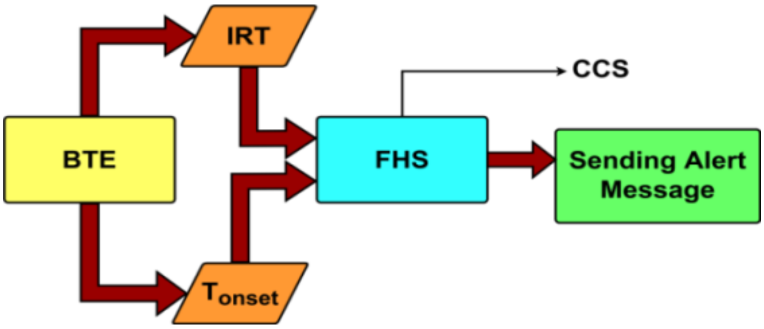

Fig. 2.1. Process Flow of the Proposed Design Setup.

Fig. 2.1 shows the process flow of this prototype, where Internal Resistance Threshold and TR onset temperature are represented as "IRT" and "T_{onset}", respectively. The values of IRT and T_{onset} are obtained from the IR and thermal behavior of the cell by monitoring it during the Battery Testing Experiment (BTE). This BTE is the main part of the whole setup. The evaluated values of IRT and T_{onset} are then used in the FHS design to sense the early TR process effectively. The ETRS unit inside the FHS is also capable of sending an alert message to the user's phone and generating a Charge Control Signal (CCS) to control the charging mechanism of the batteries.

2.2.1. Battery Testing Experiment (BTE)

In this division, the previously discharged cell was used as the device under test (DUT) and charged at a constant current of 1.5A (0.75C) with a commercial DC regulated power supply in the laboratory to push it into the overcharging region for behaviour monitoring. For monitoring, two microcontroller units were employed: Arduino-1 for thermal monitoring and Arduino-2 for internal resistance monitoring, enabling parallel data collection. This configuration reduces the processing load on each unit and ensures more accurate real-time measurements, preventing data errors. Additionally, an MLX90614 I2C-based non-contact infrared temperature sensor (I2C address 0x5A) was used to measure the cell temperature. The setup also included an INA219 DC current sensor, a DC voltage sensor, a 5Ω-5W power resistor (as load), and a dual relay module to form the online IR sensor module for measuring the cell's IR during charging. By connecting a load resistance across the cell and sensing the circuit current along with the EMF/Open Circuit Voltage (OCV), the IR was calculated using equation (2.1).

$$r = [(E / I_{dis}) - R_L] \tag{2.1}$$

In (1), "I_{dis}" is the discharging current, "r" is the cell IR, "R_L" is the load resistance and "E" is the emf/OCV of the cell. The proposed online IR computation algorithm and the block diagram representation are shown in Fig. 2.2 and Fig. 2.3, respectively. In this work, the values of charging time (t_{ch}), idle time (t_{idle}), and discharging time (t_{dis}) have been chosen as 60s, 2s, and 3s respectively by calibrating the system for efficient performance. In the algorithm, the microcontroller first sets a timer for 60 seconds and allows the cell to charge through the Charging Relay (CR). After 60s, the microcontroller sets another timer of 2s to keep the cell in idle mode for extracting the OCV. Once the OCV is extracted, the microcontroller sets a timer of 3s and allows the cell to discharge through the Discharging Relay (DR) for detecting I_{dis} . It should be noted that this IR calculation is a temporary event in each cycle and has a negligible effect on the overall charging process. Moreover, IR calculation is possible only after evaluating both OCV values and I_{dis}.

2.2.1.1. BTE Hardware Prototype

The hardware prototype of the BTE is presented in Fig. 2.4. As shown, two microcontrollers (with different COM ports) are connected to a multi-USB adapter using two USB cables. This adapter is then linked to the computer through a single USB cable, enabling simultaneous serial communication for parallel monitoring of IR and temperature variations. Another component in the experimental setup is a fire- and explosion-proof metal chamber, which ensures a safe environment during the BTE process.

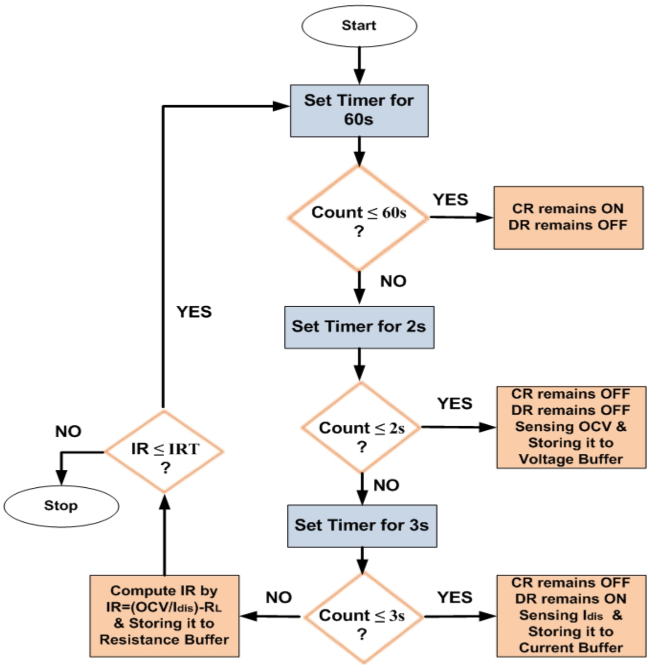

Fig. 2.2. Flowchart of the Online Internal Resistance (IR) Sensing Algorithm for ETRS.

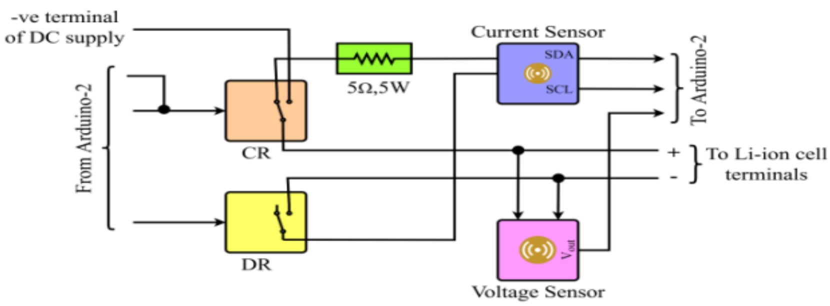

Fig. 2.3. Block Diagram of Online IR Sensor Board for Real-Time TR Monitoring.

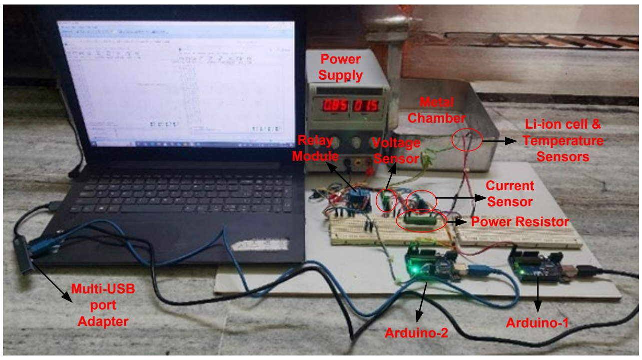

Fig. 2.4. Experimental Hardware Setup for BTE.

2.2.1.2. BTE Output Characteristics

The output curves for cell temperature and IR variations with respect to time are shown in Fig. 2.5. From Fig. 2.5, it can be observed that, the IRT value detects the TR event faster than the T_{onset} value with a time gap (also called Alarming Time Gap (ATG)) of Δt, whose value has been extracted as ~234 seconds (~3.9 minutes) using (2.2).

$$\Delta t = ATS_{IRT} - ATS_{T_{onset}} \tag{2.2}$$

Here, Arrival Time Stamp can be abbreviated as "*ATS*". The IRT and T_{onset} values along with their arrival time have been summarized in Table 2.1. After T_{onset} point, the corresponding temperature value decreases because the power supply has been turned off after extracting the required parameters successfully.

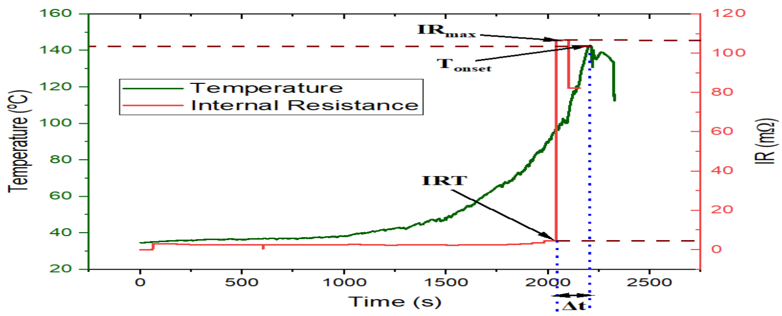

Fig. 2.5. Temperature and Internal Resistance (IR) Variation of Cell during Charging and Onset of Thermal Runaway.

Moreover, it should be noted that the TR event and IR variation are strongly influenced by the aging of the Li-ion battery. As the battery ages, it undergoes more charge-discharge cycles, which increases the total cycle count and reduces the State of Health (SOH). In [174, 175], the relationship of T_{onset} and IRT with aging has been discussed both graphically and theoretically. From their graphical relationship with SOH and/or cycle number, mathematical modelling using a curve-fitting approach can be applied, which will make the proposed algorithm more robust against the dynamic variations of T_{onset} and IRT caused by aging effects.

Table 2.1
BTE Parameters, Threshold Values and Arrival Time Stamps (very low values are artefacts due to the limitation of short OCV idle estimation)

Parameters	**Magnitude**	**ATS**
IRT	4.60 mΩ	1979.75s
IR_{max}	106.79 mΩ	2055.46s
T_{onset}	142.33°C	2213.75s

2.2.2. IR Computation Based Early Thermal Runaway Sensing

As is evident from the BTE output characteristics, the IRT point occurs earlier than the T_{onset} point. Based on this cell behaviour, an online IR sensor-based ETRS module has been designed for a smart FHS, using the IR sensor module as the primary stage marker and the thermal management module as the secondary stage marker for monitoring thermal behaviour and acting as a backup. This module was designed using the same cell model, sensors, and other components, while keeping all physical conditions constant. The proposed ETRS algorithm utilizes the IRT and T_{onset} values to reliably control the cell and prevent TR. The flowchart of the proposed online IR sensor-based ETRS algorithm is shown in Fig. 2.6. Additionally, in this design, an L293DN dual motor driver with a brushless exhaust fan was used to ventilate small amounts of vented gases released at the T_{onset} point. An extra Charging Control Relay (CCR) was added to stop cell charging, along with stage indicator LEDs and a 2-input OR gate. For sending IoT-based SMS alerts to users, an ESP8266 NodeMCU was connected to the AWS cloud server and configured with an Application Programming Interface (API).

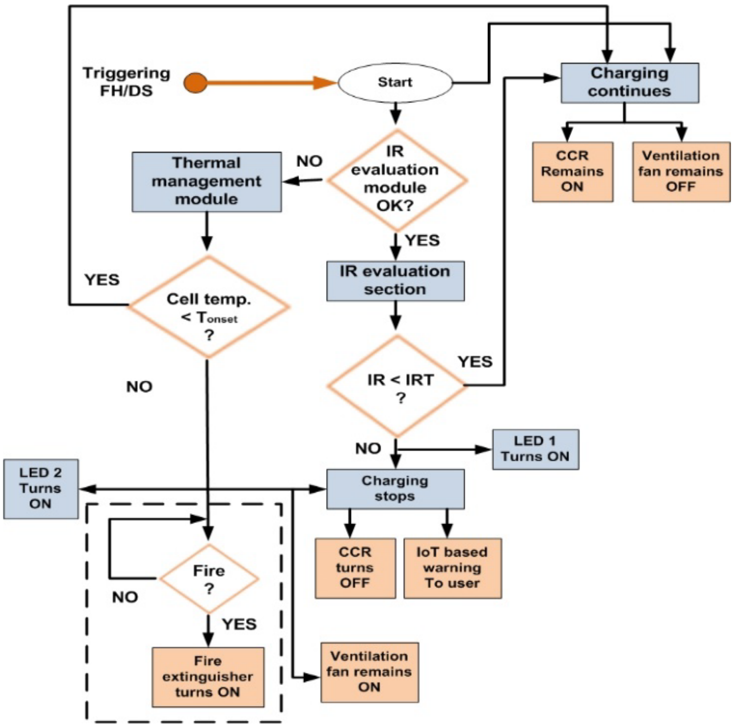

Fig. 2.6. Proposed ETRS Algorithm for FHS.

2.3. Results and Performance Evaluation

2.3.1. Result of the Proposed ETRS Technique

In this proposed ETRS technique, an online IR sensing circuit has been developed for a smart FHS, which is capable of continuously monitoring IR variations in the cell and controlling its charging status to prevent it from entering the TR region during overcharging. A thermal management system has also been designed as a secondary safety stage and backup. Based on the proposed ETRS algorithm, another cell with the same specifications as the BTE was tested by overcharging it at the same C-rate to observe its behaviour for analysis. The experiment started at 10:00:00 hrs (IST) in the laboratory. Fig. 2.7 shows the IR and temperature curves of the cell during overcharging after applying the proposed ETRS algorithm. From the curves, it is clear that they can be divided into two parts: part-A shows the cell condition before IRT detection, and part-B shows the condition after IRT detection. In part-B, after the IRmax point, the IR value of the cell drops quickly to its normal value because the charging process was immediately stopped, and the cell temperature gradually decreased. The graphical details of the curves and the SMS notification times from this experiment are summarized in Table 2.2.

2.3.2. Performance Evaluation of ETRS Techniques

Among several ETRS techniques, venting is a widely researched technique, where the authors have investigated venting based ETRS technique by analyzing the chemical phenomena and other side reactions of the cell [9, 10].

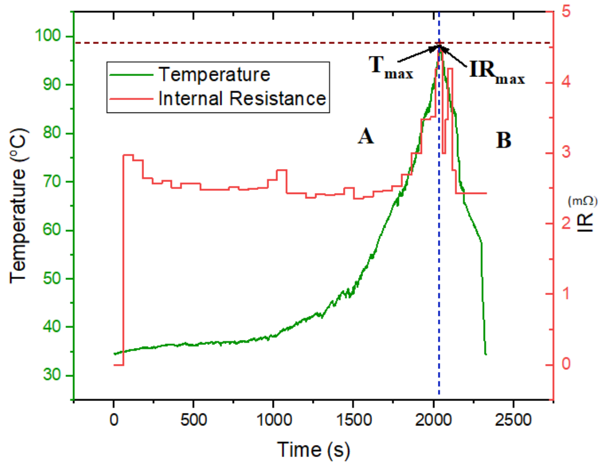

Fig. 2.7. Cell Temperature and IR Curve after Incorporation of Proposed ETRS Algorithm.

TABLE 2.2
Graphical Details in Cell Behavior Output after Incorporation of Proposed ETRS Algorithm

Parameters	**Values**
IR_{max}	4.60 mΩ
Maximum Temperature (T_{max})	96ºC
IRT time stamp	10:33:58.62 hrs (IST)
SMS time stamp	10:33:59.00 hrs (IST)

Despite the good detection speed and clear signals provided by venting gas sensors, the venting technique is not safe for real-time warning methods due to the limited feasibility of venting gas sensors and the explosive nature of vented gases (especially Volatile Organic Compounds (VOCs)) [178]. Besides the venting gas technique, several other ETRS methods have also been explored in research. Table 2.3 summarizes the ATGs of previously studied ETRS techniques along with the ATG obtained from the BTE output characteristics.

TABLE 2.3
Comparison between ETRS method of this work and other existing Studies

Alarming Method Type	**ATG Value**	**Ref.**
Venting Technique (CO_2, CO, VOCs, and solid-phase particle quantity detection)	~54s, ~(104 -103)s	[176] [177]
Mechanical Strain Detection	~167.20s	[172]
Phase Detection through EIS	~150s	[171]
This work (IR detection)	~234s	-

It can be observed from Table 2.3 that, since the ATG value of the proposed online IR-based ETRS method is higher than in other studies, it can be used as an effective practical tool to prevent cells from TR. It is because after sensing the IRT, the algorithm gives enough time for the MCU board to take the required safety measures quickly. While commercial Li-ion batteries include circuits for managing charging currents and temperature, the proposed ETRS module further improves safety by giving an early warning based on real-time internal resistance calculation. This extra response time is especially useful for EV and BESS applications, where proactive thermal management helps avoid serious accidents.

2.4 IR Sensing Methodology for Battery Pack

In a typical battery pack, different cells are connected in series and parallel fashion to optimize the net voltage and capacity of the whole battery pack. In general, a battery pack is made by connecting different battery modules (in series or parallel), which further comprises of series and parallel connection of cells. A typical battery pack design, highlighting the battery module connections, has been shown in Fig. 2.8 along with the internal architecture of battery module in Fig. 2.9. It should be noted that the parallel cell stacks have been named as Cell Array (CA) for the ease of understanding the whole concept.

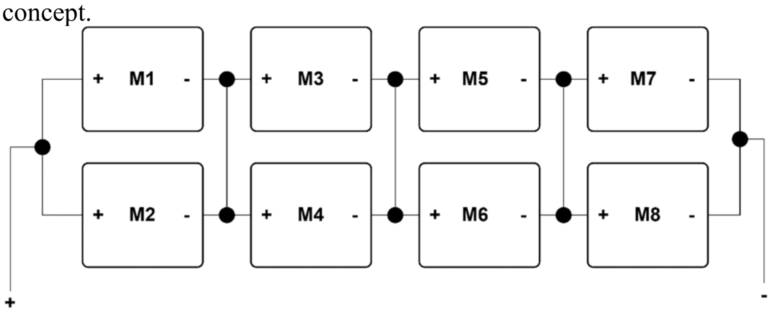

Fig. 2.8 Battery Modules

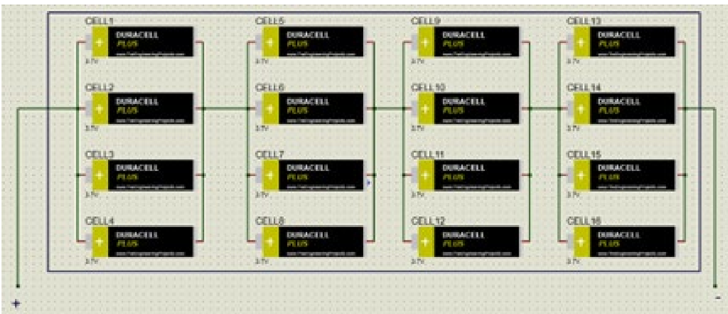

Fig. 2.9 Cells inside each Battery Module

Thus, from Fig. 2.8 it is evident that the battery pack consists of eight battery modules connected in 2P-4S (four stacks of two parallel modules connected in series). Again, from Fig. 2.9, it is quite evident that in each module, the cells are connected in a 4P-4S fashion (four Cas containing four parallel cells connected in series).

As the battery pack consists of numerous cells, any cell in any module can face the TR issue, which can also lead to a great disaster. Thus, a proper, robust, and efficient TR sensing system is utmost needed for sensing the TR in the correct area. In this work, the CA based IR sensing technique has been adopted, where a single master IR evaluation board senses the IR of all the CAs (of the battery modules) through a Time Division Multiplexing (TDM) method. During the sensing process, if any cell(s) of any CA malfunction, then the IR of that whole CA will be affected, which will be further reflected in the IR sensing terminal. Hence, as a measure, that particular CA will be replaced with a new one.

2.5. Conclusions

In this research work, a smart online IR sensor-based ETRS module has been developed for a smart FHS module, which is capable of early detection of the TR problem in Li-ion battery during overcharging. Here, two microcontroller units, non-contact temperature sensor, voltage, and current sensor, load resistance (5Ω, 5W), and a dual relay module were used for BTE and additionally an IoT module, 2- inputs OR gate IC chip, LEDs, motor driver, exhaust fan, and an extra relay module were included for designing the ETRS section in the FHS. The ETRS section disconnects the charging system after encountering abnormalities in IR variation and sends an SMS alert to the user about 3.9 minutes before the onset of TR. Based on the output results, it can also be concluded that, with the help of sophisticated microcontroller units and sensors, the proposed system works satisfactorily and can be implemented in localized mini rooftop BESS and light EVs. For commercial deployment with sophisticated hardware, this ETRS system could be implemented either at the cell level for high precision or at the battery-pack level with data aggregation to enhance scalability in large-scale battery systems. However, the IR-based monitoring methodology was constrained by several factors. Experimental low readings (~4 mΩ) for IR appeared, arising from short OCV idle estimation (2 s) and sensor resolution limits. Equation (2.1) was applied to 3s discharge steps as an approximation of pulse resistance, introducing modest deviation, and needs further investigation. Furthermore, in future research, the proposed method can be investigated to include a wider range of battery types (lithium-ion, solid-state, and lead-acid batteries) and battery aging effects (such as capacity fade, impedance growth, and thermal degradation) to increase its effectiveness and suitability for real-world scenarios.

Chapter 3

Resilient Protection Strategies for Distributed Generation and Smart Grid Integration

3.1. Introduction

Real-time internal resistance-based monitoring enhances Li-ion battery safety and fault handling at the device level. As modern power systems increasingly integrate distributed generation (DG) units, including renewable sources and battery energy storage systems (BESS), the resilience challenge extends from individual components to the entire network. The growing use of DG is largely attributed to the economic and environmental advantages of renewable energy resources [179], [180]. Despite these advantages, the magnitude and direction of the short-circuit current change after the installation of DG [181]. Short-circuit current is one of the most important parameters in selecting protective equipment such as circuit breakers (CB), fuses, current transformers, and relays. The installation of DGs alters the operation and coordination of protection devices in the power network [182]. The mis-coordination of directional overcurrent relays (DOCR) is an undeniable challenge in power systems due to the addition of DGs [183]. In a power system network, relay settings should be arranged so that, when a fault occurs, the primary relay detects it first, and if it fails, the backup relay operates after a coordination time interval (CTI). However, installing DGs changes the short-circuit (SC) level, which results in mis-coordination between DOCRs in the power network [184]. Improper tripping occurs when there is no coordination between the primary and backup relays. Hence, coordination of relays is a prime concern for power system protection. In a power system, each overcurrent relay (OCR) must be coordinated with the others for proper protection [185,186]. For optimum coordination of OCRs, various heuristic-based optimization techniques such as Genetic Algorithm (GA), Cuckoo Search, and Particle Swarm Optimization (PSO) have been used [187].

In a power system network, a change in topology may cause a change in the short-circuit (SC) level of the system. Hence, to reduce the SC level, a fault current limiter (FCL) is considered an effective solution. Optimization of the FCL impedance value is also necessary for better relay coordination. In practice, the impedance of an FCL is reduced to zero or nearly zero when there is no fault in the power system. During a fault, the FCL reduces the short-circuit level by increasing impedance, thereby restoring relay coordination. With the incorporation of DGs, the fault current may reach the fault point from different directions. Hence, reducing the short-circuit level using a single FCL becomes difficult and challenging. Therefore, applying FCLs in a network requires proper placement and optimized impedance values. In general, the impedance of an FCL increases until coordination between relays is restored. In a large power system network with many buses, transmission lines, and relays, optimization techniques like the Genetic Algorithm (GA) and Multi-Objective Genetic Algorithm (MOGA) are necessary to determine optimized values of FCLs.

Considering changes in topology is important for solving the problem of DOCR coordination in the presence of DG. Therefore, adaptive protection schemes can be used. In [188], FCLs along with adaptive protection were applied to microgrid systems. The authors of [189] adjusted DOCR settings using adaptive schemes. According to [189], when topology changes, all DOCRs are connected to a central processing unit (CPU), which adjusts the settings based on the new topology. However, these methods are very complex and time-consuming. They also require special infrastructure, which increases the cost of implementation.

In this work, the problem of finding the optimum values of Time Multiplier Setting (TMS) and Plug Setting Multiplier (PSM) for DOCRs has been addressed. For this purpose, the GA optimization method was used to determine the optimum values of TMS and PSM. To illustrate the proposed method, two case studies were considered: one with a 3-bus system including DG and 12 DOCR relays, and another 3-bus system without DG and with 11 DOCR relays. In addition, the required position of the fault current limiter (FCL) in the same network was identified to reduce the fault current and optimize the coordination time interval (CTI).

3.2 BESS as Distributed Generation

The relay coordination methodology presented in this chapter is generic and applicable to any form of distributed generation, including synchronous machines and inverter-interfaced renewables. However, in the context of this thesis, distributed generation is particularly relevant when realized as Battery Energy Storage Systems (BESS). BESS units, integrated at the distribution level, exhibit distinctive fault current profiles and dynamic behaviors compared to conventional DG sources. While the GA-based optimization described here is presented in a generic form, its implications for BESS-integrated systems are especially significant, since the diagnostic framework of Chapter 2 directly informs the health-aware operation of such assets.

3.3. Challenges for Directional Overcurrent Relays (DOCRs) in Relay Co-ordination

Different optimization methods can be used to solve relay coordination problems. The general solution to this problem can be addressed by using constrained optimization. To optimize the OCR relay coordination, the summation of operating times of used primary relays must be optimized according to the optimal settings (TMS and PSM) as presented in (3.1).

$$\min z = \sum_{i=1}^{n} t_i \tag{3.1}$$

Where Z is the objective function, i is for index, t_i is the time of operation of the i_{th} primary relay for its near-end fault, and n is the total number of DOCRs. The above optimization problem has the following constraints, which are based on characteristics and the type of relays.

3.3.1. Relay Settings

Over-current relay has TMS and PSM. The PSM limit has been chosen based on the minimum fault current to the relay and the relay characteristics. The

TMS bounds are selected depending on the current-time characteristics of the used relay.

$$PSM_{i\min} \leq PSM_i \leq PSM_{i\max} \quad (3.2)$$

$$TMS_{i\min} \leq TMS_i \leq TMS_{i\max} \quad (3.3)$$

Where, PSM_{imin} - minimum value of *PSM* of relay R_i
PSM_{imax} - maximum value of *PSM* of relay R_i
TMS_{imin} - minimum value of *TMS* of relay R_i
TMS_{imax} - maximum value of TMS of relay R_i
It should be mentioned here that TMS_{imin} and TMS_{imax} have been taken as 0.025 and 1.2, respectively, according to relay characteristics [190].

3.3.2. Relay Operating Time Bounds

The overcurrent relay requires a specific minimum duration of time for operation or to trip. However, a very large time for the operation of relays is not acceptable. Therefore, mathematically it can be represented as (3.4).

$$t_{i\min} \leq t_i \leq t_{i\max} \quad (3.4)$$

Where, t_{imin} and t_{imax} are the minimum and maximum times to operate the relay for a fault at various locations, respectively.

3.3.3.Backup-Primary Relay Coordination Time Interval

Backup and primary relay senses the fault simultaneously by the fault current. To avoid maloperation, the backup relay should be activated immediately after the failure of the primary relay. If R_i is the relay acting as primary to the fault at *k*, and R_j is the backup relay for the fault at *k*, then the coordination constraint can be represented as follows.

$$t_{j,k} - t_{i,k} \geq \Delta t \quad (3.5)$$

Where, $t_{i,k}$ -Time of operation for the primary relay R_i, for a fault at k. $t_{j,k}$ – Time of operation for backup relay R_j, for the same fault at k,
Δt - Coordination time interval (CTI).
The operating time of the relay is presented as (3.6).

$$t = \frac{A \times TMS}{PSM^{0.02} - 1} \tag{3.6}$$

As A= 0.14 for normal inverse over current relay (OCR), (3.6) is simplified as (3.7).

$$t = \frac{3 \times TMS}{\log(PSM)} \tag{3.7}$$

In this work, the relay characteristic has been chosen as in IEC 255-3 [190].

3.4. Proposed Methodology

To address the problem, the proposed methodology involves checking relay coordination, placing FCLs (Fault Current Limiters) for optimal system protection, and using an adaptive method to adjust system parameters dynamically. The Genetic Algorithm (GA) is used to optimize the configuration and restore coordination.

3.4.1. Relay Coordination Problem

A simple radial feeder system has been considered for analysis as shown in Fig. 3.1. This system is simulated using Power World Simulator.

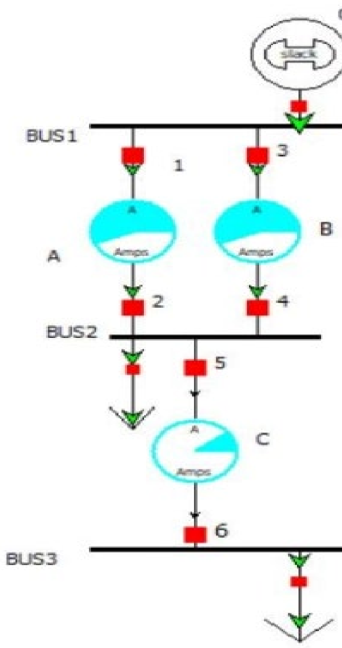

Fig. 3.1 Simple 3 bus system for analysis.

In this system, the addition of DG at bus 2 changes the topology of the existing system. The SC level in the entire network also changes with the installation of DGs in the power system. The DGs in the power network create multiple paths for the short-circuit current and increase the SC level. To determine the effect of DGs on the mis-coordination problem, DOCRs were first coordinated without DGs. Then, after adding DG, the constraints of DOCRs were evaluated based on (8) to check whether any mis-coordination occurred.

$$t_{backup} - t_{primary} \geq 0.3 \tag{3.8}$$

Considering (3.8), using GA the coordination between relays has been optimized in this study.

3.4.2. Simulation Studies of Faults at Different Line Locations with and without Distributed Generation (DG)

The next step of this method is to place and size the FCLs. By minimizing the fitness function while satisfying the constraints, the optimal number, location, and size of FCLs were determined. Therefore, the coordination of the used DOCRs was restored at minimum cost and with optimal operating time. The fitness function for FCL values was defined based on restoring DOCR coordination, reducing the operating time of relays, and considering the size and number of FCLs. Reducing the size and number of FCLs lowers the cost of the network system.

$$\text{Fitness Function} = a\sum_{i=1}^{n} t_i + b\sum_{j=1}^{m} zfcl_j + m \tag{3.9}$$

Here, a, b are weighting values, t_i is time operation of DOCRs, $Zfcl_j$ is FCL impedance of j^{th} number, and m is the number of FCLs. The constraints of the problem are specified according to (3.8), (3.10), and fitness function in (3.9).

$$zfcl_{j\min} \le zfcl_j \le zfcl_{j\max} \quad \text{j=1... m} \tag{3.10}$$

Based on these functions, the value of the FCL-based adaptive protection scheme is implemented.

3.4.3. Adaptive Protection Strategy Using Fault Current Limiter

The adaptive method relies on identifying the change in topology and, therefore, activating FCLs to suppress fault current accordingly while maintaining the coordination. Fig. 3.2 indicates the block diagram for the proposed adaptive system protection scheme.

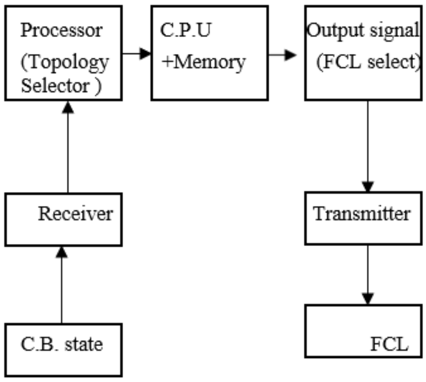

Fig. 3.2 Adaptive Protection Scheme.

As shown in Fig. 3.2 receiver receives the state of CB and sends it to the topology selector for processing. From the C.P.U., according to topology, FCLs are selected for activation. The output signal is transmitted to FCL using the transmitter to activate it.

3.4.4. GA Algorithm

Optimization has been widely used to achieve better results in various fields in recent years. One of the most used optimization techniques is GA [191]. The steps of the Genetic Algorithm are shown in Fig. 3.3 for optimizing relay coordination and FCL values. First, relay coordination was optimized using GA with the addition of DG. In the next step, the placement of FCLs was carried out using GA. Finally, constraints were checked for different fault locations, as defined in (3.2), (3.3), (3.4), (3.5), and (3.10).

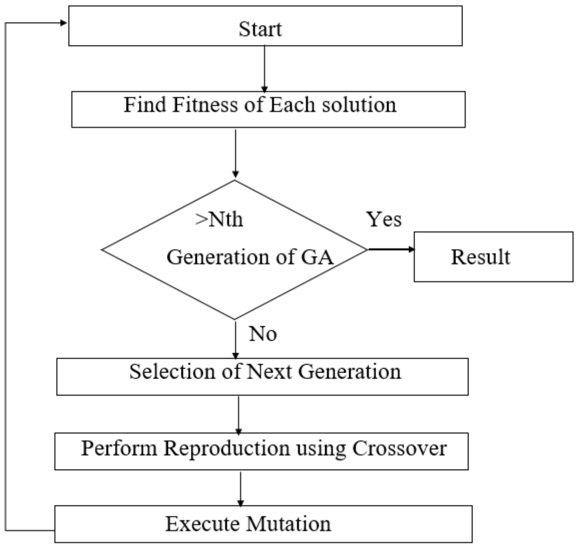

Fig. 3.3 Generalized flowchart to use Genetic Algorithm.

3.5. Results and Discussions

3.5.1. Relay operating time optimization with and without DG

The 3-bus distribution system shown in Fig. 3.4–3.7 was used to analyze the results with the proposed methodology. The system consists of 4 lines, 3 buses, and one generator. All lines were protected using DOCR relays. Faults were considered at the midpoint (50%) of each line connecting the buses in the system and named points A, B, C, and D. Fault locations A and C were taken at the midpoints of the lines where relays 1, 2, 5, and 6 are placed. Two fault points (B and D) out of four were shown pictorially with simulated values in this section.

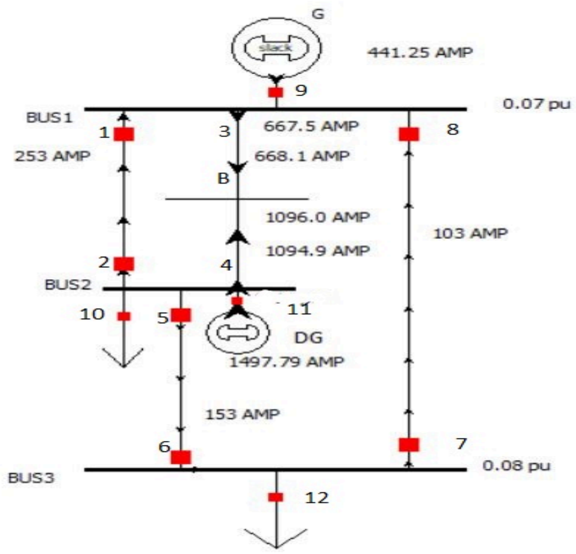

Fig. 3.4 Analysis of fault at point B with DG.

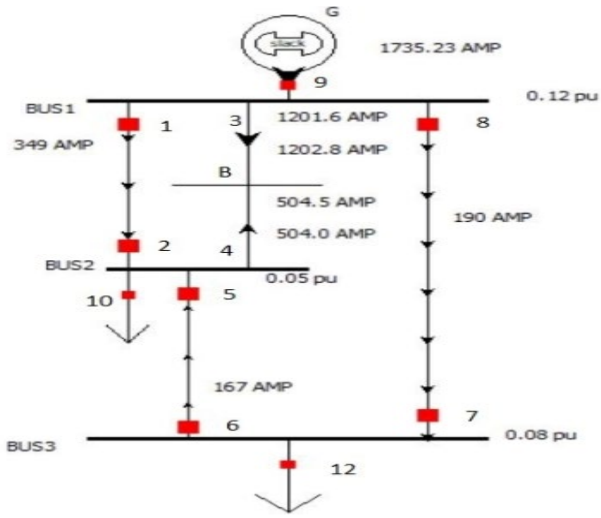

Fig. 3.5 Analysis of fault at point B without DG.

The GA method has been used to find optimum relay settings without considering DG. Fig. 3.4 and 3.5 have been considered for demonstration of fault at point B with and without DG, respectively. Similarly, Fig. 3.6 and Fig. 3.7 have been considered for the analysis of the fault at point D with and without the DG effect.

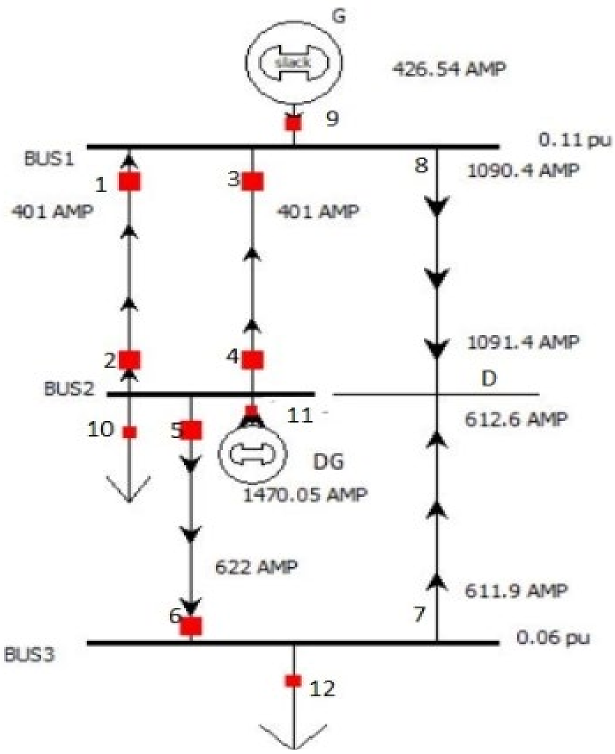

Fig. 3.6 Analysis of fault at point D with DG.

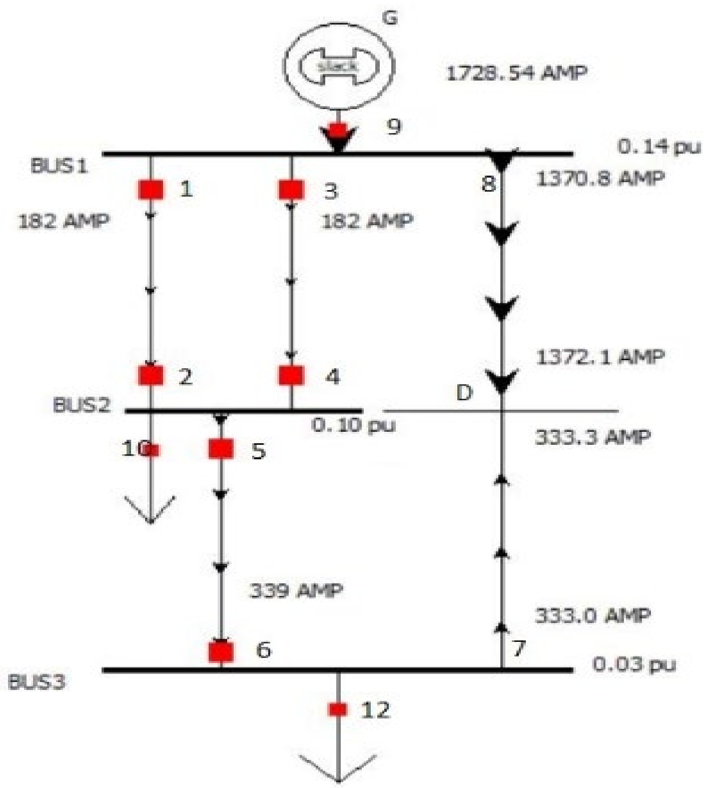

Fig. 3.7 Analysis of fault at point D without DG.

The following equations have been optimized for optimizing coordination between relays based on simulation results, considering worst-case fault current for all fault locations using equation (3.7).

CASE I : When DG set is not present.

$$\begin{aligned}\mathrm{MIN}\,(z) = {} & \frac{3X1}{\log\left(\frac{6.01}{Y1}\right)} + \frac{3X2}{\log\left(\frac{2.52}{Y2}\right)} + \frac{3X3}{\log\left(\frac{6.01}{Y3}\right)} \\ & + \frac{3X4}{\log\left(\frac{2.52}{Y4}\right)} + \frac{3X5}{\log\left(\frac{5.05}{Y5}\right)} + \frac{3X6}{\log\left(\frac{3.35}{Y6}\right)} \\ & + \frac{3X7}{\log\left(\frac{1.66}{Y7}\right)} + \frac{3X8}{\log\left(\frac{6.86}{Y8}\right)} + \frac{3X9}{\log\left(\frac{8.64}{Y9}\right)}\end{aligned} \tag{3.11}$$

CASE II : When DG set is present.

$$\begin{aligned}\mathrm{MIN}\,(z) = {} & \frac{3X1}{\log\left(\frac{3.34}{Y1}\right)} + \frac{3X2}{\log\left(\frac{5.48}{Y2}\right)} + \frac{3X3}{\log\left(\frac{3.34}{Y3}\right)} \\ & + \frac{3X4}{\log\left(\frac{5.48}{Y4}\right)} + \frac{3X5}{\log\left(\frac{7.45}{Y5}\right)} + \frac{3X6}{\log\left(\frac{2.03}{Y6}\right)} \\ & + \frac{3X7}{\log\left(\frac{3.06}{Y7}\right)} + \frac{3X8}{\log\left(\frac{5.45}{Y8}\right)} + \frac{3X9}{\log\left(\frac{2.09}{Y9}\right)} + \frac{3X11}{\log\left(\frac{7.48}{Y11}\right)}\end{aligned} \tag{3.12}$$

Where, X1, X2…X11 = TMS VALUES

Y1, Y2... Y11 = PLUG SETTING VALUE

Equations (3.11) and (3.12) are subjected to considering minimum operating time as 0.2 seconds and CTI (Co-ordination time interval) = 0.3, assuming a 200:1 C.T. ratio to get current values of relays. Next, (3.11) and (3.12) have been minimized using constraints described as in (3.8). To prepare constraints, Table 3.1 has been used. The miscoordination for some DOCRs has been shown in Table 3.2, and the optimized result of PSM and TMS values using equations (3.11) and (3.12) is represented in Table 3.3.

TABLE 3.1
Description of Primary and Secondary Relays

Fault point	Without DG		With DG	
	Primary Relay	Backup Relay	Primary Relay	Backup Relay
A	1	9	1	9
	2	3	1	4
	2	6	1	7
	NA	NA	2	11
B	3	9	3	9
	4	1	3	2
	4	6	3	7
	NA	NA	4	11
C	5	1	5	11
	5	3	6	8
	5	9	6	9
	6	8	NA	NA
D	8	9	8	9
	7	1	8	2
	7	3	8	4
	NA	NA	7	11

TABLE 3.2
Mis-coordination of DOCR Relays

Backup Relay	Primary Relay	Constraint
1	9	-0.80374
3	9	-0.45497
5	9	-0.26218

TABLE 3.3
Optimized Value for TMS and PSM

Relay Number	TMS and PSM Without DG		TMS and PSM With DG	
	TMS	PSM	TMS	PSM
1	0.137	0.91	0.440	0.964
2	0.291	0.80	0.141	0.80
3	0.137	0.91	0.411	1.046
4	0.258	0.91	0.414	0.80
5	0.326	0.804	0.163	0.841
6	0.196	0.919	0.320	1.047
7	0.226	0.828	0.343	0.80
8	0.154	0.827	0.350	0.935
9	0.064	0.968	0.050	0.80
11(DG)	NA	NA	0.065	0.80
Objective function value	9.237		13.475	

3.5.2. FCL Value Calculation

DOCRs coordination can be restored by incorporating FCLs in series in the power network. Hence, two FCLs, i.e., FCL_1 and FCL_2, have been used after the main Generator and the DG set, respectively. The optimized values of FCLs were calculated using GA and are shown in Table 3.4. In this method, all topologies were considered to calculate constraints for different scenarios. After finding the optimized FCL values, FCLs that help restore DOCR coordination in the power system were grouped together. Then, after identifying the network topology through the Topology Processor, signals were sent to the processing unit to activate or deactivate the appropriate FCLs. Again, using an adaptive protection scheme, time for optimized operation of relays has been obtained and is shown in Table 3.5, where t1, t2…tn correspond to the time of operation of relays related to the corresponding CBs.

TABLE 3.4
Optimized values of FCL in pu.

	First Group	Second Group
FCL_1	1.4	1.523
FCL_2	Not Required	2.463

TABLE 3.5
Optimized values of time after installing FCLs

Time of operations of relays	Without DG set	With DG set
t1	3.568	0.858
t2	0.551	2.51
t3	3.111	0.793
t4	0.81	2.564
t5	0.681	1.979
t6	3.315	0.967
t7	1.823	1.373
t8	0.805	1.396
t9	3.887	3.692
t11(DG)	NA	3.181

3.6. Conclusions

In this work, the impact of Distributed Generation (DG) on relay coordination has been addressed by optimizing the PSM and TMS values using a Genetic Algorithm (GA). Fault currents were simulated at different fault locations, revealing instances of relay mis-coordination, as shown in Table 3.2. These mis-coordination problems were successfully solved through GA optimization, with the optimized PSM and TMS values presented in Table 3.3. Additionally, Fault Current Limiters (FCLs) were used to reduce the short-circuit level by adding impedance into the network, which helped restore relay coordination. The objective function was optimized using MATLAB to reduce mis-coordination, and the best values of FCLs were also calculated**.** The GA-based relay coordination scheme demonstrated methodological feasibility but within a constrained scope. Validation was limited to a 3-bus test system chosen for clarity and computational tractability. Relay parameter ranges, including Plug Setting Multiplier (PSM) and Time Multiplier Setting (TMS), were bounded heuristically rather than systematically optimized. Future extensions should involve scaling the method to IEEE benchmark networks, conducting optimizer benchmarking, and evaluating FCL practicality under real-world conditions.

Chapter 4

Smart Real Time Hybrid Power Factor Selection-Based Energy Management System

4.1. Introduction

Energy demand in daily life across the globe has raised serious concern among researchers regarding better Energy Management Systems (EMS). In this context, there is a need to find a way to manage domestic electric energy consumption to embrace sustainability with energy generation. While resilient protection strategies are essential for ensuring stability and fault tolerance in distributed generation (DG) and smart grid networks, the effectiveness of DG integration also depends on how intelligently the generated energy is managed at the consumer end. Therefore, the focus extends towards smart control mechanisms such as hybrid power factor selection–based EMS, which enable optimal utilization of DG resources, improve demand-side efficiency, and enhance overall system sustainability. Advanced Metering Infrastructure (AMI) and load monitoring systems are becoming increasingly important for household energy management [192–193]. Effective implementation requires identifying high-consumption and potentially unsafe appliances by measuring real-time power usage at variable frequencies. This calls for an advanced energy measurement system with an integrated safety detection module [194–195]. Analyzing the collected data enables faulty device detection and supports better control actions, helping users optimize appliance use and reduce energy consumption [196]. Such real-time monitoring improves efficient demand-side management [197]. According to [198], Gunawan et al. employed a high-sampling-rate method for true power calculation to determine the Power Factor (PF). This approach requires significant computational power and hardware space, making it relatively complex for real-time monitoring with frequency variations. Additionally, Ibraheem Al-Naib et al. [199] implemented a PF determination algorithm using a pure Zero Crossing Detector (ZCD)-based method with optimized hardware for true power monitoring. In [199], the analog voltage and current signals were converted into digital waveforms and XOR-ed using a microcontroller program. The time delay between their rising edges was measured using the micros() function (an internal Arduino library function), which returns the elapsed time in microseconds. This delay was then used to calculate the phase difference and the corresponding PF. However, this function becomes unstable and inaccurate within the commercial frequency range (~50Hz or ~60Hz), making the pure ZCD algorithm unsuitable for real-time power monitoring across the entire range of supply frequencies in household and commercial applications.

These challenges can be addressed by implementing an efficient real-time power monitoring selection algorithm that balances accuracy with hardware complexity. This paper proposes a hybrid PF selection algorithm (HPFSA) that enables frequency-resilient load monitoring while reducing hardware requirements.

4.2. Challenges in Microcontroller-Based EMS

Microcontroller-based energy management systems (EMS) have become low-cost solutions for real-time monitoring, control, and optimization of distributed energy resources (DERs), particularly in residential and small-scale embedded applications. Although their use is growing because of low cost, simple programming, and easy modular interfacing, several technical and operational challenges still restrict their scalability, accuracy, and reliability in changing power environments.

i) Limited Precision in Timing and Measurement

Most EMS implementations rely on 8-bit or 16-bit microcontrollers such as the ATmega328P, commonly used in Arduino-based platforms. These controllers provide limited timing resolution (about 4–8 μs using functions like micros()), which reduces the accuracy of zero-crossing detection (ZCD) in PF estimation algorithms. As grid frequency increases, even small timing jitters cause large phase angle errors, which seriously affect displacement power factor (DPF) estimation. This issue becomes especially critical near the 50 Hz nominal frequency, where sensitivity to deviations rises sharply [200].

ii) Inadequacy for Harmonic-Rich Loads

Standard microcontroller-based EMSs typically measure apparent and active power using simple sampling or timing-based methods without performing spectral analysis. This works well for linear loads but causes errors in nonlinear systems such as LED drivers, SMPS, and inverter-fed equipment. These loads produce significant current harmonics, causing the true power factor (TPF) to differ from the measured displacement power factor (DPF).

Without harmonic decomposition techniques such as FFT or wavelet transforms, which are too computationally demanding for basic MCUs, accurate power quality analysis is not possible [200], [202].

iii) Static Thresholding and Lack of Adaptivity

In many embedded EMS implementations, thresholds for control logic (such as PF correction switching or load shedding) are fixed based on initial testing. In the HPFSA framework, for example, a fixed threshold frequency (49.5 Hz) is applied to switch between ZCD-based and load-analysis-based PF computation. While this is experimentally valid for a specific test set, such static logic fails to account for changing loads, grid fluctuations, or environmental noise. Adaptive thresholding or self-calibration has not been widely explored in low-cost EMS designs [200].

iv) Limited Multi-Channel Capability and Isolation

Conventional microcontroller boards offer only a limited number of analog input channels (e.g., six in Arduino Uno) and do not provide true galvanic isolation between input sensors and digital processing stages. This restricts the number of loads that can be monitored at the same time and increases the risk of electrical interference or safety hazards. Some systems use external PF transducers with analog voltage outputs (0–5 V or 4–20 mA), but these also have limited resolution and depend on accurate scaling and calibration [202].

v) Regulatory and Standards Compliance

Most microcontroller-based EMS designs, especially in academic or prototype environments, do not fully comply with grid standards such as IEEE Std 1547.2-2023. These standards set strict requirements for voltage and frequency measurement, accuracy, communication latency, and DER interoperability. For example, frequency detection must achieve ±0.1 Hz resolution within the 49.0–51.0 Hz range to ensure reliable grid operation [203]. Meeting this requirement with low-cost microcontrollers requires accurate hardware design, stable clock signals, and advanced filtering techniques, which are often missing in typical setups.

4.3. Experimental Set-Up for Microcontroller Based EMS

In this study, a cost-effective energy management system was developed and tested in a laboratory environment. The system comprises an ATmega328P-based Arduino microcontroller (with accuracy (±0.1 Hz within the 47–65 Hz range) and Timing Resolution: 4 µs (based on 16 MHz system clock)), five current sensors (ACS712-5AT), a voltage sensor (ZMP101B), a 16×2 LCD, and an ESP8266 (NodeMCU V3 with CH340 chip) module. Each current sensor is dedicated to an individual appliance, enabling real-time current measurement across five loads. The voltage sensor captures the system voltage, and both current and voltage data are processed by the microcontroller. For remote monitoring, the processed data are transmitted via the ESP8266 module and logged into a Google spreadsheet through an API, leveraging its built-in Wi-Fi capability. For industrial deployment, the STM32 Nucleo-32 board is a suitable alternative to Arduino Uno, offering a 72 MHz clock, 32-bit processing, and multiple ADC channels for higher execution speed and sensor scalability. In this work, the ACS712-5AT current sensor (5 A rating) and the ZMPT101B AC voltage sensor (250 V input, ~5 V output) were used for their compatibility and industrial-grade performance. Fig. 4.1 presents a schematic diagram of the developed power monitoring system, and Fig. 4.2 shows the actual hardware setup. As shown in Fig. 4.1, the system is equipped with current sensors that utilize a linear Hall circuit to sense the current. The sensed Hall voltage is expressed in (4.1).

$$V_H = (I \times B) / (n \times e \times t) \tag{4.1}$$

Where "V_H" represents the Hall voltage, "I" is the current flowing through the conduction path, "B" is the magnetic field strength, "n" is the number of charge carriers, "e" is the charge of an electron, and "t" is the thickness of the conductor. It should be noted that the final output voltage of the current sensor is the sum of the Hall voltage and the offset voltage. The output voltage is presented in (4.2).

$$V_{out} = V_{offset} + V_H \tag{4.2}$$

Where, "V_{out}" is the final voltage sensor output voltage and "V_{offset}" is the calibrated offset voltage.

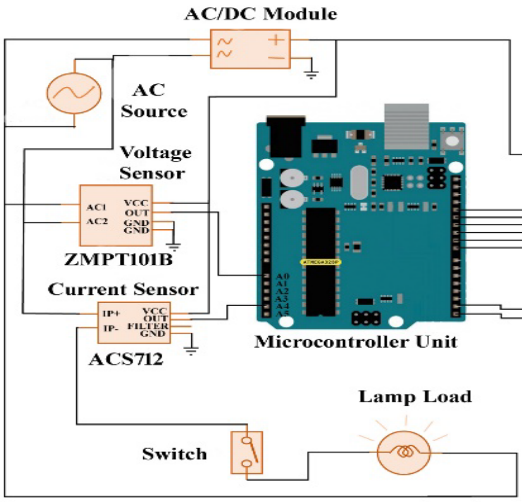

Fig. 4.1. Schematic diagram of the developed Energy Management System (EMS) for real-time true power calculation.

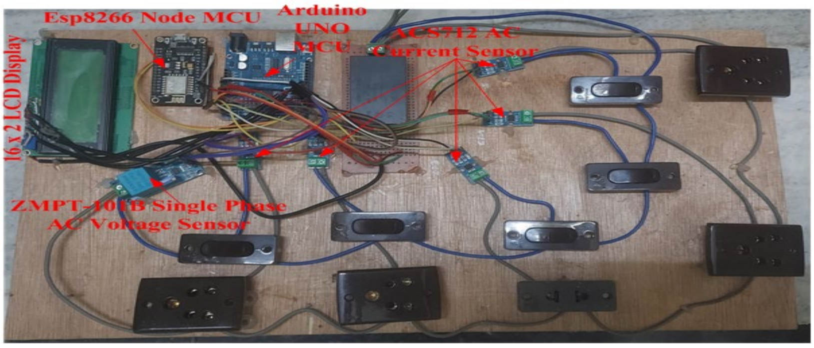

Fig. 4.2. Developed hardware-based power monitoring module developed in the laboratory.

According to (4.1), the sensor current has been modified and expressed in (4.3).

$$I_{sensor} = [((V_{out} - V_{offset}) \times n \times e \times t) / B] + V_H \tag{4.3}$$

Where, "I_{sensor}" is the sensor current, and "B" is the Magnetic field.

4.4. Proposed Methodology

Power factor (PF) estimation in embedded systems is highly sensitive to supply frequency variations, especially near the lower operational limit of 49.5 Hz. Experimental analysis on different load types revealed that PF deviations beyond this point exceed ±7%, making true power estimation unreliable. This threshold also aligns with recent under-frequency control schemes [201], reported performance degradation in low-cost APFC systems [202], and IEEE Std 1547 recommendations to maintain frequency detection accuracy within ±0.1 Hz [203]. Hence, a frequency-aware PF tracking mechanism is essential to ensure accurate load monitoring under variable grid conditions. Since true power depends on PF, which fluctuates with input frequency (due to PF calculator performance variations), an efficient load monitoring system is required to capture PF fluctuations and keep true power independent of input frequency. In this section, the proposed HPFSA is introduced along with its key characteristics. The proposed HPFSA algorithm is designed for power monitoring in systems with predominantly linear and non-linear loads with low Total Harmonic Distortion (THD). In HPFSA, the threshold frequency ($f_{threshold}$), which varies for different load types, plays an important role in deciding the switching mechanism between the two PF evaluation processes. Therefore, a threshold frequency analysis was carried out for each load to determine $f_{threshold}$. In this process, a variable-frequency power supply was used, and a frequency sweep was performed from 45 to 65 Hz (with a step size of 0.5 Hz) for a particular load. Each frequency sample was held for a time period “Thold” (60 s in this work). During this Thold interval, the absolute error for the load at each timestamp was calculated using (4.4). For that specific load, the RMS value of the absolute error (from (4.4)) was then computed using the time window (Thold) through (4.5), and the cumulative average RMSE value was calculated using (4.6) by averaging the RMSE across the three loads.

$$E_{load}^{t}(\%) = \frac{|Theoretical(PF) - Measured\,(PF)|}{Theoretical(PF)}\,x\ 100 \qquad (4.4)$$

$$E_{load}^{RMS}(\%) = \sqrt{\frac{\sum_{t=1}^{T_{hold}}(E_{load}^{t})^2}{\mathrm{T_{hold}}}} \qquad (4.5)$$

$$E_{Avg}^{RMS}(\%) = \frac{\sum_{j=1}^{3}(E_{load}^{RMS})_j}{3} \qquad (4.6)$$

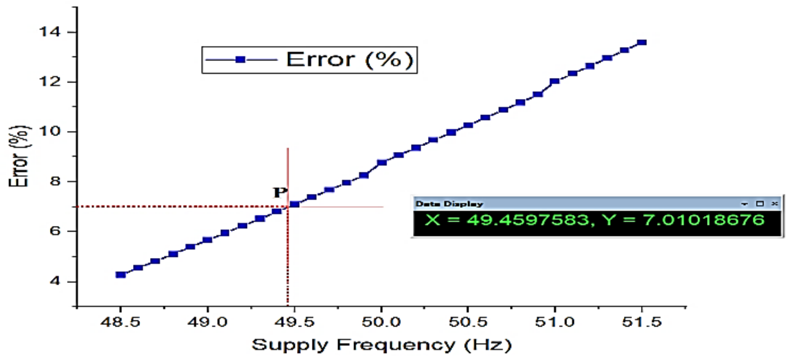

Fig. 4.3. PF computation error plotted against input supply frequency using the ZCD method. The error increases rapidly beyond ~49.5 Hz, indicating instability in PF estimation at higher frequencies

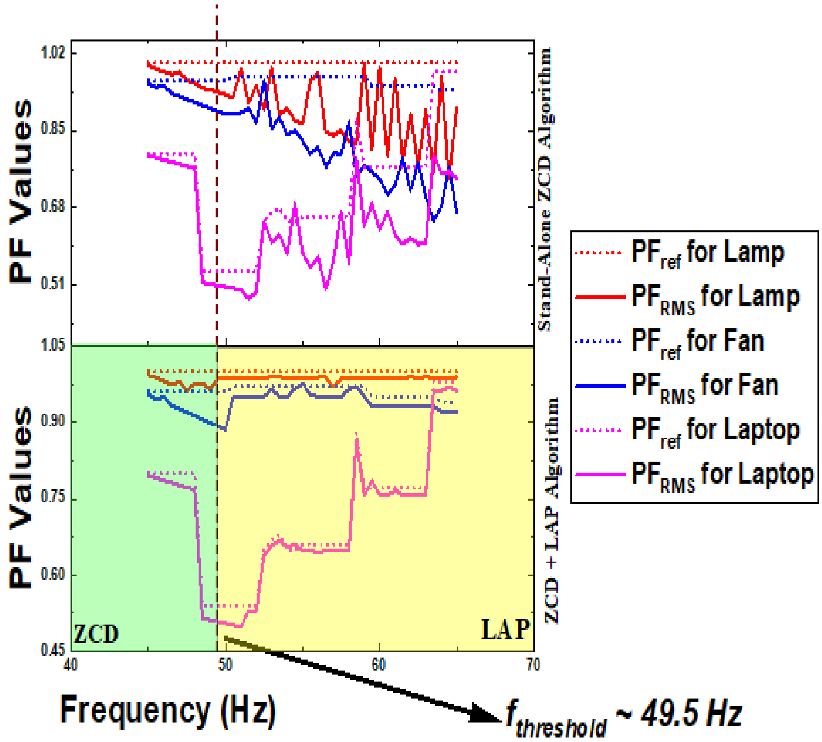

Fig. 4.4. Threshold Frequency Analysis Process of the proposed HPFSA.

The cumulative average RMSE–frequency plot is shown in Fig. 4.3, with a limited frequency range since no significant results were found beyond it. Fig. 4.4 shows the observed PF variation along with its alignment with PF_{ref} variation for three loads, using both the stand-alone ZCD and the HPFSA algorithms. The plots (Fig. 4.3 and 4.4) show that below ~49.5 Hz, the PF error stays within the acceptable margin of 7%, and phase jitter is minimal. When the supply frequency exceeds 49.5 Hz, PF error and fluctuation increase significantly across all three loads (resistive, inductive, and nonlinear, under constant load conditions), as shown in Table 4.1. Therefore, 49.5 Hz was chosen as the threshold frequency ($f_{threshold}$) in this study. To maintain PF accuracy and reduce error beyond this threshold, a high-frequency PF computation mechanism is required. Accordingly, a Load Analysis Process (LAP) block was introduced, employing a multiplication and integration-based approach for PF calculation in the higher frequency range. This mechanism ensures stable and accurate real-time power monitoring.

Table 4.1

Different Parameters for Various Loads

Load	Power (W)	Nature	Observed $f_{threshold}$ (Hz)	Execution time for ZCD (stand-alone)	PF Error Range (Below $f_{thresold}$)	PF error after $f_{threshold}$
Incandescent Lamp	60	Pure Resistive	~50.5	High	< 6.5%	Linearly increases
Pedestal Fan	70	Inductive (Motor Load)	~49.5	Moderate	< 6.8%	Linearly increases with some kink points
Laptop Charger Adapter	65	Nonlinear (SMPS-based)	~48.8	Low	< 6.2%	Non-linearly increases

To enhance performance across varying frequency ranges, the proposed system hybridizes the ZCD-based and LAP-based PF determination techniques, resulting in an efficient and adaptive real-time power computation algorithm.

Fig. 4.4 shows the RMS PF values in the threshold frequency ($f_{threshold}$) window of three loads versus input frequency to confirm the $f_{threshold}$ identified in Fig. 4.3. The upper subplot uses only the ZCD algorithm, while the lower subplot uses the hybrid HPFSA. The frequency sweep and hold procedure is the same as in Fig. 4.3. Up to about 49.5 Hz, PF varies smoothly for all loads with errors below 7%. Beyond this point, PF oscillations and error magnitudes increase sharply, confirming 49.5 Hz as the $f_{threshold}$. Hence, the proposed HPFSA performs better than the stand-alone ZCD algorithm, and the $f_{threshold}$ obtained from Fig. 4.3 is validated. In the full setup of the proposed algorithm, the MCU first determines the $f_{threshold}$ by connecting the load to a variable-frequency supply, using known PF values (from datasheets or a meter), and running an error detection routine to find the point where PF error remains within preset limits. Once this point is found, the variable supply is disconnected, and the load is switched to household mains. The MCU then measures the actual input frequency (based on the time interval between voltage and current zero crossings). If the frequency is below the threshold, the ZCD routine computes PF; if above, the MCU switches to the LAP routine. In either case, the resulting PF is then used for the true power calculation. The pseudocode of the proposed HPFSA algorithm is shown in Fig. 4.5.

Algorithm 1: Pseudo Code for Frequency Resilient HPFSA Algorithm

Input: *Voltage signal V(t), Current signal I(t),* PF_{ref}
Output: *Real Time True Power*
Computation of V_{RMS} *and* I_{RMS} *internally from V(t) and I(t);*
$RMSE = 0$;
1. Connecting the load to the system;

while $RMSE \leq 7\%$ **do**
  Load remains connected with VFPS;
  Tuning the load for time T_{hold} *with each frequency step;*
  Computing input supply frequency;
  Computing the PF at each time stamp with stand-alone ZCD algorithm;
  $e \leftarrow (PF(t)_{\text{computed}} - PF_{\text{ref}})$; **PF(t) :- PF at time stamp "t"**
  $RMSE \leftarrow \sqrt{\frac{\sum_{t=0}^{T_{\text{hold}}} e^2}{T_{\text{hold}}}}$;
end
2. $f_{\text{threshold}} \leftarrow$ *Tuned frequency where RMSE reaches 7%;*
while *!VFPS disconnected from load* **do**
  Waiting for disconnection;
end
3. Connecting the load with household power source point;
4. Computing the input supply frequency (f);

if $f \leq f_{threshold}$ **then**
  Executing ZCD algorithm;
  $PF \leftarrow PF_{\text{ZCD}}$; **Comment -** *Switching to ZCD computation routine*
else
  if $f > f_{threshold}$ **then**
    Executing LAP algorithm;
    $PF \leftarrow PF_{\text{LAP}}$; **Comment -** *Switching to LAP computation routine*
  end
end
5. $Power_{\text{true}} \leftarrow V_{\text{rms}} . I_{\text{rms}} . PF$;

Fig. 4.5. Pseudocode of the proposed algorithm. The algorithm dynamically selects between ZCD-based and LAP-based computation methods based on input supply frequency

4.4.1. Load Based Power Factor Computation

In this method, the MCU samples the voltage and current signals at 1 kHz (samples per second), which provides better accuracy while keeping the computational load optimized. Experimental results show that when the sampling frequency is increased beyond 1 kHz, accuracy decreases, and the computational load increases. In this process, each voltage sample is multiplied by its corresponding current sample. The resulting products are summed, and the result is divided by the signal's period to obtain the true power (P_{true}). The mathematical representation of this process is given in (4.7).

$$P_{true} = \sum_{T} (V_k \times I_k) / T \tag{4.7}$$

Here, "T" represents the signal time period, while "V_k" and "I_k" are the "k^{th}" voltage and current samples, respectively. Again, captured RMS values are used to compute the apparent power (P_{app}) using (4.8).

$$p_{app} = V_{rms} \times I_{rms} \tag{4.8}$$

Where, "Vrms" and "Irms" are the RMS voltage and current values, respectively. Finally, by utilizing the apparent and true power, the microcontroller calculates the PF value through (4.9). The complete flowchart of the LAP is shown in Fig. 4.6.

$$PF = P_{true} / P_{app} \tag{4.9}$$

In Fig. 4.6, T is the time period of the signals, "V_{rms}" and "I_{rms}" are the RMS voltage and current values, respectively, "LTS" is the Latch Controlling Signal, and "CS1,2,3,4" are the control signals used to operate switches "S1,2,3,4" for proper data flow paths. The voltage and current buffers store the voltage and current samples fetched from the sensors. During the first "T" cycle, the MCU fetches the voltage and current signals from the sensors and stores them in the corresponding buffers (20–25 AC cycles per interval). Initially, switches S1 and S2 are opened, allowing the MCU to multiply the buffered voltage and current samples and store the result in a latch. The MCU then waits for 1 ms, after which the switches are closed. After another 1 ms, the MCU fetches new voltage and current samples, stores them in the buffers, and reopens the switches. The new samples are multiplied and added to the previous latch value, updating it accordingly. This sampling and accumulation process continues throughout the first "T" cycle. In the next

"T" cycle, switches S1 and S2 remain closed while S3 and S4 open, sending the buffered data to the RMS calculator for further processing.

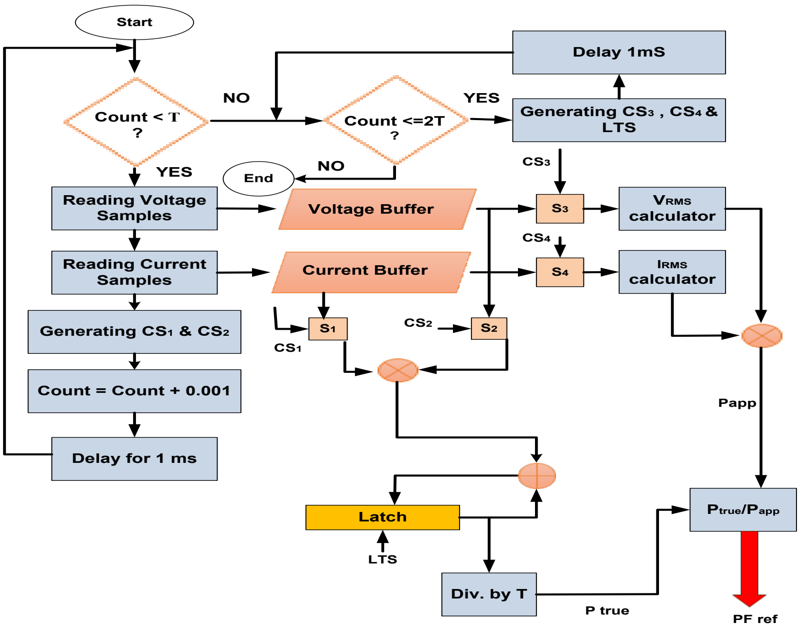

Fig. 4.6. Flowchart of the Load Analysis Process (LAP) used for PF computation.

4.4.2. Zero-Crossing Detection Logic

As mentioned earlier, the pure ZCD technique for PF measurement is not implementable for real-time monitoring due to its instability within the entire range of commercial frequencies. However, before the $f_{threshold}$, ZCD performs well. The flowchart for the ZCD mechanism of PF determination is detailed in [199].

4.5. Results and Discussions

After incorporating the HPFSA approach, the efficiency of the PF computation has been enhanced, making it feasible for real-time monitoring by optimizing the hardware space and computational accuracy.

TABLE 4.2
Performance Comparison of Pf Values

Loads	Std. PF	Ref	Proposed PF calculation method	MAE	RMSE
Lamp	1.00	[204]	0.97 – 0.99	1.77 %	0.66 %
Fan	0.94 – 0.97	[205]	0.96	1.1 %	0.3 %
Laptop	0.53-0.99	[206]	0.52 – 0.97	12.89 %	7.6 %

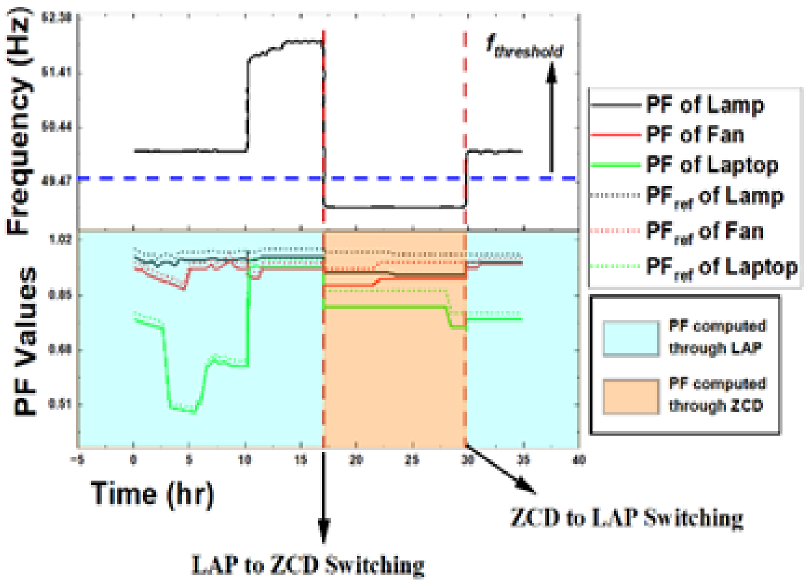

Fig. 4.7. Time Series Plot for Frequency Variation and its corresponding PF fluctuation, by taking a real-time case study.

Table 4.3
Performance Comparison with Existing Work

Refs	Loads	Hardware Complexity	PF Accuracy	Computational power
[198]	Lamp	Moderate	High	Moderate
	Fan	Moderate	High	Moderate
	Laptop	High	Moderate	High
[199]	Lamp	Low	Moderate at high frequency and high at low frequency.	Low
	Fan	Moderate	Low at high frequency and moderate at low frequency.	Moderate
	Laptop	Moderate	Extreme low at high frequency and moderate at low frequency.	Moderate
This work	Lamp	Moderate	High	Moderate
	Fan	Moderate	High	Moderate
	Laptop	Moderate	Moderate	Moderate

In this study, the term 'efficiency' refers to the system's ability to calculate PF accurately with low processing effort and reduced hardware cost. This is achieved by adaptively applying either a lightweight ZCD method or a more precise LAP method, depending on the input frequency. 'Adaptability' denotes the system's ability to dynamically switch between the two algorithms to maintain PF accuracy across a wide range of supply frequencies, as shown by the error behavior in Fig. 4.3. By connecting the selected test loads in the prototype and applying the proposed PF computation method, the PF values were extracted and compared with the standard PF values of the loads to calculate statistical deviations, as presented in Table 4.2. Table 4.2 clearly demonstrates the efficiency of the proposed method. A comprehensive comparison of the proposed model with existing models has also been made in terms of hardware cost, accuracy, and computational power, as shown in Table 4.3. Fig. 4.7 shows the system's response to real-world frequency fluctuations recorded from a nanogrid [207]. The upper subplot shows the grid frequency, while the lower subplot shows the corresponding power factor (PF) of each load. During LAP operation, the PF error remained within 2–3%, whereas during ZCD operation, it stayed below 7%. Overall, the proposed HPFSA significantly suppresses PF fluctuations while keeping deviations within the acceptable 7% limit.

4.6. Conclusions

In this work, a frequency-resilient HPFSA is proposed for accurate PF calculation, enabling real-time power and energy monitoring with improved accuracy and stability across the full permissible supply frequency range. This algorithm is adaptive, balancing the ZCD-based method with the high-sampling-rate PF detection method depending on the input supply frequency. The proposed system architecture supports future integration with intelligent load analytics, particularly Non-Intrusive Load Monitoring (NILM) using Spiking Neural Networks (SNN), which can provide more hardware-efficient NILM implementations. Although the Embedded Management System, incorporating the Hybrid Power Factor Selection Algorithm (HPFSA), showed performance improvements, it also carried methodological limitations. The fixed switching threshold of 49.5 Hz has been derived from a threshold graph and restricted to under-frequency grid control mechanisms, which limit its generalizability across diverse grids and operating conditions. Moreover, the observation that accuracy declined above 1 kHz sampling was not fundamental but rather a limitation of the prototype microcontroller, which suffered buffer overflow and timing jitter under oversampling conditions. Future research should focus on adaptive thresholding, validation across multiple datasets, and detailed quantitative benchmarking to ensure robustness.

Chapter 5

Smart Metering and Data Infrastructure for Intelligent Energy Systems

5.1. Introduction

Although hybrid power factor selection enhances real-time EMS efficiency, its effectiveness in large-scale power systems depends on accurate metering, reliable communication, and intelligent data infrastructure. The major driver behind the development of smart energy grid systems was the blackout in Ontario, Canada, on 14th August 2003 [208]. Today, one of the leading examples of a smart grid is the Independent Electricity System Operator (IESO), Ontario's modern smart grid. A layout of Ontario's Grid is shown in Fig. 5.1.

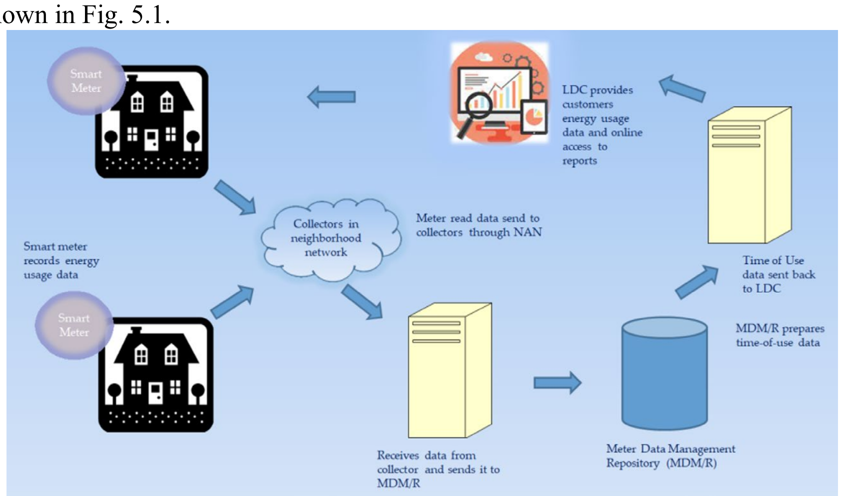

Fig. 5.1. Sample Layout of Ontario's AMI System.

Two-way data communication is regarded as extremely important for monitoring and controlling electricity usage. This type of communication not only helps in making better decisions but also enables the self-healing of the grid by supporting real-time decision-making during problems. According to [209], power demand is expected to rise by 150% to reach 53.6 billion MWh by 2050. This rising demand further increases the need for smart meters. However, with the existing AMI infrastructure, it is difficult to handle such a large volume of data, prevent theft securely through private networks, and process information using big data analytics. As highlighted in [210], nearly 700 million smart meters were installed worldwide in 2019 alone. Many of these smart meters can automatically provide real-time information about consumer load consumption, outage notifications, and power quality measurements.

In an AMI infrastructure, smart meters are installed at the consumer end and provide near real-time information on electricity usage, utility consumption, power quality, and tariffs. The data from these meters is delivered to the Local Distribution Company's (LDC) server through NAN. For further analysis, the collected data is sent to the grid's service provider and stored in MDM/R. According to the Edison Foundation, the 46 million smart meters installed in the United States alone generate about 1 billion data points per day [211]. This is a massive amount of information for the AMI system to handle. Therefore, improving the existing AMI infrastructure is essential to manage the growing data from smart meters.

In this study, recent developments in AMI infrastructures and their subcomponents, such as smart meters, NAN, and MDM/R, in smart grid technology have been discussed. Additionally, a new approach for MDM/R storage and repository services has been proposed to help consumers manage their electricity usage and control costs more effectively.

5.2. Components of AMI and Data Infrastructure

AMI stands for Advanced Metering Infrastructure. It includes Smart Meter, Advanced Metering Communication Device (AMCD), Advanced Metering Control Computer (AMCC), and Advanced Metering Regional Collector (AMRC) [212].

5.2.1 Smart Meters and Control Devices

5.2.1.1. Smart Meter

In the AMI system, the purpose of the smart meters is to transmit data over the network to the Data Collection System. The types of data that are transmitted through the smart meter are listed below.

i. Register Read: total/accumulated reading, starting from 0 on Day 1

ii. Interval Read: consumed energy over an interval of time, such as hourly usage

iii. Demand Read: maximum demand over an interval of time

iv. Events: set as flags for events such as power outage, test mode and tamper detection

5.2.1.2. Advanced Metering Communication Device (AMCD)

In the AMI system, each customer is assigned to a service delivery point (SDP), which is associated with its smart meter by its local distribution company (LDC). Again, in a multi-LDC environment, the interface that maps a particular LDC to its service delivery point is known as the Universal Service Delivery Point (USDP). The generation of USDP takes place in the MDM/R application, and responses are fed back to the LDC through the file transfer service (FTS) via LAN. Moreover, another communicating device inside the smart meter is AMCD, which stands for Advanced Metering Communication Device. The purpose of AMCD is to draw the total electrical energy by a residential house, a business, or an electrical device and transmit an amount of data to an Advanced Metering Control Computer (AMCC) [212].

5.2.1.3. Advanced Metering Control Computer (AMCC) and Advanced Metering Regional Collector (AMRC)

Another important component is AMRC, which means the Advanced Metering Regional Collector, is a sub-component of the AMI system responsible for collecting read data from Smart Meters and transmitting that same data to the AMCC.

AMCC retrieves temporarily stored data from meter reading and transfers that data to the MDM/R [212].

5.2.2. Information Flow and Meter Data Management/Repository (MDM/R)

5.2.2.1. Information Flow in AMI

In this section, information flow in the AMI system has been discussed. Information that gets stored in AMCC is used to detect maintenance and transmission level abnormalities and also to deliver reports on the general health of the AMI system to LDC, as shown in Fig. 5.2.

Under AMCC, web Services provides read-only access to LDCs or authorized agents for a Universal Service Delivery Point (USDP) for up to 100 days for the following purpose.

i. Quantity related to Billing
ii. Consumption data for Intervals (Time-of-Use only)

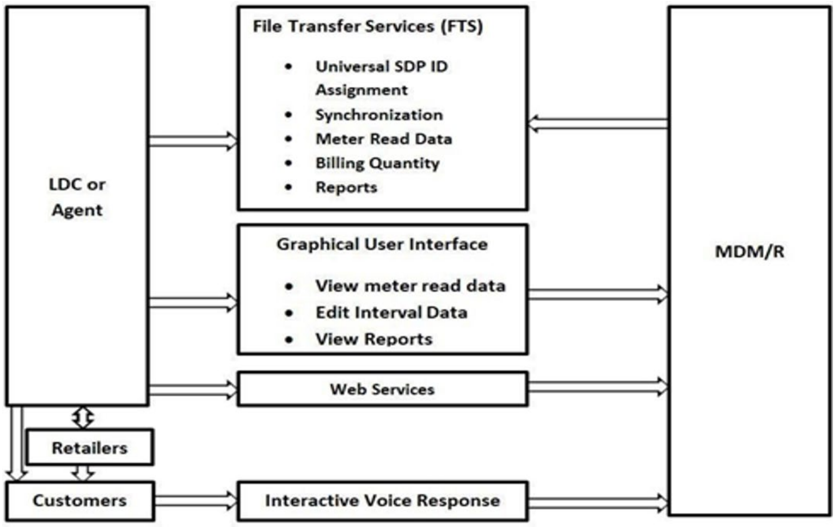

Fig. 5.2. Information Flow in AMI System.

In any metering and communicating infrastructure, there remains a gateway that monitors the transfer of data. WebSphere Partner Gateway (WPG) is a platform that helps MDM/R in business-to-business (B2B) transactions to transfer and translate files. This application provides a gateway between LDC and MDM/R for processing the data before it gets placed in MDM/R.

Meter read files from LDC and sent those files to WPG. Thereafter, from WPG, those files are copied to the FTS archive before sending them to the MDM/R system for processing. After processing, files get preserved in the MDM/R system, and those files are used for generating and sending reports to LDCs through WPG.

Modules/Applications involved in meter read processing are briefly described in the following.

• AMI Adapters: AMI adapters perform checking and parsing meter data from the meter read interface to MDM/R.

• Message Bus: This module acts as a channel for inter-process communication.

• Cleaner: This is a persistent multi-instance (meaning queues) application, used for processing and performing validations on raw data coming from smart meters into clean messages on the message bus.

• Validator: This module checks whether the data is valid or not like data with future dated is not valid so, this data is thrown as exception.

• Archiver: This module handles the things processed by validator and stores them.

• Framer: With the Framing process, interval data is assembled into Billing Quantities. Framing is a persistent single–instance application. It places intervals from smart meters read into Time-of-Use (TOU) bins, which are configured by the utility (LDC), and puts the data into different buckets, like peak data, mid-range data.

Moreover, Framer is classified into two types as stated in.

RTF (Real Time Framer): If the data can be processed in real time, it gets assigned to RTF.

PPF (Post Processing Framer): If the data cannot be processed at real time, then it is assigned to PPF, after putting the data in the database.

• AMI Database: Finally, the processed data is stored in the AMI Database.

*5.2.2.2. MDM/**R***

MDM/R is an important application in this two-way communication system. The duties performed in MDM/R are as follows.

• Once WPG validates meter read data from smart meters, MDM/R processes them in the advanced metering infrastructure.

• Consumers whose meter readings count for small volumes are transmitted as hourly data taken after the end of every hour. Generally, the demand is not monitored for small consumers every hour.

• Commercial & Industrial Consumers contribute meter reads in large volume, and the metering of load demand is needed. Meter readings are transmitted at an interval of five, fifteen, or sixty minutes, and data are taken at the end of each interval.

• Whether the correct data is coming through the AMI system to the MDM/R is being ensured by LDC.

• LDC determines and controls the use of Billing Quantity data supplied by MDM/R. Billing data is further required for preparing the billing report.

• The MDM/R processes Meter Read data files in AMCC formats, which are deployed in the Grid in a uniform format with respect to each AMCC technology.

• A relationship between Meter ID and SDP needs to be established. Hence, the MDM/R meter directory (MMD) can receive data. Meters with no SDP assigned cannot deposit data to MMD, and it is only possible after LDC establishes a relationship between the meter ID and SDP.

- Billing Quantities are framed on a daily basis and occur within calendar (EST) days.
- Response of billing quantities includes the first read of the interval of the first period of daily read data to the last interval of the last period of daily read data.
- LDCs frame billing quantity data as TOU, which gets delivered as TOU consumption data for the time period.
- LDCs frame SDPs on a Hourly basis as spot pricing. Billing data of consumption gets delivered as Hourly data of consumption corresponding to each day

5.3. AMI Protocols and Security

MDM/R uses File Transfer Services (FTS) and web service protocols for file transactions. For transferring large files in a business-to-business model, FTS is used between the LDC and MDM/R**.** The purpose of web services is to provide read-only access to LDCs and billing agents [213].

FTS commonly uses the Applicability Statement 2 (AS2) protocol. AS2 supports a feature called Message Disposition Notice (MDN)**,** which sends a confirmation back to the sender**.** The MDN is used by MDM/R and FTS to inform users about the file processing status**,** and its format varies depending on the AS2 package.

Before transmitting files to MDM/R, they must be digitally signed as explained in [214, 215]. A mutually authenticated SSL connection is used to send the signed files, allowing the sender and receiver to verify each other's identities**.** Self-signed digital certificates must be exchanged between the application server and MDM/R for SSL encryption and digital signatures.

The following types of certificates are generally used for secure transfer [216].

- Self-Signed Certificate: This type of certificate is generally issued by individual LDCs.
- Root CA Certificate: This type of certificate is common for all LDCs and can be issued by the IT service provider of the grid itself.

5.4. Application of AMI and Data infrastructure

5.4.1 Load Forecasting and Demand-Side Analytics

In any power system, load forecasting is essential to match supply with demand and to avoid disturbances in the grid. To successfully forecast a day's demand, historical time-series data of consumer load consumption for the same group of users should be available. A key role is played by smart meter data stored in the MDM/R at specific intervals. The combination of real-time load consumption data from meters and the historical database provides accurate predictions for supply and demand [217, 218].

The real-time TOU (Time-of-Use) data from the AMI system, displayed on the consumer's graphical web portal or smart meter interface, helps consumers schedule their smart appliances at suitable times of the day, as shown in Fig. 5.3 [211].

This helps the grid to maintain a flatter load curve through peak-clipping and valley-filling. Demand-side management of energy consumption during peak and off-peak hours in real time supports both grid stability and cost savings.

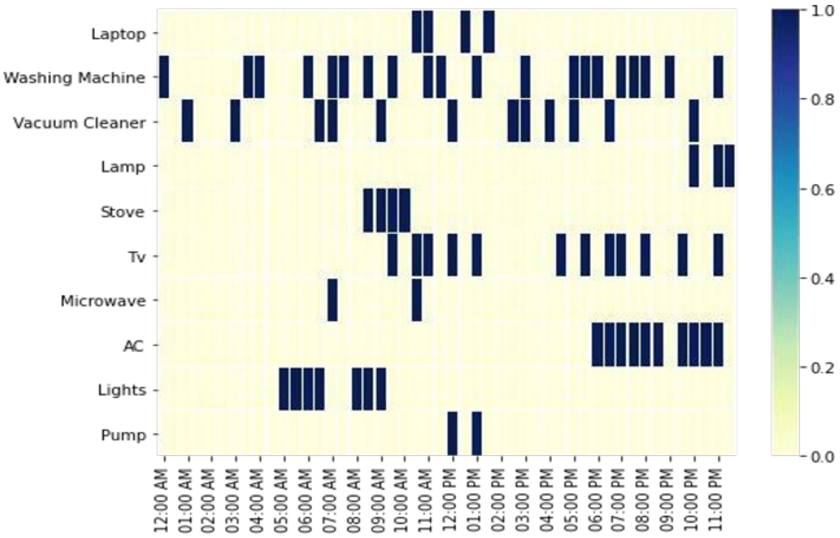

Fig 5.3. Appliance Scheduling Optimization based on TOU Data [211, 219 - 220].

An energy audit is the first step in understanding how energy is used, which in turn helps identify losses during transmission and distribution. It can also help prevent energy theft and tampering of energy data.

An energy audit report helps commercial and industrial consumers identify the costs and benefits of adopting energy-efficient measures and energy-management practices, as discussed in [221]. Everyone associated with the electrical system can benefit from efficient energy use. Participation in energy-efficiency programs helps reduce the demand for new power plants and transmission lines, thereby lowering the need for new investments, as highlighted in [222]. Another advantage of energy efficiency is that it helps businesses and communities compete more effectively—not only through cost reductions but also through broader benefits. Improved energy management methods can help organizations save money while also enhancing productivity, workplace safety, and overall performance.

5.4.2 AMI Integration with Smart Energy Systems

In this section, based on the AMI infrastructure, a networking framework has been proposed for monitoring and billing appliance-level data through the Meter Data Management and Repository (MDM/R). In a conventional AMI system, each customer is assigned a unique ID called a Service Delivery Point (SDP). Metering systems are usually installed by Local Distribution Companies (LDC) at this service point. In this work, a unique ID is also assigned to each appliance, known as an Appliance Level Delivery Point (ALDP), which acts as a subset of the consumer's SDP ID. The Advanced Metering Communication Device, implemented using an IoT-enabled ESP8266 module, transmits appliance-level energy consumption data to the Advanced Metering Control Computer (AMCC) for storage. Another important function of the AMCC is to detect abnormalities in the transmission level. The flow of the collected data in AMI is illustrated in Fig. 5.4.

.

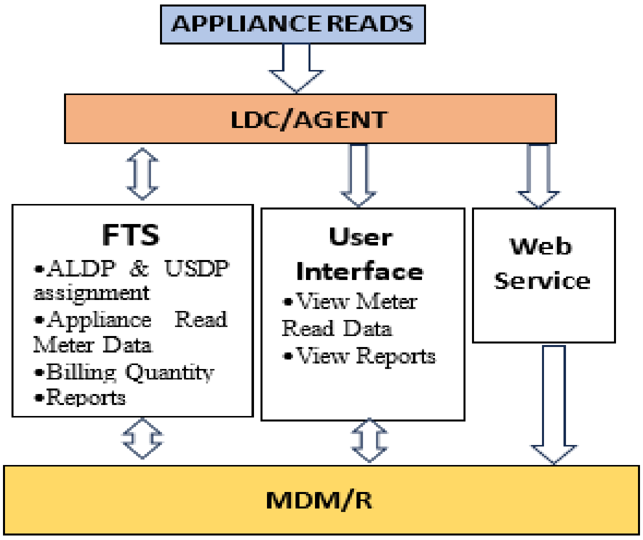

Fig. 5.4. Data Flow in AMI.

From Fig. 5.4, appliance readings are transmitted to MDM/R through the LDC, followed by the WebSphere Partner Gateway (WPG), which mainly manages business-to-business file transactions. This file transfer takes place using various protocols, such as the applicability statement defined by the File Transfer Service (FTS). MDM/R is primarily responsible for processing register reads, interval reads (data collected over specific time intervals), generating reports, and maintaining Service Level Agreements (SLA). The proposed sensing method (described in Chapter 4) ensures that appliance-level energy consumption related to USDP is recorded in MDM/R. Domestic consumers provide hourly data to MDM/R because their consumption volumes are small. However, for commercial and industrial customers, meter readings are taken every five or fifteen minutes, depending on the level of consumption [222]. For any missing data not transmitted to MDM/R, the system alerts the corresponding LDC and requests retransmission of the missing files. After this, billing reports are generated under the supervision of the LDC, which may vary from one LDC to another. Finally, appliance-level billing reports that reflect grid conditions are delivered to end customers based on Time-of-Use (TOU) tariffs.

5.5 Conclusions

This study focuses on how a smart grid communication network works, and how technologies such as AMI and MDM/R support the optimization of electricity use and management. For this purpose, recent developments in AMI infrastructures and their subcomponents, such as smart meters, Neighborhood Area Networks (NANs), and MDM/R, have been discussed. From the discussion, it can be seen that with the advent of the AMI system, the network topology has become highly complex and harder to manage and maintain communication. With the increasing demand for electrical energy, it can be concluded that in the future, the integration of renewable energy with conventional energy will become a routine practice. Moreover, in the AMI system, data flows from the end user to the management server through different file management services and a network gateway. This process helps maintain grid reliability. Nowadays, as the grid becomes more digital, the risks of data tampering and theft also increase. Therefore, this article highlights the importance of using several security protocols [223] to ensure secure data transmission between parties. Furthermore, this study proposes end-to-end encrypted communication as a solution to these security challenges, which is essential for any digital grid to operate in a smarter and safer way.

Chapter 6

Conclusions & Future Work

6.1. Conclusions

In this thesis, a comprehensive framework has been developed to address multiple challenges in advanced monitoring and control of Li-ion battery-integrated smart energy systems. This objective is achieved by investigating embedded-level diagnostics, coordinated protection, and intelligent metering strategies that enhance the safety, stability, and reliability of energy networks using Li-ion batteries. A detailed literature review is presented in Chapter 1, highlighting key challenges such as thermal instability, unreliable protection in DG-integrated systems, and limited control intelligence at the edge level.

To address these challenges, an internal resistance-based early sensing method for thermal runaway detection is proposed and implemented on a microcontroller platform. The embedded implementation has been validated for real-time use and fault detection capability, as discussed in Chapter 2. Chapter 3 introduces a GA-based coordinated protection scheme for distribution networks with DG integration, incorporating fault current limiters (FCLs) to improve selectivity, minimize tripping errors, and maintain relay grading margins. Simulation studies were carried out to evaluate system resilience under fault conditions and optimize coordination time intervals.

Chapter 4 presents the design of a microcontroller-based real-time energy monitoring platform capable of tracking power factor and frequency variations under hybrid load conditions. This system effectively identifies threshold frequency zones for different load types, thereby enabling better energy quality control in embedded applications. Chapter 5 discusses the integration of advanced metering infrastructure (AMI) and embedded control mechanisms for data-driven energy flow management. The architecture leverages smart meter intelligence and relay actuation to enable decentralized decision-making for power distribution and fault isolation.

Altogether, the thesis establishes an integrated control and monitoring platform where battery diagnostics, distributed energy control, and smart protection schemes operate together in a unified embedded ecosystem. The findings and experimental validations presented across the chapters reinforce the thesis premise and provide a clear roadmap for intelligent Li-ion battery integration in modern smart grids.

6.2 Scope of the Future Works

While this thesis has demonstrated proof-of-concept contributions in IR-based diagnostics, relay protection, EMS optimization, and AMI integration, the findings are subject to several limitations. Internal resistance values were estimated using short idle OCV methods, which introduce bias and occasional low outliers. Protection strategies were validated on a 3-bus system, and scalability to larger networks was not tested. The HPFSA framework employed a fixed switching threshold and prototype hardware with sampling constraints, limiting generalization. Integration into AMI was conceptual and lacked pilot-scale security validation. Finally, all experiments were conducted at laboratory scale on single cells and small networks; industrial-scale validation remains future work. These limitations frame the scope of the contributions and highlight avenues for further research.

To strengthen and extend the outcomes of the present work, the following future research directions are proposed:

- Integration of electrochemical–thermal coupled models to improve early fault prediction in Li-ion batteries under dynamic loading and varying environmental conditions.

- Use of data-driven and AI-based methods to enhance fault classification and state estimation through internal resistance and frequency-based monitoring parameters.

- Design of scalable embedded diagnostic units to support peer-to-peer coordinated energy sharing in distributed smart grid frameworks.

- Incorporation of wireless communication protocols (e.g., LoRa, ZigBee) with AMI-enabled battery systems for decentralized monitoring and remote protection control.

References

[1] G. Zubi, R. Dufo-López, M. Carvalho, and G. Pasaoglu, "The lithium-ion battery: State of the art and future perspectives," *Renewable and Sustainable Energy Reviews*, vol. 89, pp. 292–308, 2018.

[2] J. Li, C. Daniel, and D. Wood, "Materials processing for lithium-ion batteries," *J. Power Sources*, vol. 196, no. 5, pp. 2452–2460, 2011.

[3] A. Dey, B. Chakraborty, S. Dalai, and K. Bhattacharya, "Online Internal Resistance Computation-Based Early Sensing of Thermal Runaway for Smart Fault Handling System (FHS) of Li-Ion Batteries," IEEE Embedded Systems Letters, vol. 17, no. 4, pp. 284–287, 2025.

[4] A. Dey, B. Chakraborty, S. Dalai, and K. Bhattacharya, "Insights and New Practices for Advanced Metering Infrastructure and Smart Energy Metering Framework in Smart Grid—A Case Study," in *Proc. IEEE Calcutta Conference (CALCON)*, Kolkata, India, pp. 323–326, 2022.

[5] A. Dey, K. R. Hasabnis, B. Chakraborty, S. Mondal, S. Dalai, and K. Bhattacharya, "Enhancing Power System Resilience with DG Using GA Based Relay Coordination and FCL Integration," in *Proc. IEEE 4th Int. Conf. on Applied Electromagnetics, Signal Processing, & Communication (AESPC)*, pp. 1–6, 2024.

[6] Luo, X., et al. "Overview of current development in electrical energy storage technologies and the application potential in power system operation." Applied Energy, 2015.

[7] D. Razmi, O. Babayomi, A. Davari, T. Rahimi, Y. Miao, and Z. Zhang, "Review of model predictive control of distributed energy resources in microgrids," *Symmetry*, vol. 14, no. 8, p. 1735, 2022.

[8] R. Spotnitz and J. Franklin, "Abuse behavior of high-power, lithium-ion cells," *Journal of Power Sources*, vol. 113, no. 1, pp. 81–100, 2003.

[9] V. C. Gungor, D. Sahin, T. Kocak, S. Ergüt, C. Buccella, C. Cecati, and G. P. Hancke, "Smart grid technologies: Communication technologies and standards," *IEEE Transactions on Industrial Informatics*, vol. 7, no. 4, pp. 529–539, Nov. 2011

[10] D. Sui et al., "A comprehensive review of graphene-based anode materials for lithium-ion capacitors," Chemistry, vol. 3, no. 4, pp. 1215–1246, 2021.

[11] Nagaura, "Lithium ion rechargeable battery," *Progress in Batteries & Solar Cells*, vol. 9, p. 209, 1990.

[12] X. Feng, M. Ouyang, X. Liu, L. Lu, Y. Xia, and X. He, "Thermal runaway mechanism of lithium ion battery for electric vehicles: A review," *Energy Storage Materials*, vol. 10, pp. 246–267, 2018.

[13] Q. Wang, P. Ping, X. Zhao, G. Chu, J. Sun, and C. Chen, "Thermal runaway caused fire and explosion of lithium ion battery," *Journal of Power Sources*, vol. 208, pp. 210–224, 2012.

[14] W. Li, E. M. Erickson, and A. Manthiram, "High-nickel layered oxide cathodes for lithium-based automotive batteries," *Nature Energy*, vol. 5, no. 1, pp. 26–34, 2020.

[15] M. N. Obrovac and L. Christensen, "Structural changes in silicon anodes during lithium insertion/extraction," *Electrochemical and Solid-State Letters*, vol. 7, no. 5, p. A93, 2004.

[16] J. Vetter, P. Novák, M. R. Wagner, C. Veit, K.-C. Möller, J. O. Besenhard, M. Winter, M. Wohlfahrt-Mehrens, C. Vogler, and A. Hammouche, "Ageing mechanisms in lithium-ion batteries," *Journal of Power Sources*, vol. 147, no. 1–2, pp. 269–281, 2005.

[17] S. S. Zhang, "A review on electrolyte additives for lithium-ion batteries," *Journal of Power Sources*, vol. 162, no. 2, pp. 1379–1394, 2006.

[18] Y. Tian et al., "Promises and challenges of next-generation 'beyond li-ion' batteries for electric vehicles and grid decarbonization," Chem. Rev., vol. 121, no. 3, pp. 1623–1669, 2020.

[19] F. N. U. Khan et al., "Maximizing energy density of lithium-ion batteries for electric vehicles: A critical review," Energy Rep., vol. 9, pp. 11–21, 2023.

[20] W. Cao, J. Zhang, and H. Li, "Batteries with high theoretical energy densities," *Energy Storage Mater.*, vol. 26, pp. 46–55, 2020.

[21] G. Harper et al., "Recycling lithium-ion batteries from electric vehicles," *Nature*, vol. 575, pp. 75–86, 2019.

[22] M. Shafique et al., "Global material flow analysis of end-of-life of lithium nickel manganese cobalt oxide batteries from battery electric vehicles," Waste Manage. Res., vol. 41, no. 2, pp. 376–388, 2023.

[23] G. E. Blomgren, "The development and future of lithium-ion batteries," J. Electrochem. Soc., vol. 164, no. 1, pp. A5019–A5025, 2016.

[24] S. Hasselwander, M. Meyer, and I. Österle, "Techno-economic analysis of different battery cell chemistries for the passenger vehicle market," Batteries, vol. 9, no. 7, p. 379, 2023.

[25] Q. Li et al., "A 700 $W \cdot h \cdot kg^{-1}$ rechargeable pouch type lithium battery," Chin. Phys. Lett., vol. 40, no. 4, p. 048201, 2023.

[26] Y. Miao et al., "Current Li-ion battery technologies in electric vehicles and opportunities for advancements," Energies, vol. 12, no. 6, p. 1074, 2019.

[27] "The Nobel journey of M. Stanley Whittingham," Binghamton University. [Online]. Available: https://www.binghamton.edu/news/story/2424/the-nobel-journey-of-m-stanley-whittingham. Accessed: Mar. 10, 2024.

[28] Z. Liu et al., "Applications of graphene based composites in the anode of lithium-ion batteries," Front. Nanotechnol., vol. 4, p. 952200, 2022.

[29] H.-J. Kim et al., "A comprehensive review of Li-ion battery materials and their recycling techniques," Electronics, vol. 9, no. 7, p. 1161, 2020.

[30] H. Alizadeh et al., "Experimental investigation on thermal performance of covalently functionalized hydroxylated and non-covalently functionalized multi-walled carbon nanotubes/transformer oil nanofluid," Case Stud. Therm. Eng., vol. 31, p. 101713, 2022.

[31] P. Nzereogu et al., "Anode materials for lithium-ion batteries: A review," Appl. Surf. Sci. Adv., vol. 9, p. 100233, 2022.

[32] X. Li et al., "Study of lithium silicide nanoparticles as anode materials for advanced lithium ion batteries," ACS Appl. Mater. Interfaces, vol. 9, no. 19, pp. 16071–16080, 2017.

[33] N. Funamori and K. Tsuji, "Pressure-induced structural change of liquid silicon," *Physical Review Letters*, vol. 88, no. 25, p. 255508, 2002.

[34] Y. Deng et al., "Controllable synthesis of spinel nano-$ZnMn_2O_4$ via a single source precursor route and its high-capacity retention as anode material for lithium ion batteries," J. Mater. Chem., vol. 21, no. 32, pp. 11987–11995, 2011.

[35] S.-W. Kim et al., "Electrochemical performance and ex situ analysis of $ZnMn_2O_4$ nanowires as anode materials for lithium rechargeable batteries," Nano Res., vol. 4, pp. 505–510, 2011.

[36] C. Zhang et al., "Hierarchically designed germanium microcubes with high initial coulombic efficiency toward highly reversible lithium storage," Chem. Mater., vol. 27, no. 6, pp. 2189–2194, 2015.

[37] X. Lv et al., "Achieving high energy density for lithium-ion battery anodes by Si/C nanostructure design," J. Mater. Chem. A, vol. 7, no. 5, pp. 2165–2171, 2019.

[38] H. Wang et al., "Siligraphene as a promising anode material for lithium-ion batteries predicted from first-principles calculations," Nano Energy, vol. 49, pp. 67–76, 2018.

[39] H. J. Hwang et al., "Multilayer graphynes for lithium ion battery anode," J. Phys. Chem. C, vol. 117, no. 14, pp. 6919–6923, 2013.

[40] W. Xu et al., "Lithium metal anodes for rechargeable batteries," Energy Environ. Sci., vol. 7, no. 2, pp. 513–537, 2014.

[41] A. Dey, S. Mondal, B. Chakraborty, S. Dalai, and K. Bhattacharya, "Advancements in Li-Ion Battery Materials for Battery Energy Storage Systems," in Proc. 2025 Devices for Integrated Circuit (DevIC), pp. 749–754, 2025.

[42] E. G. Leggesse, C.-L. Chen, and J.-C. Jiang, "Lithium diffusion in graphene and graphite: Effect of edge morphology," Carbon, vol. 103, pp. 209–216, 2016.

[43] Y. Wang et al., "High-voltage 'single crystal' cathode materials for lithium-ion batteries," Energy Fuels, vol. 35, no. 3, pp. 1918–1932, 2021.

[44] Z. Li et al., "Performance improvement of Li-rich Mn-based materials with the submicron-sized single-crystal morphology and cationic doping," J. Alloys Compd., p. 173954, 2024.

[45] K. V. Kravchyk, F. Okur, and M. V. Kovalenko, "Break-even analysis of all-solid-state batteries with Li-garnet solid electrolytes," ACS Energy Lett., vol. 6, no. 6, pp. 2202–2207, 2021.

[46] W. Huang et al., "Elastic lattice enabling reversible tetrahedral Li storage sites in a high-capacity manganese oxide cathode," Adv. Mater., vol. 34, no. 30, p. 2202745, 2022.

[47] M. B. Dixit et al., "Understanding implications of cathode architecture on energy density of solid-state batteries," Energy Storage Mater., vol. 40, pp. 239–249, 2021.

[48] M.-K. Tran et al., "Comparative study of equivalent circuit models performance in four common lithium-ion batteries: LFP, NMC, LMO, NCA," Batteries, vol. 7, no. 3, p. 51, 2021.

[49] J. P. Mwizerwa et al., "Activated carbon/reduced graphene oxide wrapped $LiFePO_4$ cathode for Li-ion batteries with ultrahigh capacities and high specific energy density," FlatChem, vol. 34, p. 100393, 2022.

[50] J. Sun et al., "High volumetric energy density of $LiFePO_4$/C microspheres based on xylitol-polyvinyl alcohol complex carbon sources," J. Alloys Compd., vol. 773, pp. 788–795, 2019.

[51] W. Pfleging, "Recent progress in laser texturing of battery materials: A review of tuning electrochemical performances, related material development, and prospects for large-scale manufacturing," Int. J. Extrem. Manuf., vol. 3, no. 1, p. 012002, 2020.

[52] D. Commandeur et al., "Combinatorial performance mapping of near-NMC111 Li-ion cathodes," J. Materiomics, vol. 8, no. 2, pp. 437–445, 2022.

[53] A. A. Savina and A. M. Abakumov, "Benchmarking the electrochemical parameters of the $LiNi_{0.8}Mn_{0.1}Co_{0.1}O_2$ positive electrode material for Li-ion batteries," Heliyon, vol. 9, no. 12, 2023.

[54] "Flash battery," Flash Battery. [Online]. Available: https://www.flashbattery.tech/en/types-of-lithium-batteries-which-chemistry-use. Accessed: Mar. 10, 2024.

[55] U.-H. Kim et al., "High-energy-density Li-ion battery reaching full charge in 12 min," ACS Energy Lett., vol. 7, no. 11, pp. 3880–3888, 2022.

[56] P. Singh, V. Dudeja, and A. K. Panwar, "Electrochemical performance of NCA based cathodes for variable thickness of electrode through modelling and simulation," Mater. Today: Proc., vol. 62, pp. 3742–3748, 2022.

[57] X. Xia et al., "Ni-rich $LiNi_{0.82}Co_{0.15}Al_{0.03}O_2$ (NCA) as a high specific capacity thermal battery cathode material," Ionics, vol. 30, no. 1, pp. 607–615, 2024.

[58] Y. Han et al., "Improving electrochemical performance of $LiCoPO_4$ via Mn substitution," Mater. Technol., vol. 28, no. 5, pp. 265–269, 2013

[59] G. Rancilio et al., "Modeling a large-scale battery energy storage system for power grid application analysis," Energies, vol. 12, no. 17, p. 3312, 2019.

[60] S. Liu et al., "Reviving the lithium-manganese-based layered oxide cathodes for lithium-ion batteries," Matter, vol. 4, no. 5, pp. 1511–1527, 2021.

[61] T. A. Wani and G. Suresh, "A comprehensive review of $LiMnPO_4$ based cathode materials for lithium-ion batteries: Current strategies to improve its performance," J. Energy Storage, vol. 44, p. 103307, 2021.

[62] W. Du et al., "Prospect and status of polyanionic lithium cobalt silicates as high energy-density and safe cathode materials for lithium-ion batteries," Phys. Status Solidi B, vol. 258, no. 9, p. 2000420, 2021.

[63] H. Zhao et al., "The modification of natural pyrite and its electrochemical properties in Li/FeS_2 batteries," Funct. Mater. Lett., vol. 7, no. 01, p. 1350069, 2014.

[64] M. Li et al., "New concepts in electrolytes," Chem. Rev., vol. 120, no. 14, pp. 6783–6819, 2020.

[65] E. Logan and J. Dahn, "Electrolyte design for fast-charging Li-ion batteries," Trends Chem., vol. 2, no. 4, pp. 354–366, 2020.

[66] T. Gao and W. Lu, "Mechanism and effect of thermal degradation on electrolyte ionic diffusivity in Li-ion batteries: A molecular dynamics study," Electrochim. Acta, vol. 323, p. 134791, 2019.

[67] W.-Y. Kim, P.-Y. Lee, J. Kim, and K.-S. Kim, "A nonlinear-model-based observer for a state-of-charge estimation of a lithium-ion battery in electric vehicles," Energies, vol. 12, no. 17, p. 3383, 2019.

[68] J. Xie, X. Wei, X. Bo, P. Zhang, P. Chen, W. Hao, and M. Yuan, "State of charge estimation of lithium-ion battery based on extended Kalman filter algorithm," Frontiers in Energy Research, vol. 11, p. 1180881, 2023.

[69] J. Zhou, B. Xing, and C. Wang, "A review of lithium ion batteries electrochemical models for

electric vehicles," in *E3S Web of Conferences*, vol. 185, p. 04001, 2020.

[70] S. Sarkar, S. Z. Halim, M. M. El-Halwagi, and F. I. Khan, "Electrochemical models: Methods and applications for safer lithium-ion battery operation," *Journal of The Electrochemical Society*, vol. 169, no. 10, p. 100501, 2022.

[71] X. Xu, M. Bishop, D. G. Oikarinen, and C. Hao, "Application and modeling of battery energy storage in power systems," *CSEE Journal of Power and Energy Systems*, vol. 2, no. 3, pp. 82–90, 2016.

[72] G. Saldana, J. I. San Martín, I. Zamora, F. J. Asensio, O. Onederra, and M. Gonzalez-Perez, "Empirical calendar ageing model for electric vehicles and energy storage systems batteries," *Journal of Energy Storage*, vol. 55, p. 105676, 2022.

[73] D. Karimi, H. Behi, J. Van Mierlo, and M. Berecibar, "Equivalent circuit model for high-power lithium-ion batteries under high current rates, wide temperature range, and various state of charges," *Batteries*, vol. 9, no. 2, p. 101, 2023.

[74] Q. Wang, T. Gao, and X. Li, "SOC estimation of lithium-ion battery based on equivalent circuit model with variable parameters," *Energies*, vol. 15, no. 16, p. 5829, 2022.

[75] J. Meng, G. Luo, M. Ricco, M. Swierczynski, D.-I. Stroe, and R. Teodorescu, "Overview of lithium-ion battery modeling methods for state-of-charge estimation in electrical vehicles," Applied Sciences, vol. 8, no. 5, p. 659, 2018.

[76] J. Guo, Q. Guo, J. Liu, and H. Wang, "The polarization and heat generation characteristics of lithium-ion battery with electric–thermal coupled modeling," Batteries, vol. 9, no. 11, p. 529, 2023.

[77] R. Guo and W. Shen, "A review of equivalent circuit model based online state of power estimation for lithium-ion batteries in electric vehicles," Vehicles, vol. 4, no. 1, pp. 1–29, 2021.

[78] M. Tekin and M. I. Karamangil, "Development of dual polarization battery model with high accuracy for a lithium-ion battery cell under dynamic driving cycle conditions," Heliyon, vol. 10, no. 7, 2024.

[79] C. Hu, B. D. Youn, and J. Chung, "A multiscale framework with extended Kalman filter for lithium-ion battery SOC and capacity estimation," *Applied Energy*, vol. 92, pp. 694–704, Apr. 2012.

[80] T. Feng, L. Yang, X. Zhao, H. Zhang, and J. Qiang, "Online identification of lithium-ion battery parameters based on an improved equivalent-circuit model and its implementation on battery state-of-power prediction," Journal of Power Sources, vol. 281, pp. 192–203, 2015.

[81] Y. Wang, M. Li, and Z. Chen, "Experimental study of fractional-order models for lithium-ion battery and ultra-capacitor: Modeling, system identification, and validation," Applied Energy, vol. 278, p. 115736, 2020.

[82] Y. Zou, S. E. Li, B. Shao, and B. Wang, "State-space model with non-integer order derivatives for lithium-ion battery," Applied Energy, vol. 161, pp. 330–336, 2016.

[83] G. Dong, J. Wei, and Z. Chen, "Kalman filter for onboard state of charge estimation and peak power capability analysis of lithium-ion batteries," Journal of Power Sources, vol. 328, pp. 615–626, 2016.

[84] Y. Wang, R. Pan, C. Liu, Z. Chen, and Q. Ling, "Power capability evaluation for lithium iron phosphate batteries based on multi-parameter constraints estimation," Journal of Power Sources, vol. 374, pp. 12–23, 2018.

[85] S. Xiang, G. Hu, R. Huang, F. Guo, and P. Zhou, "Lithium-ion battery online rapid state-of-power estimation under multiple constraints," Energies, vol. 11, no. 2, p. 283, 2018.

[86] Y. Geng, H. Pang, and X. Liu, "State-of-charge estimation for lithium-ion battery based on PNGV model and particle filter algorithm," Journal of Power Electronics, vol. 22, no. 7, pp. 1154–1164, 2022.

[87] S. Nejad, D. Gladwin, and D. Stone, "A systematic review of lumped-parameter equivalent circuit models for real-time estimation of lithium-ion battery states," Journal of Power Sources, vol. 316, pp. 183–196, 2016.

[88] N. Tian, Y. Wang, J. Chen, and H. Fang, "On parameter identification of an equivalent circuit model for lithium-ion batteries," in Proc. IEEE Conf. Control Technology and Applications (CCTA), pp. 187–192, 2017.

[89] N. Biju and H. Fang, "Battx: An equivalent circuit model for lithium-ion batteries over broad current ranges," Applied Energy, vol. 339, p. 120905, 2023.

[90] S. J. Navas, G. C. González, F. Pino, and J. Guerra, "Modelling li-ion batteries using equivalent circuits for renewable energy applications," Energy Reports, vol. 9, pp. 4456–4465, 2023.

[91] J. Conzen, S. Lakshmipathy, A. Kapahi, S. Kraft, and M. DiDomizio, "Lithium ion battery energy storage systems (BESS) hazards," Journal of Loss Prevention in the Process Industries, vol. 81, p. 104932, 2023.

[92] M. Rouholamini, C. Wang, H. Nehrir, X. Hu, Z. Hu, H. Aki, B. Zhao, Z. Miao, and K. Strunz, "A review of modeling, management, and applications of grid-connected Li-ion battery storage systems," IEEE Transactions on Smart Grid, vol. 13, no. 6, pp. 4505–4524, 2022.

[93] N. Lebedeva, Li-ion batteries for mobility and stationary storage applications, Publications Office of the European Union, 2018.

[94] BloombergNEF, "Annual battery price survey," [Online]. Available: https://about.bnef.com/blog. [Accessed: Mar. 10, 2024].

[95] C. Parthasarathy, H. Hafezi, and H. Laaksonen, "Integration and control of lithium-ion BESSs for active network management in smart grids: Sundom smart grid backup feeding case," Electrical Engineering, vol. 104, no. 2, pp. 539–553, 2022.

[96] U.S. Energy Information Administration, "Energy storage for electricity generation," [Online]. Available: https://www.eia.gov/energyexplained/electricity/energy-storage-for-electricity-generation.php. [Accessed: Mar. 15, 2024].

[97] Energy Storage World Forum, "Applications of Energy Storage," [Online]. Available: https://energystorageforum.com/energy-storage-technologies/applications-of-energy-storage. [Accessed: Mar. 18, 2024].

[98] M. Alrashidi, "Community battery storage systems planning for voltage regulation in low-voltage distribution systems," Applied Sciences, vol. 12, no. 18, p. 9083, 2022.

[99] International Renewable Energy Agency, "Future of Solar Photovoltaic: Deployment, Investment, Technology, Grid Integration, and Socio-Economic Aspects," [Online]. Available: https://www.irena.org/-/media/Files/IRENA/Agency/Publication/2019/Nov/IRENA_Future_of_Solar_PV_2019.pdf. [Accessed: Mar. 20, 2024].

[100] Y.-K. Wu and K.-T. Tang, "Frequency Support by BESS–Review and Analysis," Energy Procedia, vol. 156, pp. 187–191, 2019.

[101] C. Jamroen, A. Pannawan, and S. Sirisukprasert, "Battery Energy Storage System Control for Voltage Regulation in Microgrid with High Penetration of PV Generation," in Proc. 53rd Int. Universities Power Eng. Conf. (UPEC), 2018, pp. 1–6.

[102] M. Zeraati, M. E. H. Golshan, and J. M. Guerrero, "Distributed Control of Battery Energy Storage Systems for Voltage Regulation in Distribution Networks with High PV Penetration," IEEE Trans. Smart Grid, vol. 9, no. 4, pp. 3582–3593, 2016.

[103] C. Zhao, P. B. Andersen, C. Træholt, and S. Hashemi, "Grid-Connected Battery Energy Storage System: A Review on Application and Integration," Renew. Sustain. Energy Rev., vol. 182, p. 113400, 2023.

[104] C. A. Cañizares, K. Bhattacharya, D. Sohm, et al., "Frequency Regulation Model of Bulk Power Systems with Energy Storage," IEEE Trans. Power Syst., vol. 37, no. 2, pp. 913–926, 2021.

[105] D. Ribó-Pérez, L. Larrosa-López, D. Pecondón-Tricas, and M. Alcázar-Ortega, "A Critical Review of Demand Response Products as Resources for Ancillary Services: International Experience and Policy Recommendations," Energies, vol. 14, no. 4, p. 846, 2021.

[106] P. Ponnaganti, B. Bak-Jensen, B. V. Wæhrens, and J. Asmussen, "Assessment of Energy Arbitrage Using Energy Storage Systems: A Wind Parks Perspective," Energies, vol. 14, no. 16, p. 4718, 2021.

[107] "Energy Arbitrage by Load Shifting," [Online]. Available: http://patentimages.storage.googleapis.com/pdfs/US20090326729.pdf. [Accessed: Mar. 20, 2024].

[108] T. T. Kim and H. V. Poor, "Scheduling Power Consumption with Price Uncertainty," IEEE Trans. Smart Grid, vol. 2, no. 3, pp. 519–527, 2011.

[109] "Difference Between Brownouts and Blackouts," [Online]. Available: https://www.gotpower.com/brownouts-and-blackouts. [Accessed: Mar. 25, 2024].

[110] M. Shahidehpour, F. Tinney, and Y. Fu, "Impact of Security on Power Systems Operation," Proc. IEEE, vol. 93, no. 11, pp. 2013–2025, 2005.

[111] F. I. Khan, M. Ahmed, and T. Aziz, "A Novel Framework for Restoration Technique of an Industrial Microgrid Using Black Start Units," Int. Trans. Electr. Energy Syst., vol. 30, no. 12, p. e12636, 2020.36, 2020.

[112] M. E. Glavin, P. K. W. Chan, S. Armstrong, and W. G. Hurley, “A standalone photovoltaic supercapacitor battery hybrid energy storage system,” in IEEE Transactions on Power Electronics, vol. 25, no. 12, pp. 3419–3428, Dec. 2010.

[113] A. Yazdani, and R. Iravani, Voltage-Sourced Converters in Power Systems: Modeling, Control, and Applications. John Wiley & Sons, 2010.

[114] T. Logenthiran, D. Srinivasan, and T. Z. Shun, “Intelligent control of distributed energy resources in microgrids,” in IEEE Transactions on Smart Grid, vol. 3, no. 4, pp. 2019–2028, Dec. 2012.

[115] S. H. E. Abdel Aleem et al., “Optimal sizing and design of a hybrid solar PV–diesel–battery system for a remote area in Egypt,” in IEEE Access, vol. 6, pp. 27202–27215, May 2018.

[116] B. Xu, D. Cui, Y. Zhang, and B. Zhang, “Energy arbitrage with energy storage systems: a

review," in CSEE Journal of Power and Energy Systems, vol. 6, no. 1, pp. 143–153, Mar. 2020.

[117] D. Di Domenico, G. Fiengo, and A. Stefanopoulou, "Lithium-ion battery state of charge estimation with a kalman filter based on a electrochemical model," Proc. 2008 American Control Conference, 2008.

[118] P. Rong and M. Pedram, "An analytical model for predicting the remaining battery capacity of lithium-ion batteries," in IEEE Transactions on Very Large Scale Integration (VLSI) Systems, vol. 14, no. 5, pp. 441–451, May 2006.

[119] A. T. Elsayed, A. A. Mohamed, and O. A. Mohammed, "DC microgrids and distribution systems: An overview," in Electric Power Systems Research, vol. 119, pp. 407–417, Feb. 2015.

[120] M. Yilmaz and P. T. Krein, "Review of battery charger topologies, charging power levels, and infrastructure for plug-in electric and hybrid vehicles," in IEEE Transactions on Power Electronics, vol. 28, no. 5, pp. 2151–2169, May 2013.

[121] M. Ceraolo, "New dynamical models of lead-acid batteries," in IEEE Transactions on Power Systems, vol. 15, no. 4, pp. 1184–1190, Nov. 2000.

[122] G. Liu, D. P. Chassin, and N. Djilali, "Simulating microgrids with a hierarchical control architecture," in IEEE Transactions on Smart Grid, vol. 2, no. 3, pp. 392–399, Sept. 2011.

[123] H. Farhangi, "The path of the smart grid," in IEEE Power and Energy Magazine, vol. 8, no. 1, pp. 18–28, Jan.–Feb. 2010.

[124] A. Khaligh and Z. Li, "Battery, ultracapacitor, fuel cell, and hybrid energy storage systems for electric, hybrid electric, fuel cell, and plug-in hybrid electric vehicles: State of the art," in IEEE Transactions on Vehicular Technology, vol. 59, no. 6, pp. 2806–2814, Jul. 2010.

[125] L. Xie, Y. Gu, A. Eskandari, and M. Ehsani, "Fast MPC-based coordination of wind power and battery energy storage systems," in Journal of Energy Engineering, vol. 139, no. 4, pp. 205–213, Dec. 2013.

[126] R. H. Lasseter, "Microgrids," in *IEEE Power Engineering Society Winter Meeting*, vol. 1, pp. 305–308, Jan. 2002.

[127] A. Ipakchi and F. Albuyeh, "Grid of the future," in *IEEE Power and Energy Magazine*, vol. 7, no. 2, pp. 52–62, Mar.–Apr. 2009.

[128] M. A. Hannan, M. M. Hoque, A. Mohamed, and A. Ayob, "Review of energy storage systems for electric vehicle applications: Issues and challenges," in *Renewable and Sustainable Energy Reviews*, vol. 69, pp. 771–789, Mar. 2017.

[129] N. Javaid et al., "A review of energy management strategies for smart homes," in *Renewable and Sustainable Energy Reviews*, vol. 74, pp. 335–349, July 2017.

[130] S. S. R. Depuru, L. Wang, and V. Devabhaktuni, "Smart meters for power grid: Challenges, issues, advantages and status," in *Renewable and Sustainable Energy Reviews*, vol. 15, no. 6, pp. 2736–2742, Aug. 2011.

[131] S. Bellocchi, K. Klöckner, M. Manno, M. Noussan, and M. Vellini, "On the role of electric vehicles towards low-carbon energy systems: Italy and Germany in comparison," *Applied Energy*, vol. 255, p. 113848, 2019.

[132] V. V. Viswanathan et al., "Cost and performance model for redox flow batteries," in Pacific Northwest National Laboratory Report, PNNL-19377, 2010.

[133] D. Doughty and E. P. Roth, “A general discussion of Li-ion battery safety,” in The Electrochemical Society Interface, vol. 21, no. 2, pp. 37–44, 2012.

[134] M. Wakihara and O. Yamamoto, Lithium-Ion Batteries: Fundamentals and Performance. Wiley-VCH, 1998.

[135] J. Jaguemont, L. Boulon, and Y. Dube, “A comprehensive review of lithium-ion batteries used in hybrid and electric vehicles at cold temperatures,” in Applied Energy, vol. 164, pp. 99–114, Feb. 2016.

[136] G. Plett, “Extended Kalman filtering for battery management systems of LiPB-based HEV battery packs Part 3: State and parameter estimation,” in Journal of Power Sources, vol. 134, no. 2, pp. 277–292, Aug. 2004.

[137] B. Scrosati and J. Garche, “Lithium batteries: Status, prospects and future,” in Journal of Power Sources, vol. 195, no. 9, pp. 2419–2430, May 2010.

[138] J. A. Peças Lopes, N. Hatziargyriou, J. Mutale, P. Djapic, and N. Jenkins, “Integrating distributed generation into electric power systems: A review of drivers, challenges and opportunities,” in Electric Power Systems Research, vol. 77, no. 9, pp. 1189–1203, July 2007.

[139] N. Hatziargyriou, Microgrids: Architectures and Control. John Wiley & Sons, 2014.

[140] F. Katiraei and M. R. Iravani, “Power management strategies for a microgrid with multiple distributed generation units,” in IEEE Transactions on Power Systems, vol. 21, no. 4, pp. 1821–1831, Nov. 2006.

[141] R. D. Zimmerman, C. E. Murillo-Sánchez, and R. J. Thomas, “MATPOWER: Steady-state operations, planning, and analysis tools for power systems research and education,” in IEEE Transactions on Power Systems, vol. 26, no. 1, pp. 12–19, Feb. 2011.

[142] A. Hahn, A. Ashok, S. Sridhar, and M. Govindarasu, “Cyber-physical security testbeds: Architecture, application, and evaluation for smart grid,” in IEEE Transactions on Smart Grid, vol. 4, no. 2, pp. 847–855, Jun. 2013.

[143] A. M. Amnesty International, “This is what we die for: Human rights abuses in the Democratic Republic of the Congo power the global trade in cobalt,” Amnesty International Report, Jan. 2016.

[144] B. Swain, “Recovery and recycling of lithium: A review,” in Separation and Purification Technology, vol. 172, pp. 388–403, Oct. 2017.

[145] D. Ellingsen, L. Majeau-Bettez, C. Hung, A. Hammer Strømman, and G. Singh, “Life cycle assessment of lithium-ion batteries for plug-in hybrid electric vehicles,” in Environmental Science & Technology, vol. 47, no. 7, pp. 3502–3510, Apr. 2013.

[146] X. Li, M. Feng, J. Wang, and M. Ouyang, “A review on recycling technology and management of spent lithium-ion batteries,” in Waste Management, vol. 84, pp. 188–200, Aug. 2019.

[147] BloombergNEF, “Battery Pack Prices Fall to an Average of $130/kWh,” BloombergNEF, Dec. 2023.

[148] A. Zakeri and S. Syri, “Economical and environmental analysis of electricity storage systems: A review,” in Renewable and Sustainable Energy Reviews, vol. 42, pp. 569–596, Feb. 2015.

[149] P. V. Chombo and Y. Laoonual, "A review of safety strategies of a Li-ion battery," *Journal*

of Power Sources, vol. 478, p. 228649, 2020.

[150] S. Onori, P. Spagnol, V. Marano, Y. Guezennec, and G. Rizzoni, "A new life estimation method for lithium-ion batteries in plug-in hybrid electric vehicles applications," International Journal of Power Electronics, vol. 4, no. 3, pp. 302–319, 2012.

[151] International Electrotechnical Commission, "Secondary lithium-ion cells for the propulsion of electric road vehicles - Part 2: Reliability and abuse testing," *IEC Standard 62660-2*, 2010.

[152] A. A. Pesaran, "Battery thermal management in EVs and HEVs: Issues and solutions," *Battery Man*, vol. 43, no. 5, pp. 34–49, 2001.

[153] C. F. Lopez, J. A. Jeevarajan, and P. P. Mukherjee, "Characterization of lithium-ion battery thermal abuse behavior using experimental and computational analysis," *Journal of The Electrochemical Society*, vol. 162, no. 10, pp. A2163–A2173, 2015.

[154] M. Y. Kim, H. Kim, and S. Lee, "Battery thermal management systems: A review of passive and active designs," *Energies*, vol. 13, no. 20, pp. 5217, 2020.

[155] F. Mocera, A. Somà, and D. Clerici, "Study of aging mechanisms in lithium-ion batteries for working vehicle applications," in *Proc. 2020 Fifteenth International Conference on Ecological Vehicles and Renewable Energies (EVER)*, pp. 1–8, 2020.

[156] M. Dubarry, N. Vuillaume, and B. Y. Liaw, "From single cell model to battery pack simulation for Li-ion batteries," *Journal of Power Sources*, vol. 186, no. 2, pp. 500–507, Jan. 2009.

[157] S. B. Peterson, J. Apt, and J. F. Whitacre, "Lithium-ion battery cell degradation resulting from realistic vehicle and vehicle-to-grid utilization," *Journal of Power Sources*, vol. 195, no. 8, pp. 2385–2392, Apr. 2010.

[158] H. He, R. Xiong, X. Zhang, and F. Sun, "State-of-charge estimation of the lithium-ion battery using an adaptive extended Kalman filter based on an improved Thevenin model," *IEEE Transactions on Vehicular Technology*, vol. 60, no. 4, pp. 1461–1469, May 2011.

[159] G. L. Plett, "Extended Kalman filtering for battery management systems of LiPB-based HEV battery packs Part 2. Modeling and identification," *Journal of Power Sources*, vol. 134, no. 2, pp. 262–276, Aug. 2004.

[160] S. Zhang and J. Lee, "A review on prognostics and health monitoring of Li-ion battery," *Journal of Power Sources*, vol. 196, no. 15, pp. 6007–6014, Aug. 2011.

[161] K. Smith, C.-Y. Wang, A. Pesaran, and M. Kim, "Predicting battery thermal abuse behavior using electro-thermal simulation," in *Proc. Advanced Automotive Battery Conf.*, Long Beach, CA, 2010.

[162] T. Ackermann, G. Andersson, and L. Söder, "Distributed generation: A definition," Electric Power Systems Research, vol. 57, no. 3, pp. 195–204, Apr. 2001.

[163] M. H. Syed and S. M. Islam, "Protection challenges in microgrids with renewable energy sources and battery storage: A review," Energies, vol. 14, no. 18, pp. 5863, 2021.

[164] M. Kezunovic, S. Meliopoulos, and V. Venkatasubramanian, "Application of time-synchronized measurements in power system protection and control," IEEE Transactions on Smart Grid, vol. 11, no. 3, pp. 2367–2375, May 2020.

[165] H. Bevrani, T. Ise, and Y. Miura, Power System Monitoring and Control, John Wiley & Sons, 2014.

[166] S. Chaitusaney and A. Yokoyama, “Impact of protection coordination on DG penetration,” IEEE Transactions on Power Delivery, vol. 23, no. 2, pp. 926–932, Apr. 2008.

[167] L. A. Kojovic and D. R. Novak, “Role of intelligent electronic devices in grid modernization and distributed energy integration,” IEEE Transactions on Smart Grid, vol. 9, no. 6, pp. 6325–6332, Nov. 2018.

[168] W. Gao et al., “Case study of an electric vehicle battery thermal runaway and online internal short-circuit detection,” IEEE Transactions on Power Electronics, vol. 36, no. 3, pp. 2452–2455, 2020.

[169] F. Wan et al., “High-sensitivity lithium-ion battery thermal runaway gas detection based on fiber-enhanced raman spectroscopy,” IEEE Sensors Journal, vol. 23, no. 7, pp. 6849– 6856, 2023.

[170] Z. Sun et al., “An online data-driven fault diagnosis and thermal runaway early warning for electric vehicle batteries,” IEEE Transactions on Power Electronics, vol. 37, no. 10, pp. 12636–12646, 2022.

[171] D. Kong, H. Lv, P. Ping, and G. Wang, “A review of early warning methods of thermal runaway of lithium ion batteries,” Journal of Energy Storage, vol. 64, no. 107073, pp. 1-21, 2023.

[172] S. Chen et al., “Mechanical strain signal based early warning for failure of different prismatic lithium-ion batteries,” Journal of Power Sources, vol. 580, no. 233397, pp. 1-8, 2023.

[173] D. Li, Z. Zhang, Z. Wang, P. Liu, Z. Liu and N. Lin, "Timely Thermal Runaway Prognosis for Battery Systems in Real-World Electric Vehicles Based on Temperature Abnormality," IEEE Journal of Emerging and Selected Topics in Power Electronics, vol. 11, no. 1, pp. 120-130, 2023.

[174] D. Ren et al., “A comparative investigation of aging effects on thermal runaway behavior of lithium-ion batteries,” ETransportation, vol. 2, pp. 100034, 2019.

[175] Z. Chen et al., “Capacity prediction and validation of lithium-ion batteries based on long short-term memory recurrent neural network,” IEEE access, vol. 8, pp.172783–172798, 2020.

[176] L. You et al., “Research on proactive diagnosis and early warning method for monitoring thermal runaway products of lithium iron phosphate battery in energy storage power station,” in 2023 4th International Conference on Advanced Electrical and Energy Systems (AEES). IEEE, pp. 603–608, 2023.

[177] J. Yu et al., “Fire accident simulation and fire emergency technology simulation research of lithium iron phosphate battery in prefabricated compartment for energy storage power station,” in 2022 7th International Conference on Power and Renewable Energy (ICPRE). IEEE, pp. 1021–1027, 2022.

[178] S. Koch, K. P. Birke, and R. Kuhn, “Fast thermal runaway detection for lithium-ion cells in large scale traction batteries,” Batteries, vol. 4, no. 2, pp. 1-11, 2018.

[179] C. D. Iweh, et al., "Distributed generation and renewable energy integration into the grid: Prerequisites, push factors, practical options, issues and merits," Energies, vol. 14, no. 17, p. 5375, 2021.

[180] H. HassanzadehFard and A. Jalilian, "Optimal sizing and location of renewable energy based DG units in distribution systems considering load growth," Int. J. Electr. Power Energy Syst., vol. 101, pp. 356-370, 2018.

[181] N. Bayati, A. Hajizadeh, and M. Soltani, "Protection in DC microgrids: a comparative review," IET Smart Grid, vol. 1, no. 3, pp. 66-75, 2018.

[182] H. M. Sharaf, et al., "A proposed coordination strategy for meshed distribution systems with DG considering user-defined characteristics of directional inverse time overcurrent relays," Int. J. Electr. Power Energy Syst., vol. 65, pp. 49-58, 2015.

[183] M. Meskin, et al., "Enhancement of overcurrent protection in active medium voltage distribution networks," in Proc. IEEE 6th Int. Conf. Renewable Energy Res. Appl. (ICRERA), 2017.

[184] A. S. Noghabi, H. R. Mashhadi, and J. Sadeh, "Optimal coordination of directional overcurrent relays considering different network topologies using interval linear programming," IEEE Trans. Power Del., vol. 25, no. 3, pp. 1348-1354, Jul. 2010.

[185] Y. G. Paithankar and S. R. Bhide, Fundamentals of Power System Protection, New Delhi, India: Prentice Hall, 2007.

[186] A. Elmitwally, E. Gouda, and S. Eladawy, "Optimal allocation of fault current limiters for sustaining overcurrent relays coordination in a power system with distributed generation," Alexandria Eng. J., vol. 54, no. 4, pp. 1077-1089, 2015.

[187] Y. Damchi, et al., "Optimal coordination of directional overcurrent relays in a microgrid system using a hybrid particle swarm optimization," in Proc. Int. Conf. Adv. Power Syst. Autom. Prot., 2011, vol. 2.

[188] N. Tummasit, S. Premrudeepreechacharn, and N. Tantichayakorn, "Adaptive overcurrent protection considering critical clearing time for a microgrid system," in Proc. IEEE Innovative Smart Grid Technol. Asia (ISGT Asia), Nov. 2015.

[189] A. Ukil, B. Deck, and V. H. Shah, "Smart distribution protection using current-only directional overcurrent relay," in Proc. IEEE PES Innovative Smart Grid Technol. Conf. Europe (ISGT Europe), 2010.

[190] P. Jamborsalamati, et al., "Implementation of an agent based distributed FLISR algorithm using IEC 61850 in active distribution grids," in Proc. Int. Conf. Renewable Energy Res. Appl. (ICRERA), 2015.

[191] D. S. Alkaran, M. R. Vatani, M. J. Sanjari, G. B. Gharehpetian, and M. S. Naderi, "Optimal overcurrent relay coordination in interconnected networks by using fuzzy-based GA method," IEEE Trans. Smart Grid, vol. 9, no. 4, pp. 3091-3101, Jul. 2018.

[192] A. Ghosal and M. Conti, “Key management systems for smart grid advanced metering infrastructure: A survey,” IEEE Communications Surveys & Tutorials, vol. 21, no. 3, pp. 2831–2848, 2019.

[193] O. Kebotogetse, R. Samikannu, and A. Yahya, "Review of key management techniques for advanced metering infrastructure," *Int. J. Distrib. Sensor Netw.*, vol. 17, no. 8, pp. 1–17, 2021.

[194] A. H. Tan, D. S. Ong, and M. Foo, "Estimation of battery internal resistance using built-in self-scaling method," *J. Energy Storage*, vol. 59, Art. no. 106481, 2023.

[195] J. Han, C.-S. Choi, W.-K. Park, I. Lee, and S.-H. Kim, “Smart home energy management system including renewable energy based on zigbee and plc,” IEEE Transactions on Consumer Electronics, vol. 60, no. 2, pp. 198–202, 2014.

[196] S. Sykiotis, S. Athanasoulias, M. Kaselimi, A. Doulamis, N. Doulamis, L. Stankovic, and V. Stankovic, “Performance-aware nilm model optimization for edge deployment,” IEEE Transactions on Green Communications and Networking, vol. 7, no. 3, pp. 1434–1446, 2023.

[197] Y. Zhang, H. Wu, Q. Ma, Q. Yang, and Y. Wang, “A learnable image-based load signature construction approach in nilm for appliances identification,” IEEE Transactions on Smart Grid, vol. 14, no. 5, pp. 3841–3849, 2023.

[198] T. S. Gunawan, M. H. Anuar, M. Kartiwi, and Z. Janin, “Development of power factor meter using arduino,” in 2018 IEEE 5th International Conference on Smart Instrumentation, Measurement and Application (ICSIMA). IEEE, 2018, pp. 1–4.

[199] A. MT Ibraheem Al-Naib, and B. Abdullah Hamad, “A cost-effective method for power factor metering systems,” International journal of electrical and computer engineering systems, vol. 13, no. 5, pp. 409–415, 2022.

[200] A. Dey, S. Mondal, B. Chakraborty, S. Dalai, and K. Bhattacharya, "Microcontroller Based Real-Time Power Monitoring Module by Hybrid Power Factor Selection Algorithm," in *IEEE Embedded Systems Letters*, 2025.

[201] Dedović, Maja Muftić, et al. "Enhancing power system stability with adaptive under frequency load shedding using synchrophasor measurements and empirical mode decomposition." International Journal of Electrical Power & Energy Systems, vol. 160, Art. no. 110133, 2024.

[202] S. Mane, R. Sapat, P. Kor, J. Shelar, R. D. Kulkarni, and J. Mundkar, “Microcontroller based automatic power factor correction system for power quality improvement,” in Proc. Int. Conf. for Emerging Technology (INCET), Belgaum, India, pp. 1–4, Jun. 2020.

[203] IEEE Std 1547.2-2023, IEEE Application Guide for IEEE Standard 1547-2018: Interconnection and Interoperability of Distributed Energy Resources with Electric Power Systems, IEEE Standards Association, 2023.

[204] M. J. Ghorbani and H. Mokhtari, “Impact of harmonics on power quality and losses in power distribution systems.” International Journal of Electrical & Computer Engineering (2088-8708), vol. 5, no. 1, 2015.

[205] P. Meehan, C. McArdle, and S. Daniels, “An efficient, scalable time-frequency method for tracking energy usage of domestic appliances using a two-step classification algorithm,” Energies, vol. 7, no. 11, pp. 7041–7066, 2014.

[206] M. S. Hussain, “Development and deployment of a high-precision power factor measurement meter,” Available at SSRN 4826204, 2024.

[207] J. Nömm, S. K. Rönnberg, and M. H. J. Bollen, “An analysis of frequency variations and its implications on connected equipment for a nanogrid during islanded operation,” Energies, vol. 11, no. 9, p. 2456, Sep. 2018.

[208] J. W. Bialek, "Blackouts in the US/Canada and continental Europe in 2003: Is liberalisation to blame?," 2005 IEEE Russia Power Tech, 2005, pp. 1-7.

[209] M. Islam, A. Khan and M. Khan, "A Way to Unlock The Electricity Energy Market for The Common People Using CP Model", Engineering International, vol. 4, no. 2, p. 63, 2016.

[210] M. Horváth et al., "Large scale smart meter data assessment for energy benchmarking and occupant behaviour profile development", IOP Conference Series: Earth and Environmental Science, vol. 323, no. 1, p. 012121, 2019.

[211] F. A. Qayyum et. al., "Appliance Scheduling Optimization in Smart Home Networks," IEEE Access, vol. 3, pp. 2176-2190, 2015.

[212] R. Rashed Mohassel, A. Fung, F. Mohammadi and K. Raahemifar, "A survey on Advanced

Metering Infrastructure", International Journal of Electrical Power & Energy Systems, vol. 63, pp. 473-484, 2014.

[213] N. Saputro, K. Akkaya and S. Uludag, "A survey of routing protocols for smart grid communications", Computer Networks, vol. 56, no. 11, pp. 2742-2771, 2012.

[214] P. Kumar, Y. Lin, G. Bai, A. Paverd, J. Dong and A. Martin, "Smart Grid Metering Networks: A Survey on Security, Privacy and Open Research Issues", IEEE Communications Surveys & Tutorials, vol. 21, no. 3, pp. 2886-2927, 2019.N.

[215] E. Ancillotti, R. Bruno and M. Conti, "The role of communication systems in smart grids: Architectures, technical solutions and research challenges", Computer Communications, vol. 36, no. 17-18, pp. 1665-1697, 2013.

[216] X. Fang, S. Misra, G. Xue and D. Yang, "Smart Grid — The New and Improved Power Grid: A Survey", IEEE Communications Surveys & Tutorials, vol. 14, no. 4, pp. 944-980, 2012.

[217] D. Mahmood et al., "Realistic Scheduling Mechanism for Smart Homes", Energies, vol. 9, no. 3, p. 202, 2016.

[218] "Innovative Smart Grid Technologies Conference NIST 2010", IEEE Power and Energy Magazine, vol. 8, no. 1, pp. 81-81, 2010.

[219] U. R. Anuebunwa, H. Rajamani, P. Pillai and O. Okpako, "Novel genetic algorithm for scheduling of appliances," 2016 IEEE PES PowerAfrica, 2016, pp. 57-61.

[220] A. Ahmad et al., "An Optimized Home Energy Management System with Integrated Renewable Energy and Storage Resources", Energies, vol. 10, no. 4, p. 549, 2017. Available: 10.3390/en10040549.

[221] N. Uribe-Pérez, L. Hernández, D. de la Vega and I. Angulo, "State of the Art and Trends Review of Smart Metering in Electricity Grids", Applied Sciences, vol. 6, no. 3, p. 68, 2016.

[222] Shaukat et al., "A survey on consumers empowerment, communication technologies, and renewable generation penetration within Smart Grid", Renewable and Sustainable Energy Reviews, vol. 81, pp. 1453-1475, 2018.

[223] Y. Kabalci, "A survey on smart metering and smart grid communication," Renewable and Sustainable Energy Reviews, vol. 57, pp. 302–318, 2016.

Abhijit Dey
09.10.25